To the Graduate Council:

I am submitting herewith a dissertation written by Kimberlee D. Payne entitled "Characterization and Structure Elucidation of Sodium Di-n-Alkylsulfosuccinate Surfactants in Water." I have examined the final copy of this dissertation for form and content and recommend that it be accepted in partial fulfillment of the requirements for the degree of Doctor of Philosophy, with a major in Chemistry.

Linda J. Magid
Linda J. Magid, Major Professor

We have read this dissertation
and recommend its acceptance:

Kelsey D. Cook

George Kabalka

George C. Fazio

Accepted for the Council:

Lew Minkel
Vice Provost
and Dean of The Graduate School

CHARACTERIZATION AND STRUCTURE ELUCIDATION OF SODIUM DI-N-ALKYLSULFOSUCCINATE SURFACTANTS IN WATER

A Dissertation

Presented for the

Doctor of Philosophy

Degree

The University of Tennessee, Knoxville

Kimberlee D. Payne

June 1987

To Don

ACKNOWLEDGEMENTS

The author wishes to express her deep gratitude and appreciation to Dr. Linda Magid for her guidance and encouragement. Her enthusiasm and energy has been truly inspirational.

The author also wishes to extend her gratitude to Paul Butler for invaluable computer assistance and discussions over the years and to Terri Smith for many synthetic ideas.

Appreciation is extended to the University of Tennessee, the United States Army, Sun Oil Corporation and the Atlantic Richfield Company for financial assistance during five years of graduate study.

The author wishes to convey her deep appreciation to her husband Don for his assistance in preparing this dissertation and for his love and understanding.

The author's parents, Ron and Betty Daus, have provided much love and encouragement over the years. The author is extremely grateful to them for their influence in her life.

ABSTRACT

The micellar structures and properties of a homologous series of double-tailed surfactants were determined using a number of techniques. Phase studies and conductivity, electromotive force and ^{23}Na nuclear magnetic resonance measurements were performed on aqueous solutions of the dihexyl, diheptyl, dioctyl, dinonyl and didecyl members of the sodium di-n-alkylsulfosuccinates in order to determine the change in the degree of cooperativity of micellization that occurred as a function of the surfactant chain length. Small-angle neutron scattering experiments were conducted to determine the size and shape of the sulfosuccinate micelles as a function of surfactant and salt concentration. The change in micellar size that occurred upon the addition of a counterion complexing agent to solutions of anionic surfactants was ascertained using small-angle neutron scattering.

The dinonyl and didecyl members of the sulfosuccinates were found to have limited solubility in water whereas the dihexyl, diheptyl and dioctyl members possessed fairly extensive isotropic micellar solution regions; results indicated that the latter members formed normal micelles in water over a fairly wide concentration range. Aggregation of these surfactants in water was characterized by lower optimum aggregation numbers and higher extents of counterion dissociation. The micelles consisted of a disordered hydrocarbon core surrounded by a hydrated shell. Compared to micelles formed from single-tailed surfactants, the micelles of the di-n-alkylsulfosuccinates experienced more rapid growth upon increasing surfactant concentration and upon

addition of salt. As the micellar solubility limit was approached, a transition in micellar shape from spheres to ellipsoids occurred for the dihexyl and diheptyl members. The addition of the cryptand, 4,7,13,16,21,24-hexaoxa-1,10-diazabicyclo[8.8.8]hexacosane, C222, to sodium dodecylsulfate solutions resulted in the formation of smaller, more highly charged micelles whereas the effect of C222 upon the structure of micelles formed by sodium di-n-heptylsulfosuccinate was concentration dependent. The observed differences in micellar structure and behavior between single- and double-tailed surfactants were explained in terms of headgroup areas and hydrocarbon-water contact.

TABLE OF CONTENTS

LIST OF TABLES

LIST OF FIGURES

FIGURE PAGE

CHAPTER I

INTRODUCTION

A. Background

The class of compounds known as surfactants displays unique physico-chemical properties that are a consequence of their amphiphilic nature. Surfactants possess distinct regions of hydrophobic and hydrophilic character. The hydrophobic region, or tail, is nonpolar whereas the hydrophilic region, or headgroup, is polar. When placed in aqueous solution surfactants may form spherical aggregates in which the tails cluster together while the headgroups remain in contact with the solvent; these aggregates are called micelles. Micelles are also possible in hydrocarbon solvents; here the roles of the tails and headgroups are reversed, thus the term "reverse micelles" is applied. Other types of surfactant aggregates are also possible, such as vesicles and bilayers.

Surfactants may be classified as either ionic or nonionic, depending on the nature of their headgroup. Headgroups may be cationic (e.g., ammonium), anionic (e.g., sulfonate), neutral (e.g., ethylene oxide) or zwitterionic (e.g., ammoniopropanesulfonate). The nonpolar region is typically a hydrocarbon which may have different chain lengths, unsaturation and/or two or more tails. This dissertation will deal exclusively with ionic surfactants, specifically double-tailed anionic surfactants.

The unique properties displayed by surfactants depend directly on the amphiphile concentration. In a concentration region characteristic

of the surfactant, the solution properties start to deviate substantially from those displayed by monomeric surfactant. Techniques such as EMF measurements, conductimetry, NMR and surface tension measurements[1] are able to detect this deviation; the concentration (region) at which this deviation occurs is termed the critical micelle concentration (cmc). For ionic surfactants, cmc's typically lie in the range 10^{-4} M - 10^{-2} M; cmc values for nonionics are usually lower.[2] An excellent compilation of cmc values and techniques is available.[3] The cmc is obtained by plotting the measured physico-chemical property versus concentration and extrapolating the results at high and low concentration. The point of intersection is the cmc. Figure 1 illustrates this method for sodium di-n-heptylsulfosuccinate.

The free energy of micellization is composed of two opposing forces: an attractive force due to the mutual attraction of the hydrocarbon tails and, for ionic surfactants, a repulsive force due to electrostatic repulsions between headgroups. Nonionics have lower cmc's because the repulsive contribution is from hydration forces rather than electrostatic repulsions.

Changes in the chemical structure of the amphiphile can result in changes in the cmc. For a single-tailed surfactant, the cmc can be related directly to the number of carbon atoms, n_c, as shown below:

$$\log \text{cmc} = a - bn_c \qquad (1)$$

where a and b are constants. For ionic surfactants b is approximately 0.3 and for nonionic and zwitterionic surfactants b is usually 0.5. The

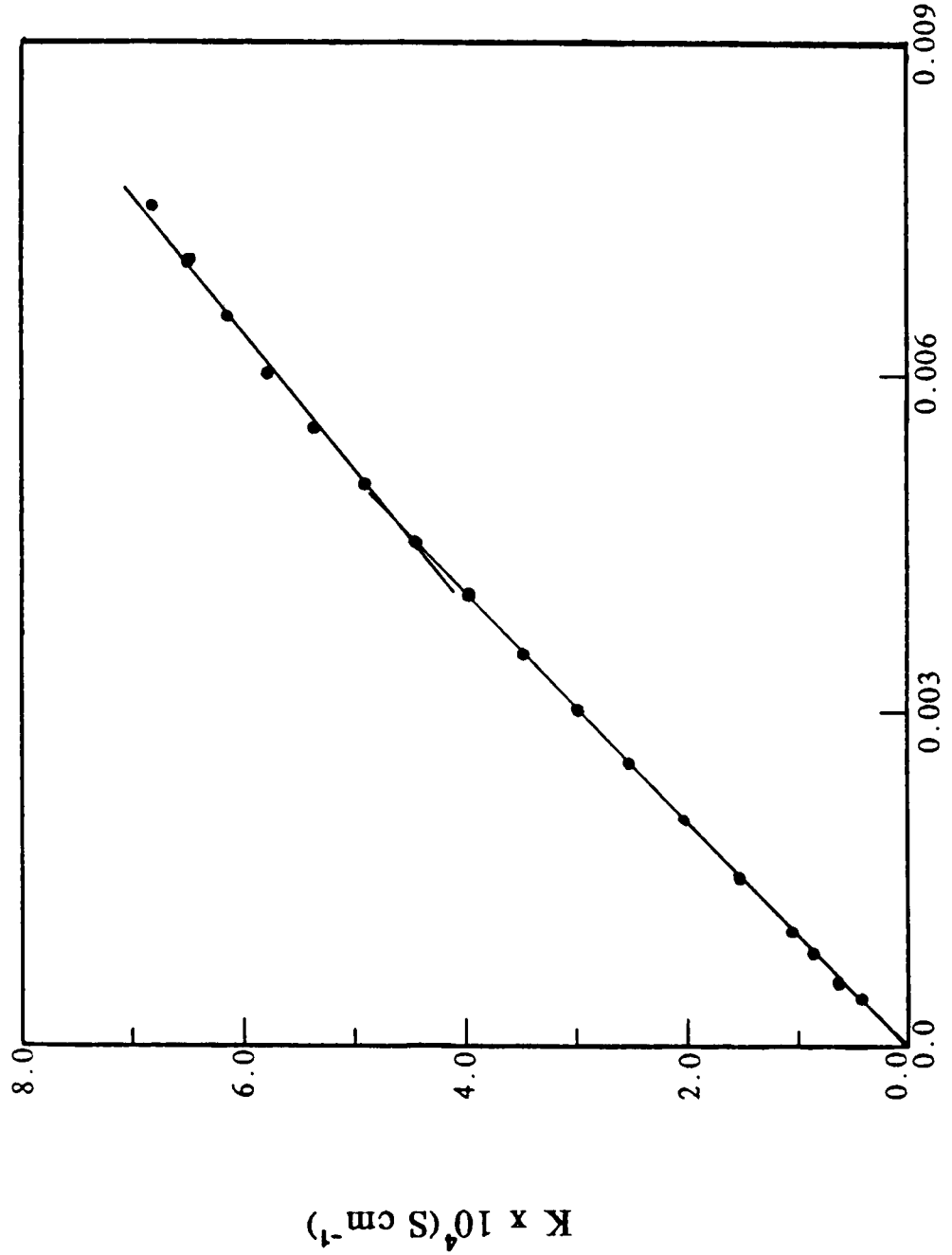

Figure 1. Plot of specific conductivity versus concentration for C_7SS.

value of b increases for ionic surfactants in the presence of added electrolyte.

Changing the hydrocarbon structure of the surfactants will also result in a change in the cmc. The cmc is increased by the addition of unsaturation, chain branching and polar groups, such as hydroxyl groups. However, the cmc decreases upon the addition of a benzene ring. (The above comparisons are valid for surfactants with comparable alkyl chain lengths.)

The main influence of the headgroup on the cmc is due to its charge. Thus nonionic surfactants possess lower cmc's than do ionics, whereas the cmc values of zwitterionic surfactants fall between the two groups. Only small differences in cmc's are found for ionic surfactants with different headgroups. The presence of two ionic headgroups leads to an increase in the cmc.[4]

Generally, the effects of counterions on the cmc have been found to be small for anionic surfactants. For a series of alkali dodecylsulfates, Mukerjee et al.[5] found that the cmc's increased slightly in the order $Cs^+ < K^+ < Na^+ < Li^+$. With tetraalkylammonium counterions, the cmc's decreased with increasing alkyl chain length for the dodecylsulfates.[5] Evans and co-workers[6] discovered recently that the addition of a macrocyclic ligand to aqueous solutions of sodium dodecylsulfate resulted in a decrease in the cmc.

Counterion effects on cationic surfactants are usually more substantial. The cmc's for dodecyltrimethylammonium salts were found to follow the sequence $NO_3^- < Br^- < Cl^-$.[7] Increasing the hydrophobicity of

the counterion has the effect of decreasing the cmc for alkylpyridinium surfactants.[8] The same effect is seen for hexadecyltrimethylammonium surfactant solutions with chlorobenzoates as the counterion.[9]

The addition of simple electrolytes to nonionic surfactants has only negligible effects on the cmc, whereas substantial effects are seen for ionic systems. The cmc is related to the salt concentration through[10]

$$\log \text{cmc} = -(m/n)\log C_s + \text{constant} \qquad (2)$$

where m is the number of bound counterions, n is the micellar aggregation number and C_s is the total concentration of counterion.

Besides decreasing the cmc, addition of simple electrolytes containing the counterion to ionic surfactants may also induce a change in the micellar shape. For hexadecyltrimethylammonium chlorobenzoates, shape changes occur upon simple substitution of the counterion. Counterions with chlorine atoms in the ortho position were found to induce the formation of "normal" micelles whereas surfactants with counterions containing chlorines in the meta or para position had lower cmc values and formed large cylindrical micelles.[9]

Hartley[11] is credited with first envisioning micelles as spherical aggregates; Figure 2 illustrates a Hartley micelle. On the average, spherical micelles contain 20-100 monomers and have radii in the range 12-30 Å.[2] The hydrocarbon tails of the surfactants make up the micellar core, whose radius is roughly equivalent to the extended length of the longest tail. Hartley[11] proposed that the micellar core was liquid-like

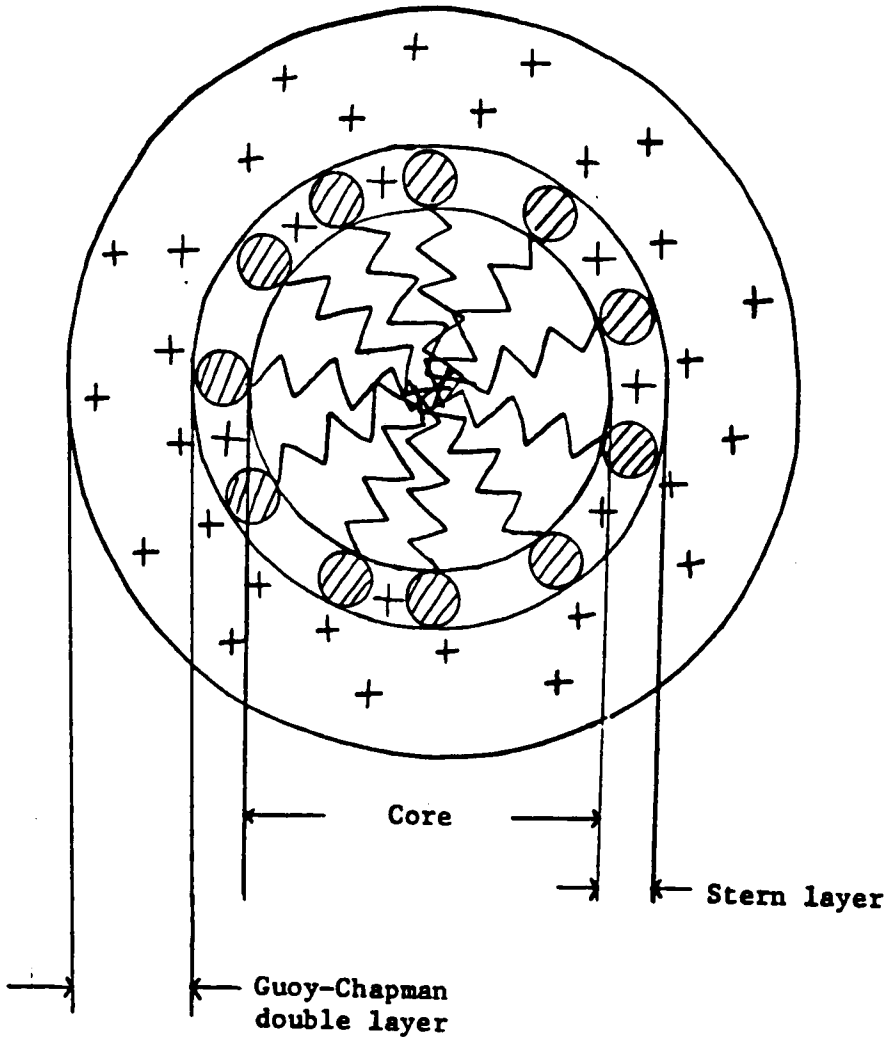

Figure 2. The Hartley model of the micelle.

circles: surfactant headgroups, crosses: counterions,
wavy lines: surfactant tail groups.

since micelles are able to solubilize nonpolar substances. The liquid-like nature of the core was later confirmed by thermodynamic,[12,13,14] fluorescence depolarization[15] and electron spin resonance[16] studies. The Stern layer consists of the headgroups, bound counterions and any associated waters of hydration. Typically the Stern layer coincides within 1 Å with the shear surface of the micelle.[17] The Guoy-Chapman layer, which surrounds the Stern layer, contains the majority of the dissociated counterions. The dissociated counterions exchange with the ions present in the bulk solution.

Much controversy has centered upon the Hartley model, particularly on the extent of water penetration into the micellar core. The extreme views, that of no water penetration and of extensive water penetration, are known as the fjord and reef models respectively.[18] One of the first proponents of a dry core was Stigter,[19] who determined that even the α-methylene groups (α to the headgroup) were contained in the core. More recently Dill and Flory[20] developed a statistical theory based on a lattice model which dealt with the constraints imposed by the space-filling requirements of the hydrocarbon chain segments. From their theory Dill and Flory[20] concluded that extensive water/hydrocarbon contact occurred at the surface but no water penetrated into the core.

Intermediate views on water penetration also exist. Fromherz[21] developed a surfactant block model incorporating both a compact drop model and a bilayer fragment model. In this model the micellar core was found to be rough with substantial wetting of the methylenes. Using ^{19}F NMR spin lattice relaxation of perfluorinated and partially fluorinated

surfactants in H_2O and D_2O, Ulmuis and Lindman[22] found appreciable H_2O contact only with the α-CF_2.

Menger has been the sharpest critic of the Hartley model. Through the use of spectroscopic studies[18,23] and CPK molecular models,[24] Menger has presented evidence that deep crevices exist in the core through which water penetrates almost to the end of the hydrocarbon chains. Menger supports his conclusions by earlier SAXS[25] and ^{19}F NMR studies[26] which also reported the presence of strong water penetration. Wennerstrom and Lindman[27] have pointed out that the interpretations of the data in these last two studies were not correct. Menger's spectroscopic technique and his interpretations of the data were also criticized by them. The use of probes in spectroscopic techniques is always questionable since (1) the introduction of the probe itself may perturb the micellar structure and (2) the exact location of the probe is not known accurately. Wennerstrom and Lindman[27] point out that spectroscopic techniques only measure the closeness of the probe to the water, whereas the amount of water actually present in the core is measured by thermodynamic and transport techniques. Indeed, studies performed using these techniques conclude that no water is present in the core.[27]

The most concrete evidence concerning the extent of water penetration comes from small-angle neutron scattering and NMR studies by Cabane and co-workers.[28,29] To measure the short distances involving water penetration into the sodium dodecylsulfate micelle (SDS), experiments were performed at high Q values in the SANS study. Scattering from sharp interfaces are known to follow Porod's law: $I(Q)\alpha Q^{-4}$, whereas

diffuse boundaries will produce scattering that drops off faster than Q^{-4} at large Q. Cabane et al.[28] obtained good fits to their data with a theoretical curve for spheres that had sharp boundaries. Therefore, on a scale comparable with the resolution of the experiment, SDS micelles have sharp water/hydrocarbon boundaries; overall penetration of water into the core must be no more than one water molecule per SDS molecule. Results from the NMR study also indicated a smooth surface with no penetration of water into the core.[29]

Besides spheres, other possible shapes exist for micellar aggregates; prolate and oblate ellipsoids and rods are a few of the possibilities. The shape of aggregates can be predicted by the surfactant packing parameter on the basis of the surfactant's structure.[30,31,32] Israelachvilli et al.[30,31,32] define the surfactant packing parameter, spp, in the following manner:

$$spp = v/al_c \tag{3}$$

where v is the volume per hydrocarbon region, a is the area per headgroup in the planar bilayer and l_c is the extended (all trans) length of the longest hydrocarbon tail. Israelachvilli et al.[30,31,32] applied the zero-order theory which requires an optimum area per headgroup.

The spp is derived for each shape from surface-to-volume considerations. The case of spherical micelles will be considered in detail. First the volume is defined as:

$$V = \bar{n}v = (4/3)\pi l_c^{\,3} \tag{4}$$

where $\bar{n}$ is the mean aggregation number. The surface of a spherical micelle may be given as

$$S = \bar{n}a = 4\pi l_c^2 \tag{5}$$

Dividing equation (4) by (5) yields

$$v/a = (1/3)l_c \tag{6a}$$

or

$$v/al_c = 1/3 \tag{6b}$$

According to this theory, once v/al_c becomes larger than 1/3 spheres can no longer exist. In the same manner as above, it can be shown[30,31,32] that for cylinders $v/al_c = 1/2$, for planar bilayers $v/al_c = 1$ and for reverse micelles and microemulsions $v/al_c > 1$ (microemulsions are thermodynamically stable systems which can be formed from oil/surfactant/water mixtures). Figure 3 shows the shape and spp values for a number of micellar forms. By manipulation of the surfactant packing parameter, changes in surfactant systems can be induced. For example, the addition of a simple electrolyte of the counterion is known to induce a sphere-to-rod transition for some surfactants. The area per headgroup is decreased due to the salt effectively screening charges between headgroups and v/al_c becomes larger. Routinely, microemulsion systems are prepared with alcohols. The alcohol increases the volume of

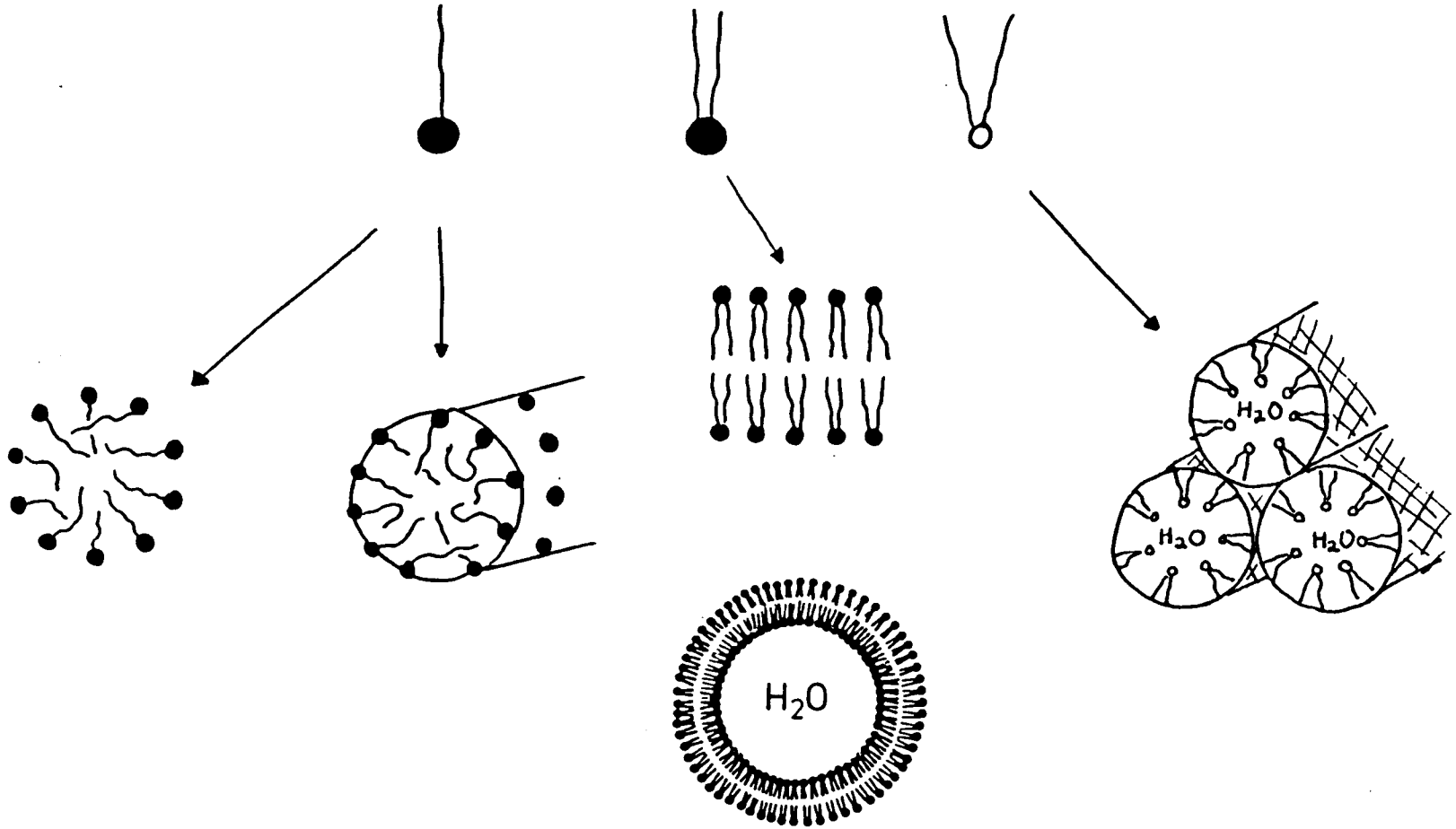

v/al_c

1/3 1/2 1 >1

Figure 3. Surfactant packing parameter.

the hydrocarbon tail without increasing l_c; this results in increasing v/al_c.

The aggregation of surfactant monomers into micelles has been described by a number of models.[1,33] The thermodynamics for three of the models will be reviewed here.

The phase-separation model views the aggregation process as being analogous to a phase transition. The micellization that occurs is highly cooperative. It is within this model that the cmc has its most clear-cut interpretation. In this model the cmc is defined as the saturation concentration of the surfactant monomers. Thus, below the cmc only monomers exist and above the cmc the concentration of nonmicellar surfactant is constant. This model is particularly useful for describing the dependence of micellar properties on surfactant concentration. The use of this model in describing NMR phenomena will be elaborated upon in Chapter II. It is important to note that the phase-separation model assumes an oversimplified view of the cooperativity of aggregation and does not account for premicellar aggregation.

The second model, the mass action law model, treats the equilibrium between monomeric surfactant and a micelle of aggregation number n:

$$nS \rightleftharpoons S_n \tag{7}$$

The equilibrium constant, K, is defined as

$$K = [S_n]/[S]^n \tag{8}$$

and the cmc is approximated by

$$cmc \simeq K^{(1/n-1)} \tag{9}$$

Two results of this model are worthy of note: (1) the larger the value of n, where n reflects the degree of cooperativity, the closer this model approaches the phase-separation model; (2) the occurrence of premicellar aggregation is still not accounted for.

The multiple equilibrium model formulates aggregation in two ways: either as the formation of each aggregate directly from monomers:

$$nS_1 \rightleftharpoons S_n \qquad n = 2,3... \tag{10}$$

with

$$K_n = [S_n]/[S]^n \tag{11}$$

or as the formation of micelles through a stepwise aggregation process:

$$S_1 + S_{n-1} \rightleftharpoons S_n \qquad n = 2,3... \tag{12}$$

where

$$K_{n'} = [S_n]/[S_1][S_{n-1}] \tag{13}$$

The two schemes shown above are thermodynamically but not kinetically equivalent. The equilibrium constants are related as shown in equation (14):

$$K_n = \prod_{i=2}^{n} K \qquad (14)$$

If the equilibrium constants are assumed equal, i.e., $K_1 = K_2 = K_3 = K_n$, then association occurs indefinitely, eventually leading to phase separation. Since this is not usually the case, modification of this model may be made in order to describe more aptly the system under study.

Tanford's[34] analysis of the contributions to the free energy of micellization is based upon the hydrophobic effect. Micelle formation is commonly viewed as arising from repulsion between the water and the hydrocarbon tails and the attraction between the tails. Tanford argues that this is not the true origin of the hydrophobic effect. Instead, it is the strong attraction of water for itself that is the main driving force behind the hydrophobic effect. Furthermore, the hydrocarbon-hydrocarbon and hydrocarbon-water attractions (and repulsions) are very slight. In pure water, the water molecules are arranged so that the molecules can hydrogen bond to four other water molecules. When a solute is placed in water, these hydrogen bonds must be either broken or distorted. However, if the solute is ionic or polar, it is able to compensate for the broken or distorted hydrogen bonds by forming strong bonds to the water molecules. Consequently, these molecules are easily soluble in water.

Results of recent experiments performed at temperatures up to 166°C conflict with Tanford's view of the hydrophobic effect. Evans et al.[35,36,37] studied the thermodynamics of micellization of alkyltrimethylammonium bromides in water from 25°C to 166°C. They found that

the free energy of hydrocarbon transfer is almost independent of temperature. At 166°C, a large negative entropy was obtained that was ascribed to the transfer of the hydrocarbon tail from bulk water to the micelle interior where movement is restricted. Since the unique structural properties of water are negligible at 166°C, the aggregation is driven solely by the energetics of transfer of hydrocarbon out of water. The same entropic and enthalpic factors operate at 25°C and must have the same magnitude as at 166°C since these factors are almost independent of water structure. However, at 25°C, a large positive entropy is obtained, which, when combined with the enthalpy change, gives a free energy that is almost temperature independent. Evans and co-workers[35,36,37] suggest that the entropy change is composed of two contributions. The first contribution is the same contribution of hydrocarbon transfer that operates at 166°C. The second contribution accounts for the restructuring of water which operates at 25°C. These same two contributions also make up the enthalpy change. The water restructuring effects must cancel out in order to obtain an almost constant free energy of micellization; therefore the water restructuring is only a small part of the free energetics of micelle formation.

Tanford's[34] thermodynamical approach will be outlined in the following paragraphs. First, let us consider the free energy of a surfactant monomer in water and in a micelle. The free energy of an amphiphile in water may be written as follows:

$$\mu_w = \mu_w^o + RT\ln(X_w) \qquad (15)$$

where Xw is the mole fraction of the monomer in water and μ_w^o is the standard unitary free energy of monomer in aqueous solution. Likewise, one can write for micelles in water

$$\mu_{mic} = \mu_{mic}^o + RT\ln(X_{mic}) \tag{16}$$

where μ_{mic}^o is the standard unitary free energy of a monomer in a micelle. The difference between the standard free energies of the monomers in micelles and in aqueous solution determines the equilibrium between micelles and free monomer. This is also the determinant of the size distribution of the micelles.

As seen earlier, the most simplistic approach is to treat micelle formation as a phase separation. The Gibbs phase rule will then apply. One can define the solubility as that single fixed mole fraction X_w at which the equilibrium between monomers and micelles occurs at a specific temperature and pressure. Thus

$$\mu_{mic}^o - \mu_w^o = RT\ln(X_w) \tag{17}$$

Obviously, micelles cannot be viewed as a separate phase since they are dispersed in solution. In order to correctly describe the thermodynamics of micelle formation, the contribution to μ_{mic}^o which arises from the mixing of micelles with solvent must also be considered.

Two approaches are available that treat micelles as a component of the aqueous phase. One approach views the micelles as comprising a

single element of the solution, regardless of their size. The other approach considers micellar aggregates of different n to be distinct species; each species has its own chemical potential. Here we shall consider only the first approach. The average number of monomers in the micelle is represented by $\bar{n}$, therefore the mole fraction of monomers present in the micelles (X_{mic}) is expressed by $\bar{n}$ times the mole fraction of the micelles. Thus

$$\mu_{mic} = \mu^{o}_{mic} + (RT/\bar{n})\ln(X_{mic}/\bar{n}) \qquad (18)$$

At equilibrium $\mu_{mic} = \mu_{w}$ so that

$$\mu^{0}_{mic} - \mu^{0}_{w} = RT\ln(X_{w}) - (RT/\bar{n})\ln(X_{mic}/\bar{n}) \qquad (19)$$

The probability of finding a monomer in a micelle is given by μ^{o}_{mic}. In order to incorporate the concept of a cmc into the thermodynamic equations, one can make use of the fact that the concentration of free monomers in equilibrium with the micelles changes very slowly with the concentration of micelles. Therefore, one can write for an extensive range of conditions that $X_{w} \sim$ cmc. Equation (18) may be rewritten as

$$\mu^{o}_{mic} - \mu^{o}_{w} = [(\bar{n}-1)/\bar{n}]RT\ln(cmc) + (RT/\bar{n})\ln(X_{mic}/\bar{n}) \qquad (20)$$

where the cmc is expressed in mole fraction units. For very large micelles $(\bar{n} - 1)/\bar{n}$ can be neglected and the above equation is then simplified to

$$\mu^{o}_{mic} - \mu^{o}_{w} = RT\ln(cmc) \qquad (21)$$

which resembles equation 17. It is important to note that as $\bar{n}$ is increased, the treatment of micelle formation as a phase separation becomes a much better approximation.

What is the driving force behind substantial micellar growth that occurs in some surfactant systems when the amphiphile concentration is increased? This issue can be addressed by considering the Benedek thermodynamic treatment[38,39] for micellar growth which is based upon the following assumptions: (1) a minimum micelle size, of aggregation number n_o, exists such that aggregation numbers must be greater than or equal to n_o; (2) there is no dependence of the size distribution upon the effects of micellar interactions at low surfactant concentration or for weakly interacting systems; and (3) the chemical potential of a micelle has the following form:

$$\mu^{o}_{n} = n\mu^{o}_{1} + \Delta + (n - n_0)\delta \quad \text{for } n \geq n_0 \qquad (22)$$

where μ^{o}_{n} and μ^{o}_{1} are the standard chemical potentials for a micelle with aggregation number n and for the monomer, respectively, and Δ is the lowering of the chemical potential that occurs when a minimum size micelle is formed from n monomers. The addition of more monomers to the minimum size micelle results in lowering of the chemical potential of a monomer in a micelle by a constant value, δ. This type of model is a "step plus ladder model" for the chemical potential of a micelle.

In order for micelles to grow, $|\delta|$ must be sufficiently larger than $|\Delta|/n_o$. For a sphere-to-rod transition, this condition is met when there is a free energy advantage for the monomer to be in the straight portion of the rod rather than in its hemispherical endcap.

The weight average, $\bar{n}$, and number average aggregation numbers, $\bar{n}'$, have the form

$$\bar{n} = n_0 + \frac{\beta}{1 - \beta} \left[1 + \frac{1}{n_0(1 - \beta) + \beta} \right] \tag{23}$$

$$\bar{n}' = n_0 + \frac{\beta}{1 - \beta} \tag{24}$$

where $\beta = X_1 e^{-\delta/kT}$ and X_1 is the monomer concentration. The determining factor in micellar growth is β. If β is close to one, a slight increase in β will result in a rapid increase in $\bar{n}$; for this condition an increase in surfactant concentration will result in rapid micellar growth. The mean aggregation numbers will be so much larger than that of the minimum size micelles that a polydisperse system forms. On the other hand, if β is considerably smaller than one, (e.g., 0.75), then n is not sensitive to slight changes in β as the amphiphile concentration is increased. In this case, a nearly monodisperse system results, with the value of mean aggregation numbers not deviating substantially from the minimum value as the concentration is increased.

The kinetics of micellization has been measured using a number of techniques. Depending upon the technique used, two different relaxation times were found: a fast relaxation process, τ_1, was found by

ultrasonic absorption,[40] NMR[41] and epr[42] spectroscopy, whereas T-jump,[43] pressure-jump[44] and stopped-flow[4] experiments yield a slow relaxation process, τ_2. On the average, the time domains of the two processes differed by a factor of 100. The fast process was assigned to the equilibrium between surfactant monomers and micelles and the slow process to the micellization-dissolution equilibrium.[40] Aniansson and Wall[46,47] explained the above phenomena by developing a theory using heat conduction and diffusion as analogies to the kinetics of micellization.

The relaxation time of the fast process, τ_1^{-1} is given below:

$$\tau_1^{-1} = k^-/\sigma^2 + ak^-/\bar{n} \quad . \tag{25}$$

where $\bar{n}$ is the mean aggregation number, σ is the standard deviation of the monomer distribution which is usually assumed to be a gaussian distribution. The relative amount of micellized monomer, a, is given by

$$a = (A_{tot} - \bar{A}_1)/\bar{A}_1 \tag{26}$$

where $\bar{A}_1$ is the equilibrium concentration of A. It has been found experimentally[40] that the length of the alkyl tails of the surfactant and the surfactant concentration affect τ_1. Typically τ_1 is in the range 10^{-3} - 10^{-8} s.

The second process is also described by an exponential decay whose relaxation time is given by

$$\tau_2^{-1} = (n^2/\bar{A}_1)R^{-1}[1 + \sigma^2 a/\bar{n}]^{-1} \quad (27)$$

The resistance for aggregates to "flow" through the region of intermediate aggregate sizes is denoted R and is defined as

$$R = \sum_{n_1+1}^{n_2} (k_n - \bar{A}_n) \quad (28)$$

$\bar{A}_N$ is the mean concentration of A_n and n_1 and n_2 are aggregation numbers between monomer and micelles. Temperature and salt concentration appear to have the most influence on τ_2. The value of τ_2 range from 10^{-3} - 1 s.

B. Statement of the Problem

The sensitivity of micellar properties to changes in the nonpolar region of the surfactant is exemplified by changes in the cmc. Thus, when a normal alkyl tail is replaced by a branched chain, surfactant association becomes less cooperative and cmc values increase. As a result, double-tailed surfactants are often characterized by a broadened cmc region, a decrease in optimum aggregation numbers and an increase in counterion dissociation.

The purpose of this dissertation is to determine the micellar structures and properties for a homologous series of double-tailed surfactants; features that will be focused upon include the evolution of micelle size and shape as the chain length is increased and as a function of concentration and salt; and the extent of hydration, as well as

properties associated with the cooperativity of micellization. Also, the effect of counterion complexation upon the size of micelles of anionic surfactants will be considered.

The physical properties of the sodium di-n-alkylsulfosuccinates (I) were determined; the amphiphiles studied and their abbreviations are as

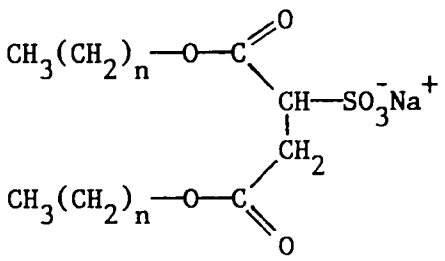

(I)

follows: di-n-hexyl (C_6SS), di-n-heptyl (C_7SS), di-n-octyl (C_8SS), di-n-nonyl (C_9SS) and di-n-decyl ($C_{10}SS$).

Similarities in structure exist between the sulfosuccinates and phospolipids (II). Phospholipids are the main constituents of

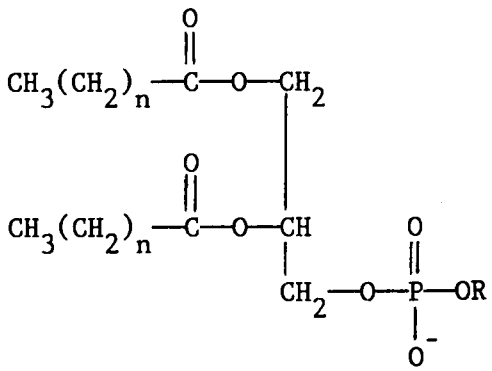

(II)

biomembranes and are used extensively to study membrane systems; however, the synthesis of these amphiphiles is not facile on a large scale. On the other hand, sulfosuccinates are much easier to synthesize in large quantities and therefore, can be used in model studies. Sulfosuccinates are also important because they are part of a family of surfactants that form microemulsions without the aid of a cosurfactant.

This dissertation is divided into three parts. The first part will focus upon the change in the degree of cooperativity of micellization that occurs for a double-tailed surfactant as a function of the chain length. Determination of the size and shape of the sulfosuccinate micelles as a function of surfactant and salt concentration form the focus of the second part of this dissertation. The final portion of this dissertation will consider the changes in micellar size that result from counterion complexation by a macrocyclic ligand for anionic surfactants.

An overview of the micellar behavior of double-tailed surfactants in water is presented in the first part of Chapter II; results from phase studies and conductivity measurements are then presented for the C_6 through C_{10} sulfosuccinates. The second half of Chapter II considers the application of NMR to the study of micellar systems and the results obtained using ^{23}Na NMR for C_6SS and C_7SS are presented. Small-angle neutron scattering (SANS) was employed for the determination of the size and shape of the micelles; because SANS is a relatively new technique, Chapter III gives the necessary theoretical background. Chapter IV discusses the application of SANS to other micellar systems as well as the

studies performed in this work on the sulfosuccinates. These studies were concerned with the determination of micellar size and shape, monomer hydration and volume. Dramatic counterion effects on the size and shape of micelles are reviewed in Chapter V and results from SANS experiments of micellar solutions containing counterion-complexing ligands are presented. Chapter VI discusses the results and conclusions from the various studies.

CHAPTER II

PHYSICO-CHEMICAL PROPERTIES OF DOUBLE-TAILED SURFACTANTS

A. Phase Behavior, CMC, Counterion Binding

According to the packing constraint theory,[13,14,15] single-tailed surfactants should form spherical micelles whereas double-tailed surfactants, with a spp > 1/2, should form vesicles or bilayers. For double-tailed surfactants containing relatively short tails, normal micelles exist.

Surfactants can be classified according to their phase behavior in water into one of three categories. The first category includes surfactants exhibiting substantial solubility in water; these systems are characterized by an extensive isotropic micellar solution region, L_1 (see Figure 4a). In the L_1 region normal spherical micelles are present whose shape may change as the micellar solubility limit is approached. The micellar solubility limit is defined as the boundary between the isotropic micellar solution region and the two phase region which is a dispersion of the isotropic micellar solution plus a liquid crystalline mesophase. Liquid crystalline phases normally seen for surfactants include cubic, hexagonal and lamellar. Examples of surfactants in this first category include sodium dodecylsulfate (SDS) and cetyltrimethylammonium bromide (CTAB).

Surfactants of limited solubility in water belong in the second category; these surfactants are typified by large spp's. The phase

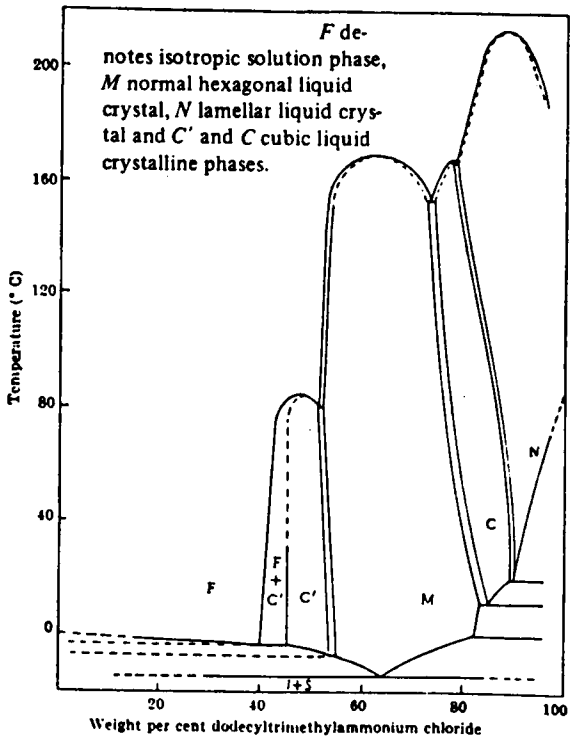

(a)

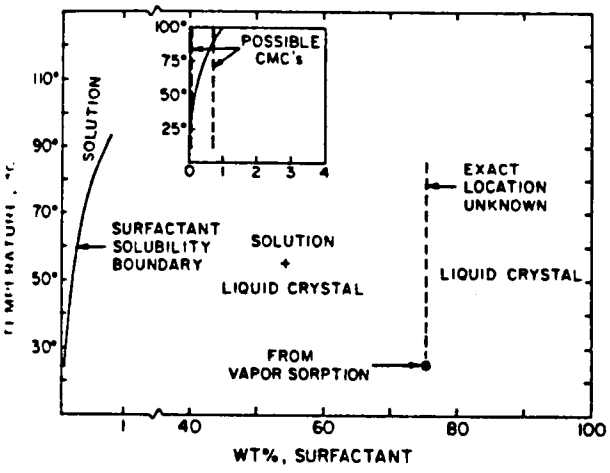

(b)

Figure 4. Phase diagram for the binary systems (a) dodecyltrimethylammonium chloride/H_2O,[1] (b) Texas #1/water.[54]

diagram in Figure 4b is representative of many double-tailed surfactants such as sodium p-(1-heptylnonyl)sulfonate (Texas #1)[48] and dioctadecyldimethylammonium chloride. For these surfactants, the L_1 region is extremely limited; in fact, the micellar solubility limit is observed at such low concentrations that it often lies below the hypothetical cmc. Vesicles do form upon sonication of aqueous dispersions of these surfactants.

The third category contains surfactants which form vesicles spontaneously upon dissolving in water; surfactants displaying such behavior normally possess two tails and a highly hydrated counterion. Examples of surfactants in this category include didodecyldimethylammonium surfactants with hydroxide or acetate counterions, Texas #1 with Kryptofix 2.2.2. and $C_{16}C_8N(CH_3)_2Br$ (even though it does not fit the counterion criteria). At low surfactant concentrations (below ca. 10^{-3} M) the L_1 region contains spontaneously formed vesicles; at higher concentrations, mixtures of micelles and vesicles are present. The vesicle-to-micelle transition is normally complete in the concentration range 10^{-2} to 10^{-1} M.

The shape changes that occur as surfactant concentration is increased in the L_1 region and as the micellar solubility limit is approached can be predicted based upon the proximate mesophase idea.[49] For surfactants, the lyotropic phases usually observed are the cubic, the hexagonal and the lamellar phase. Therefore, based upon the structures present in the liquid crystalline phase, spherical micelles are

expected before the cubic phase, rodlike micelles before the hexagonal phase and disk-like micelles before the lamellar phase.

Kunitake and co-workers[50,51] have studied extensively the formation of bilayers and vesicles by double-tailed surfactants. The dialkyldimethylammonium surfactants with chain lengths of 10-20 carbons have been thoroughly investigated;[50,52] the phase behavior of dioctadecyldimethylammonium chloride resembles that of phospholipids.[52] Double-tailed surfactants containing anionic[50] (phosphate, sulfonate, carboxylate), nonionic[51] or zwitterionic[51] headgroups also form bilayers; di-n-alkylsulfosuccinates with relatively long tails (C_{10}, C_{12}, C_{16}) fall in this category.[50] Upon sonication, large vesicles were present in aqueous solutions of $C_{10}SS$ and $C_{12}SS$ whereas no change occurred in the aqueous dispersions of $C_{16}SS$, i.e., only liquid crystals were present. This trend is in agreement with those of other two-tailed surfactants in that as the chain length is increased, the lamellar structure is formed more readily.

Several members of the sodium alkylbenzenesulfonate family (see below) have been studied in detail.[53-58]

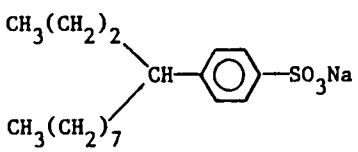

I

cmc 1.75×10^{-3} M

(25 C)

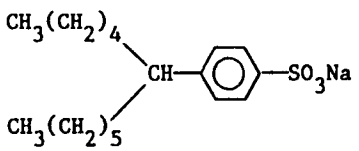

II

2.1×10^{-3} M

(30 C)

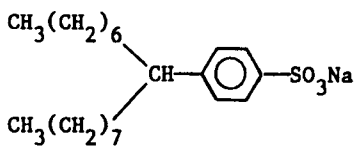

III

9.6×10^{-4} M,est.

Sodium p-(1-propylnonyl)benzenesulfonate,[53] I, and sodium p-(1-pentylheptyl)benzenesulfonate,[55] II, form normal micelles in water, whereas sodium p-(1-heptylnonyl)benzenesulfonate, III, exhibits very limited solubility in water: 0.06 weight % at 25°C.[54] Magid et al.[58] demonstrated by SANS that aqueous solutions of Texas #1 contained small, spherical micelles at concentrations of a few times the cmc. Sonication of aqueous dispersions of liquid crystals of Texas #1 led to the formation of unstable vesicles.[57]

A member of the sulfosuccinate family, sodium di-2-ethylhexylsulfosuccinate (Aeorosol OT or AOT), IV,

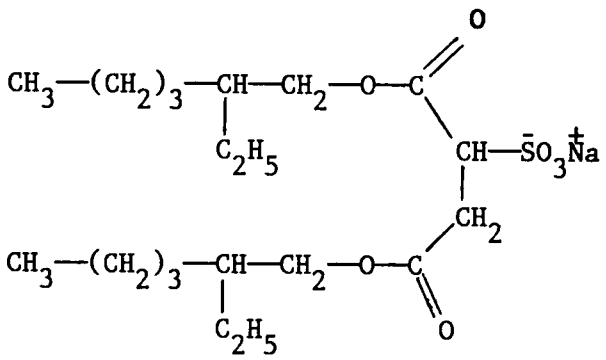

(IV)

shows phase behavior similar to that of Texas #1. AOT is of limited solubility in water; it does form micelles in water with a cmc in the range 2.3-5.1 x 10^{-3} M.[59] Likewise AOT tends to form liquid crystals at low surfactant concentrations. AOT is extremely soluble in hydrocarbon solvent and is able to solubilize large amounts of water. Figure 5 shows the ternary phase diagram for the system AOT/n-decanol/water. The reverse micellar region, L_2, is fairly extensive; the large amount of

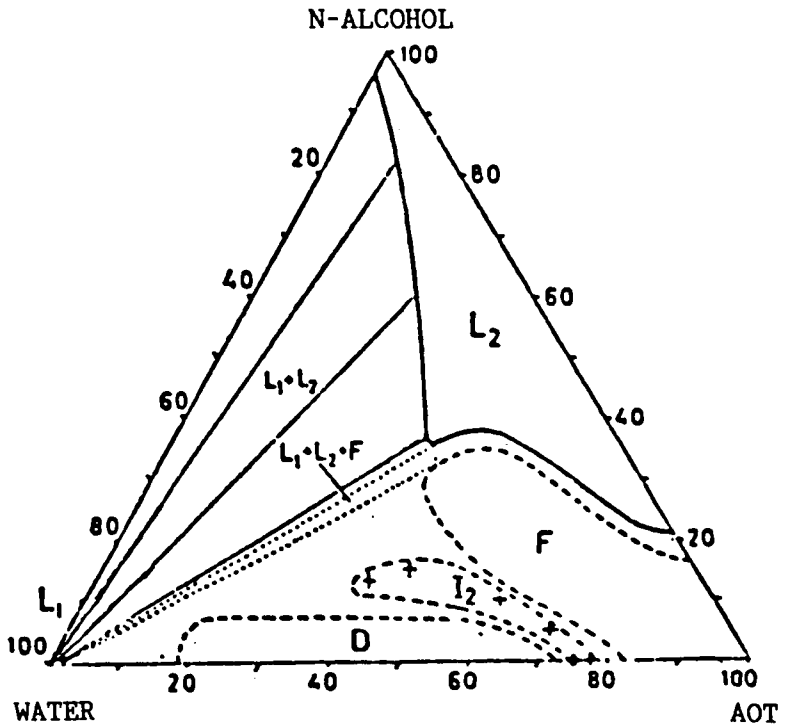

Figure 5. Phase diagram for the ternary system AOT/n-alcohol/water.

water taken up reflects the presence of microemulsions. AOT is an extremely important surfactant because it can form microemulsions without the aid of cosurfactants which are typically medium chain length alcohols. The solution properties of AOT have been studied in great detail; for a comprehensive review see reference 60.

Techniques such as conductimetry and electromotive force measurements (EMF) can be used to assess the effect that a second tail has on the cmc and extent of counterion binding. The most systematic study of this effect was conducted by H. C. Evans in 1958.[61] Evans studied sodium alkylsulfates in which the alkyl group consisted of 8-19 carbon atoms and the headgroup was either in the terminal position or attached to various interior carbons. The cmc values obtained from conductimetry were found to decrease and the extent of counterion dissociation to increase as the headgroup was placed closer to the middle of the chain. Evans noted some curvature at the point of intersection in plots of specific conductivity vs. concentration for some of the lower molecular weight compounds. This curvature indicates that micellization is occurring over a small range of concentrations as opposed to occurring at a single concentration.

Tausk and co-workers[62] determined the physico-chemical properties of a series of short-chain lecithin homologues containing either two hexanoyl, heptanoyl, octanoyl or nonanoyl tails. The di-C_8 lecithin was the highest homologue to form normal micelles. Surface tension measurements were used to determine the cmc's, which were found to decrease with increasing chain length.

The effect of the size of the hydrophobic moiety on the degree of ionization was investigated by Zana;[63] the cmc and extent of counterion dissociation of the dodecyldimethylalkylammonium bromide series $(C_{12}H_{25})(C_mH_{2m+1})N(CH_3)_2Br$, with m = 1, 2, 3, 4, 8, 10) were measured using conductimetry and/or Br^- specific electrodes. The C_mH_{2m+1} moiety was determined to begin associating with the hydrophobic region when m is three. The cmc's decreased and the extent of counterion dissociation increased with increasing alkyl chain length. Based on calculations of a, area per headgroup, Zana[63] found that a increased with increasing chain length. Lianos and Lang[55] also reported a larger area per headgroup for the double-tailed surfactant sodium p-(1-propylnonyl)-benzenesulfonate, 140 $Å^2$ vs 80 $Å^2$ for SDS.

Miller and Dixon[64] first reported conductivity data for sodium dialkylsulfosuccinates. Surfactants with di-n-octyl, di-n-hexyl, di-n-amyl, di-n-butyl and di-(2-ethylhexyl) tails were investigated at 29.92°C; the cmc's were obtained from plots of specific conductivity vs concentration. Results are listed in Table I along with cmc values obtained from surface tension measurements.[65]

More recently, Jobe and Reinsborough[66] compared the micellar properties of two related families: the sodium alkylsulfoacetates, V, and the sodium dialkylsulfosuccinates. Sodium alkylsulfoacetates contained

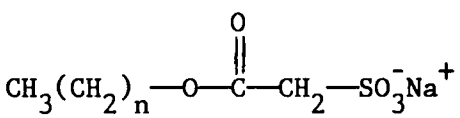

(V)

TABLE I

CMC VALUES FOR SODIUM DIALKYLSULFOSUCCINATES[a]

Surfactant	CMC (mol/L) Surface Tension 25°C	Specific Conductance 29.92°C
n-butyl	0.20	0.21
n-amyl	0.053	0.073
n-hexyl	0.0124	0.0128
n-octyl	0.00068	-
2-ethylhexyl	0.0025	0.0061

[a]From ref. 65.

chain lengths of six (SHSA), eight (SOSA) and ten (SDSA) carbons and the sulfosuccinates consisted of either dihexyl (C_6SS) or dioctyl (C_8SS) tails. The cmc's determined from conductivity and viscosity measurements at 25.0°C are listed in Table II. The cmc of the double-tailed surfactant with six-carbon tails is approximately the same as that of the single-tailed surfactant with a ten carbon tail. This trend in cmc values agrees with the trend usually observed;[66] for double-tailed surfactants with chain lengths n_m and n_n, $n_c < n_m + n_n$, where n_c is related to the cmc via equation 1 (p. 2).

B. Physico-Chemical Properties of Sodium Di-n-Alkylsulfosuccinates

1. Phase Behavior

The partial phase diagrams for di-C_6, di-C_8 and di-C_{10} sulfosuccinates are shown in Figure 6, and those for di-C_7 and di-C_9 sulfosuccinates in Figure 7. The Krafft temperatures are: C_6SS: 16.0°C; C_7SS: 31.5°C; C_8SS: 32.0°C; C_9: 45.0°C; and $C_{10}SS$: 49.5°C. This behavior resembles the even-odd alternation found in melting points of compounds containing one or more alkyl chains.[67] The first formed liquid-crystalline phase is lamellar.[68] The surfactant concentrations at the boundary between L_1 and L_1 + LC (biphasic dispersion transition) at 45°C are: C_6SS: 1.2 M(extrapolated); C_7SS: 0.57 M; C_8SS: 0.05 M; C_9SS: 0.020 M; and $C_{10}SS$: 0.0014 M. This boundary is susceptible to isotope effects: for di-C_8 in D_2O this concentration is 0.041 M.

TABLE II

CMC VALUES FOR SODIUM DIALKYLSULFOSUCCINATES AND SODIUM ALKYLSULFOACETATES[b]

Surfactant	CMC (mol/L) Viscosity 25°C	Specific Conductance 25°C
SHSA	0.21	0.17
SOSA	0.070	0.066
SDSA	0.025	0.022
C_6SS	0.014	0.0138
C_8SS	-	0.00068

[b]From ref. 66.

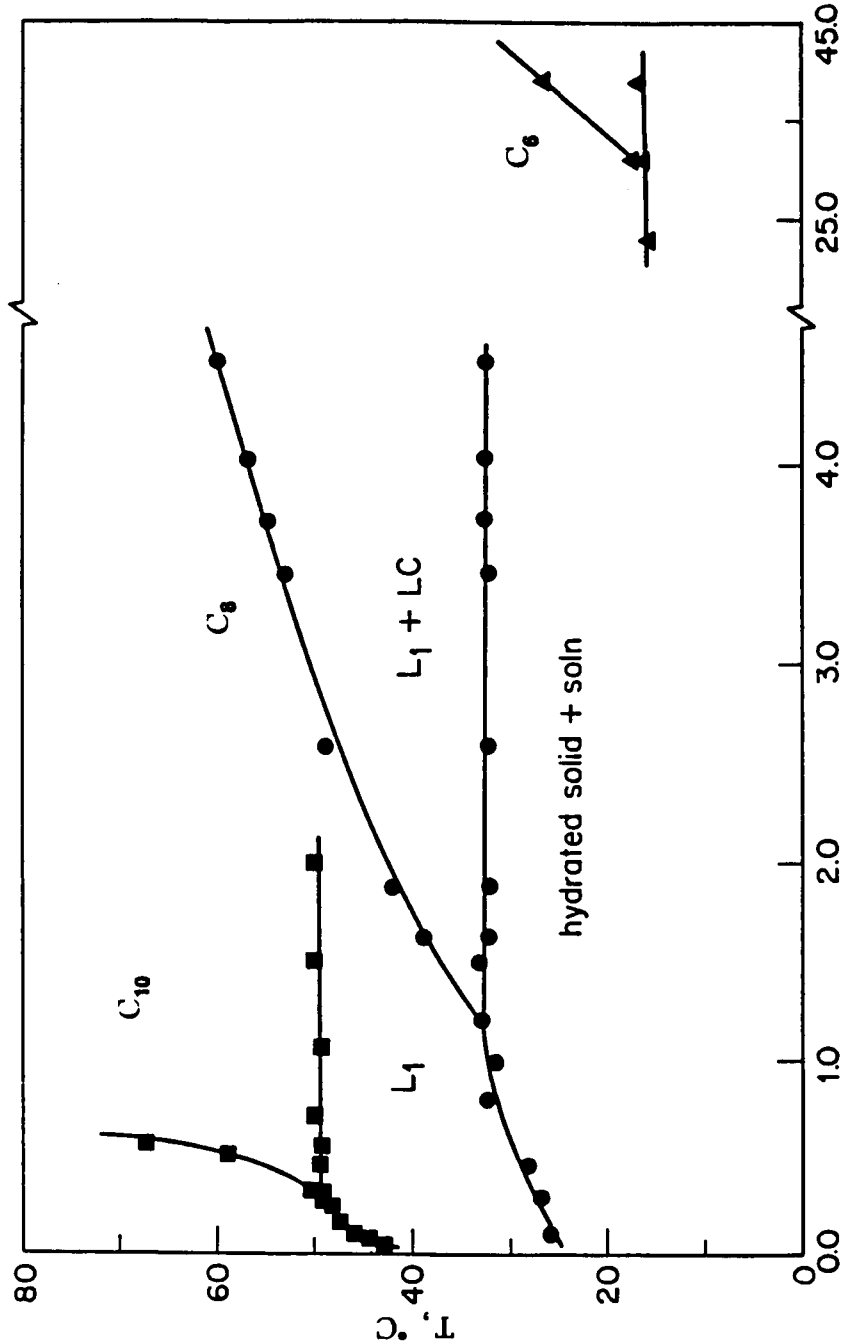

Figure 6. Partial binary phase diagrams for C_6SS, C_8SS and $C_{10}SS$.

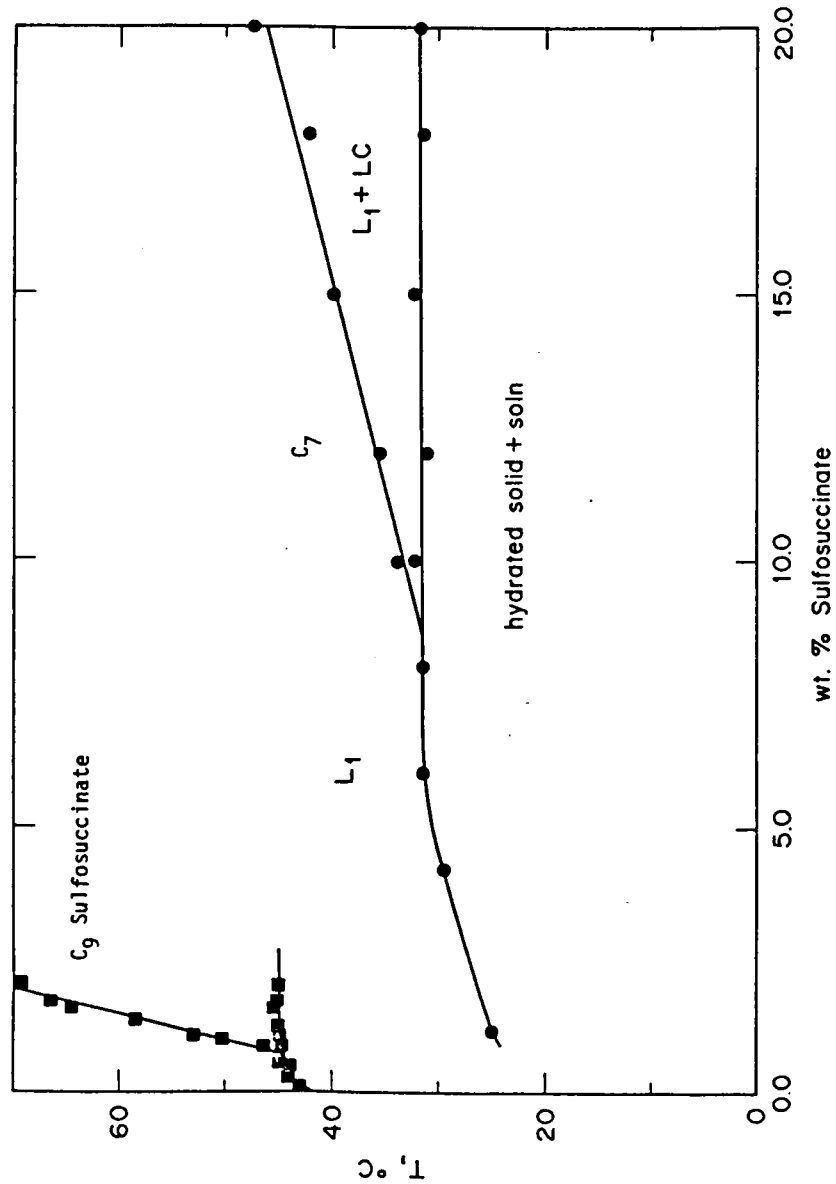

Figure 7. Partial binary phase diagrams for C_7SS and C_9SS.

2. EMF Measurements

EMF measurements for di-C_6 and di-C_8 sulfosuccinates were made in our lab[69] using the Fisher Na^+ electrode. Results are presented in Figures 8 and 9. The author made numerous attempts to apply this technique to the di-C_7 sulfosuccinate; erratic results were obtained which are believed to be a consequence of the surfactant adsorbing onto the surface of the Na^+ electrode. This type of behavior has been noted for other double-tailed surfactants[63] (using Br^- electrodes). The breaks in the mV vs. log concentration plots designate the onset of micellization. The break for C_6SS occurred at 0.0120 M, for C_8SS at 0.00114 M. The slope below the cmc for C_6SS was close to the Nernstian value (63.1 mV at 45.0°C) which suggests that little if any premicellar association is occurring. This slope for C_8SS is greater than that Nernstian; Texas #1 has been observed to behave similarly.[53]

The method of Kale et al.[70] was used to determine the extent of counterion binding; details are given elsewhere.[69] The results for C_6SS and C_8SS are presented in Table III. These results show that α, the extent of counterion dissociation, decreases with increasing surfactant chain length and decreases with increasing surfactant concentration. These trends are in agreement with those seen earlier.

3. Conductimetry

Conductivity measurements were made for di-C_6, di-C_7 and di-C_8 sulfosuccinates at 45.0°C. Plots of specific conductivity vs. concentration for these surfactants are shown in Figures 10, 11 and 12. Di-C_{10} sulfosuccinate was also studied by this technique,[69] but the

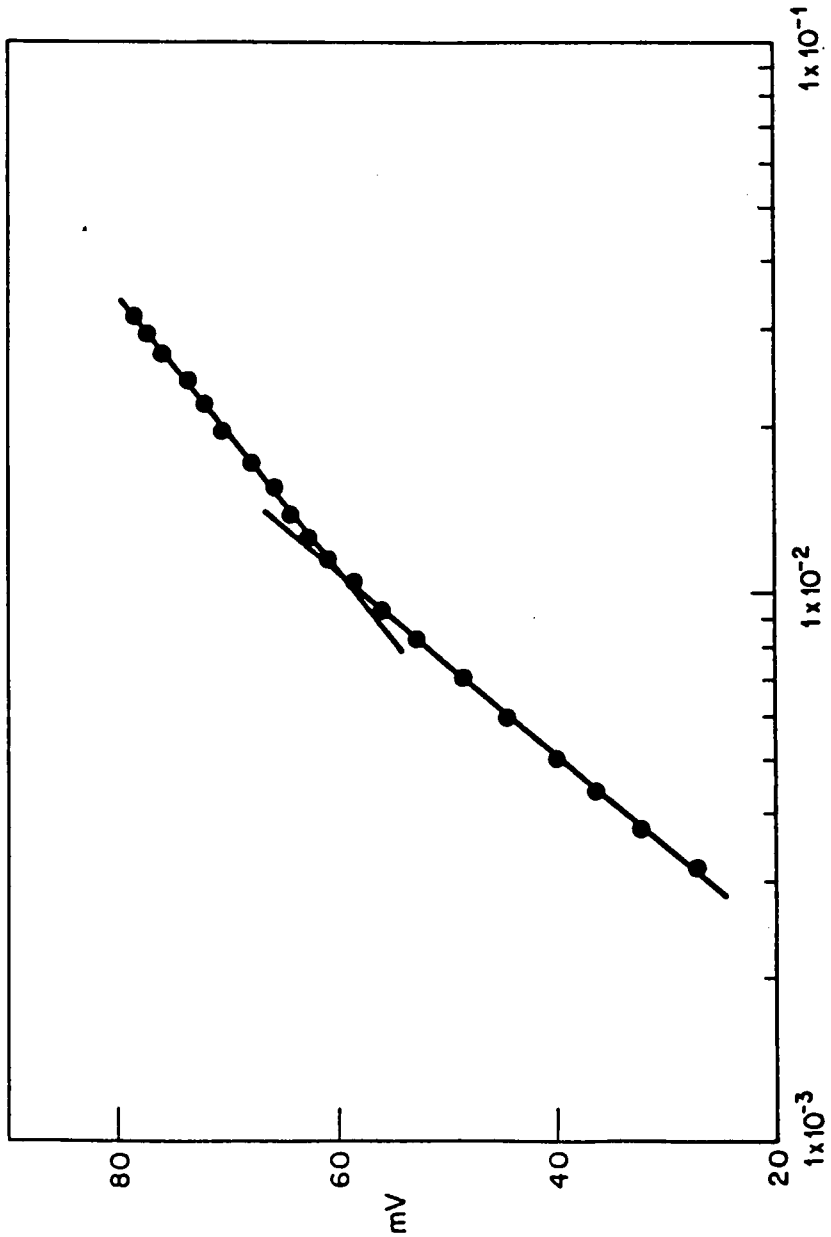

Figure 8. Plot of EMF versus surfactant activity for C_6SS.

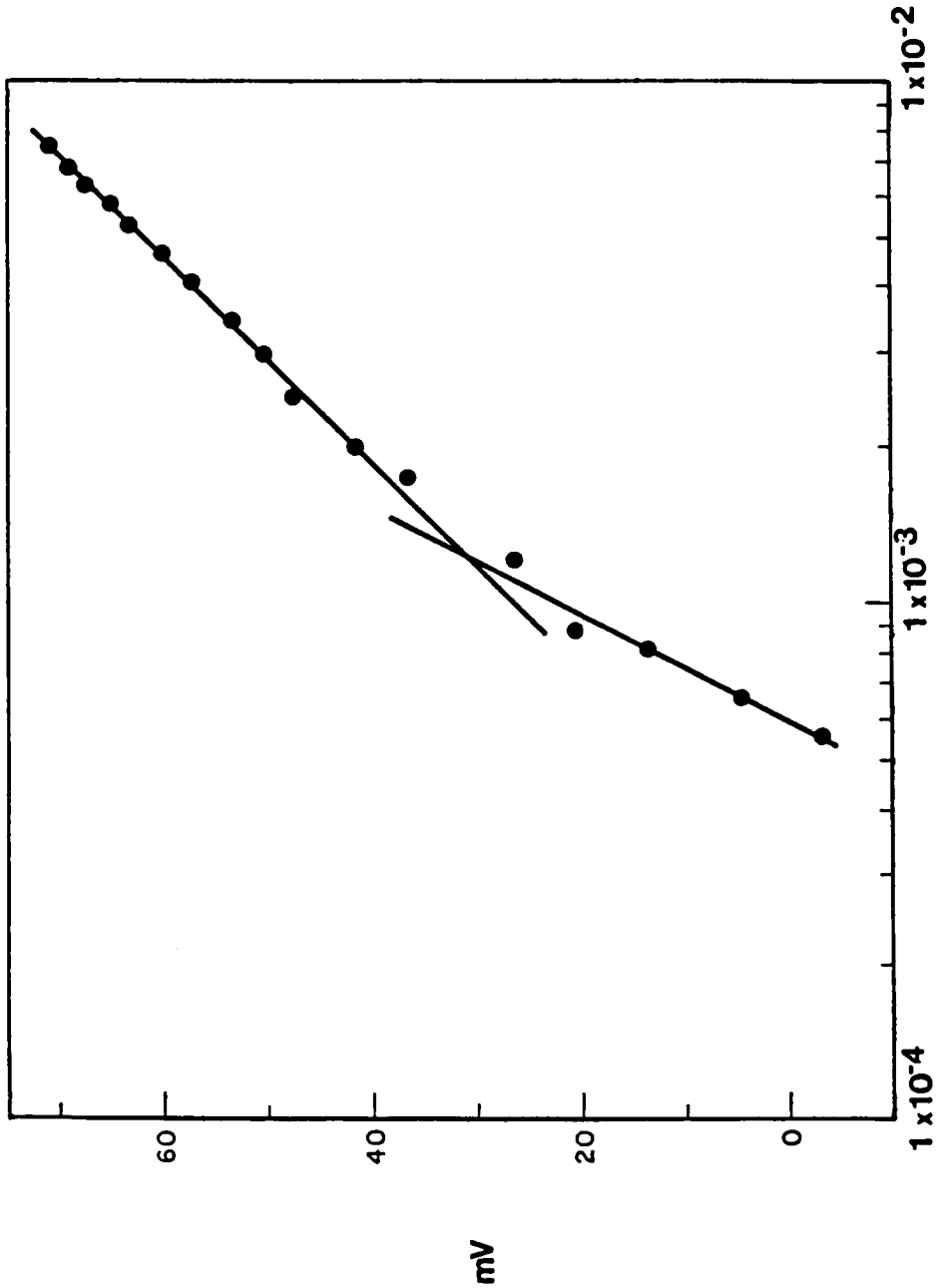

Figure 9. Plot of EMF versus surfactant concentration for C_8SS.

TABLE III

FRACTION OF DISSOCIATED COUNTERIONS IN AQUEOUS C_6 AND C_8 SULFOSUCCINATE SOLUTIONS: EMF

Surfactant	Conc, M	α	Surfactant	Conc, M	α
C_6	0.0131	0.63	C_8	0.00171	0.46
"	0.0145	0.65	"	0.00201	0.44
"	0.0160	0.63	"	0.00254	0.41
"	0.0179	0.62	"	0.00296	0.39
"	0.0202	0.60	"	0.00346	0.37
"	0.0229	0.60	"	0.00405	0.36
"	0.0260	0.61	"	0.00467	0.34
"	0.0291	0.57	"	0.00532	0.33
"	0.0328	0.54	"	0.00577	0.32
"	0.0358	0.53	"	0.00627	0.31
"	0.0388	0.53	"	0.00750	0.29

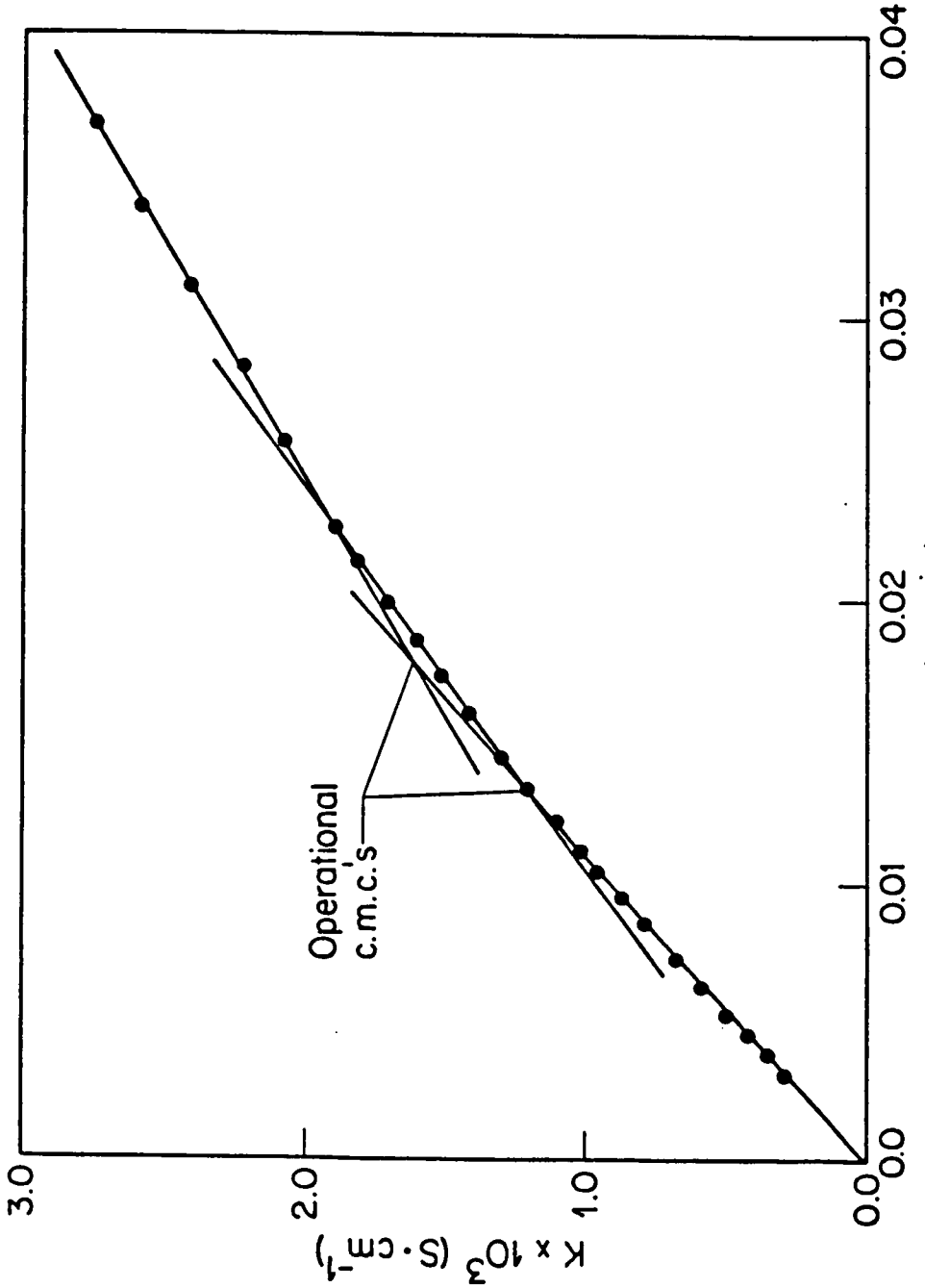

Figure 10. Plot of specific conductivity versus concentration for C_6SS.

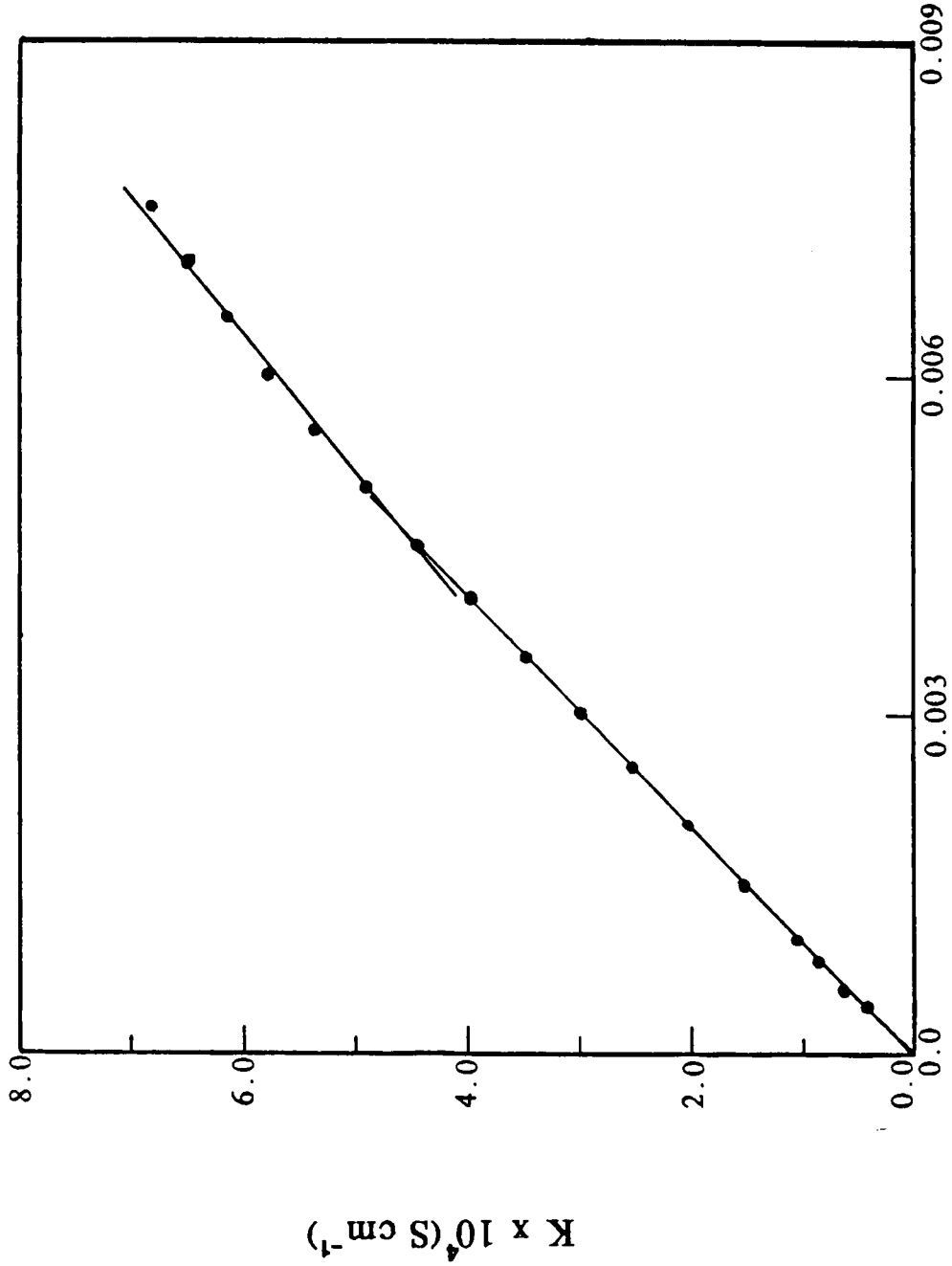

Figure 11. Plot of specific conductivity versus concentration for C_7SS.

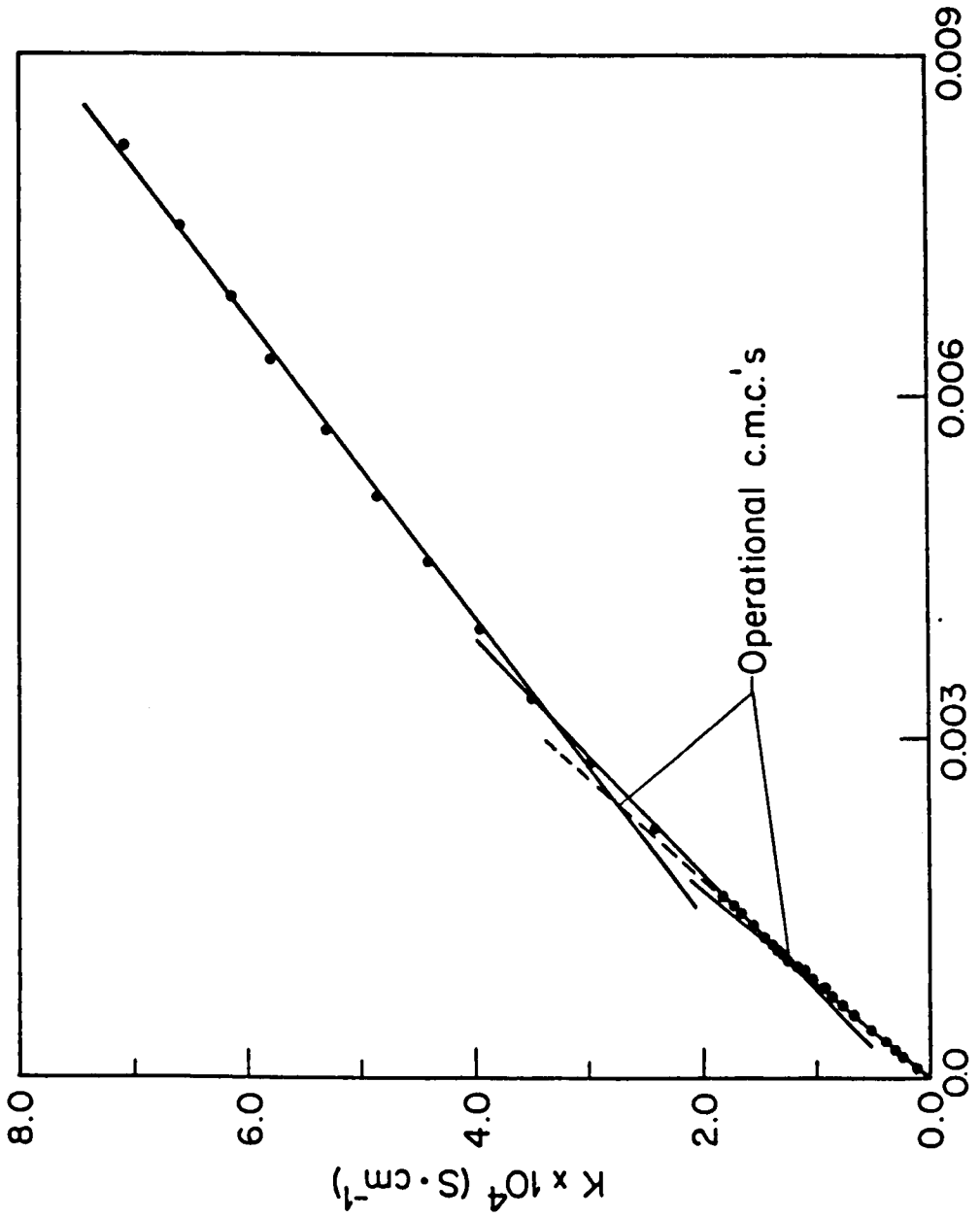

Figure 12. Plot of specific conductivity versus concentration for C_8SS.

results will not be presented since the solutions showed aging effects. Aging effects have been related to low solubilities which makes surfactants extremely sensitive to trace amounts of electrolyte impurities including Na^+, which is leachable from glass. Like Texas #1, di-C_{10} sulfosuccinate has a very limited solubility range; Texas #1 has also shown this type of behavior.[53,54]

Two operational cmc's are found for C_6SS and C_8SS. The lower of these values corresponds to the cmc's determined by EMF measurements. The continuous decrease in α (seen by EMF) as the surfactant concentration is increased is responsible for the multiple breaks. Second breaks have also been found for micelles undergoing a shape change.[9,71] The conductivity of C_7SS was measured up to 0.320 M. Plots of equivalent conductivity vs. concentration showed a gradual curvature in the graphs at high concentration but no second break. The continual change from high to low counterion dissociation resulted in a gentle slope change for the conductivity data of these surfactants. It should be noted at this point that the cmc values determined from the conductivity data are "operational cmc's" and were obtained in order to analyze the SANS data.

To a first approximation, α may be found from the ratio of the slopes above and below the cmc. However, in determining α in this manner, one must assume that the equivalent conductivity of the surfactant ions is equivalent to that of the ionized surfactant in the micelles. Here, Evan's equation[61] was used to obtain values of α from the conductivity data:

$$(1000)S_2 = \frac{(\bar{n} - m)^2}{\bar{n}^{4/3}} (1000S_1 - \Lambda_{Na^+}) + \frac{\bar{n} - m}{\bar{n}} \Lambda_{Na^+} \qquad (29)$$

S_1 and S_2 are the slopes below and above the cmc, $\bar{n}$ is the average micellar aggregation number, m is the average number of associated counterions and Λ_{Na^+} is the equivalent conductivity of the sodium ion. At 45°C this value is 73.7. The degree of counterion dissociation, α, is equivalent to $(1 - m/\bar{n})$. The aggregation numbers used to evaluate α were obtained from the analysis of SANS data for samples having concentrations near the cmc (see Chapter IV). Values for α are tabulated in Table IV along with the aggregation numbers used. These values are in qualitative agreement with those obtained from the EMF measurements. The cmc determined for C_8SS by Miller and Dixon,[64] 6.4×10^{-4} M, was from a shallow maximum present in the plot of the equivalent conductivity *vs.* $(\text{conc.})^{1/2}$. The same slight inflection in the 45°C data appears, but the main break occurs at 0.0012 M.

C. Study of Surfactant Behavior by NMR

Micellar systems contain a large number of elements having isotopes with magnetic nuclei that can be studied by NMR; typically, it is possible to determine more than one NMR parameter for the nuclei under investigation. ^1H and ^{13}C NMR studies of the alkyl tails constitute the majority of the NMR investigations that have been performed on surfactant systems. Many structural features of micelles have been determined by NMR; for example, NMR studies have investigated the trans gauche conformational equilibrium of micellar alkyl tails,[72] the extent of water

TABLE IV

CMC'S AND FRACTION OF DISSOCIATED COUNTERIONS FOR C_6SS, C_7SS AND C_8SS: CONDUCTIMETRY

Surfactant	CMC (mol/L)	$\bar{n}$	α
C_6SS	0.0135	25	0.523
	0.0178		0.460
C_7SS	0.0043	30	0.450
C_8SS	0.00112	34	0.402
	0.00256		0.341

penetration,[22,29] the sphere-to-rod transition[73,74] and the presence of premicellar aggregates.[75]

Nuclear quadrupole relaxation and chemical shift measurements have been used to assess the effect of micellization upon the counterion; the study of sodium counterions is of particular interest. ^{23}Na NMR has demonstrated that both quadrupole relaxation and chemical shift measurements are sensitive probes of changes in the surfactant headgroup, but are relatively insensitive to changes in the alkyl tail length.[76,77] Whereas simple electrostatic interactions explained the observed trends in counterion binding for the octylsulfate micelles, hydrogen bonding effects were also important for the octanoate micelles; the shielding of the sodium ion at the micelle surface was found to follow the sequence $-OSO_3^-$ > aryl-SO_3^- > alkyl-SO_3^- > $-CO_2^-$.

Micelles are dynamic entities in which monomers are continuously entering and leaving the micelles. The observed NMR parameter is thus actually a weight average of monomer and micellar values due to this rapid exchange between monomers and micelles.

Many authors have adopted the phase separation model in order to evaluate NMR data for micellar solutions. This model assumes that only two types of counterions exist: free counterions, denoted by the subscript f, which are not associated with the micelle and bound counterions denoted by the subscript m. The observed NMR parameter can then be written in terms of the two counterion populations:

$$B_{obs} = (C_m/C_t) \cdot B_m + (C_t - C_m)/C_t \cdot B_f \qquad (30)$$

where C_m is the concentration of counterions bound to the micelle, C_t is the total amphiphile concentration, and B_f and B_m are the intrinsic NMR parameters of the two sites. The parameter, β, is assumed to be independent of concentration. Then, $C_m = (C_t - C_c)$ where C_c = cmc. Equation 30 can then be rewritten as

$$B_{obs} = B_f + \beta(B_m - B_f) - \beta cmc/Ct(B_m - B_f) \qquad (31)$$

Equation 31 applies to systems where the amphiphile concentration is greater than the cmc. A plot of the observed NMR parameter vs. inverse total surfactant concentration should yield two straight lines that intersect at the cmc.

Kilpatrick and Miller[78] applied a more realistic model to their ^{23}Na chemical shift data for SDS, AOT and Texas #1. The limitations of the pseudo-phase separation model were circumvented through the use of a mass-action model which allowed for the existence of micellar aggregates of all sizes and of a β that varies with aggregate size. Kilpatrick and Miller[78] evaluated the association of monomers as being anti- or weakly cooperative except in the region where micellization occurs; the association of monomers to form micelles was evaluated as being highly cooperative. The extent of counterion binding was treated either by assuming a constant charge density at the aggregated surface or by assuming a step function in which increased as aggregate size increased. Based on a determination of equilibrium constants, AOT and SDS displayed highly cooperative association; however, the Texas #1 data was not consistent

with micelle formation in that noncooperative association was found except for dimerization.

D. ^{23}Na NMR Chemical Shift Study of C_6SS and C_7SS

The formalism of the model of Kilpatrick and Miller[78] is useful for assessing cooperativity of aggregation and therefore, was applied in the interpretation of ^{23}Na chemical shift data. The ^{23}Na chemical shifts of C_6SS and C_7SS were determined at 45°C; Figures 13 and 14 show the data plotted as a function of inverse total surfactant concentration. The linewidth data are presented in Figures 15 and 16. The behavior seen in the figures is typical for surfactants that display strong cooperativity of association, i.e., micellization. In fact, the same three features are seen in the plots for C_6SS and C_7SS as Kilpatrick and Miller[78] saw for SDS and AOT: (1) below the cmc, the measured NMR parameters were independent of concentration and approached the values found for dilute NaCl solutions; (2) at intermediate concentrations, the NMR parameters were seen to change monotonically with inverse concentration; and (3) at high concentrations near the solubility limit, the NMR parameters change quickly with increasing concentration.

The mass action model of Kilpatrick and Miller[78] will be presented in detail. This model views the association processes as involving step-wise addition of monomer, with each step characterized by an equilibrium constant:

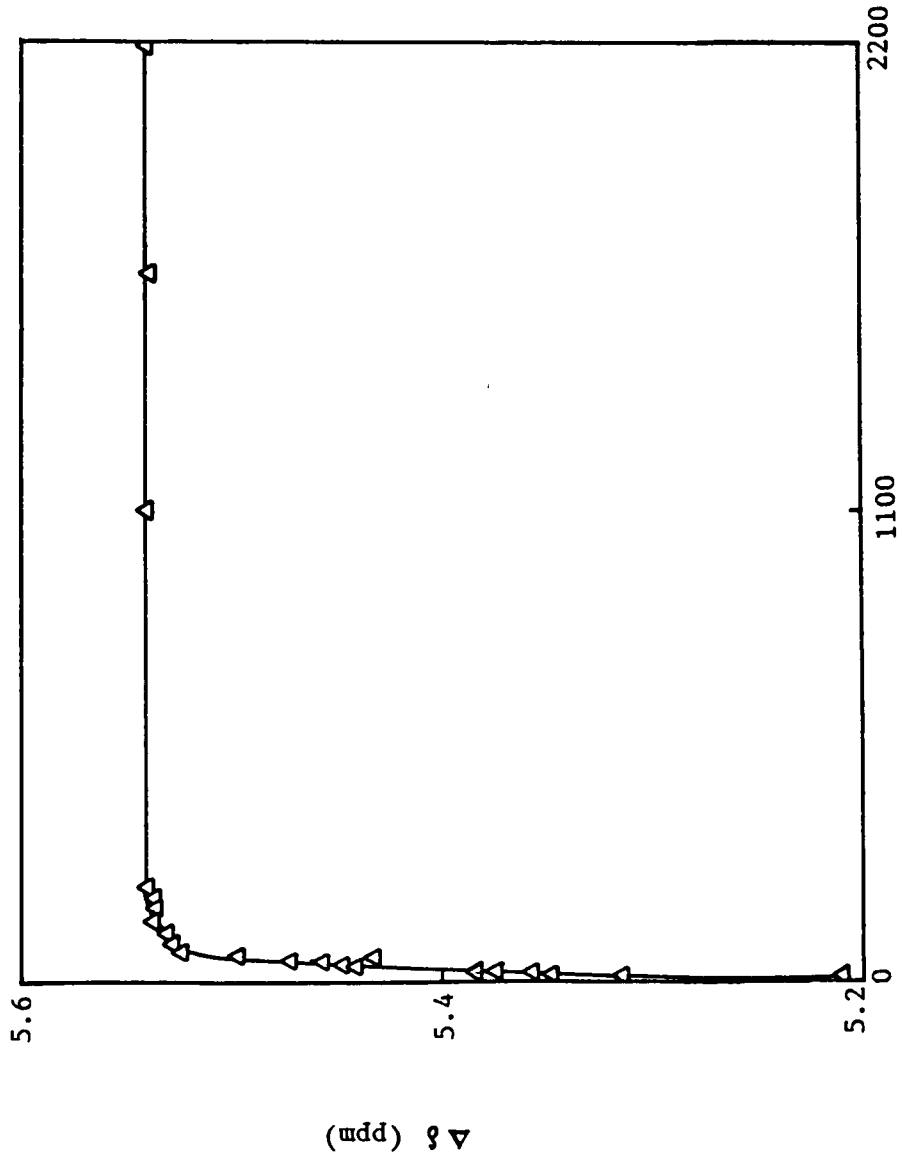

Figure 13. Concentration dependence of ^{23}Na chemical shifts: C_6SS.

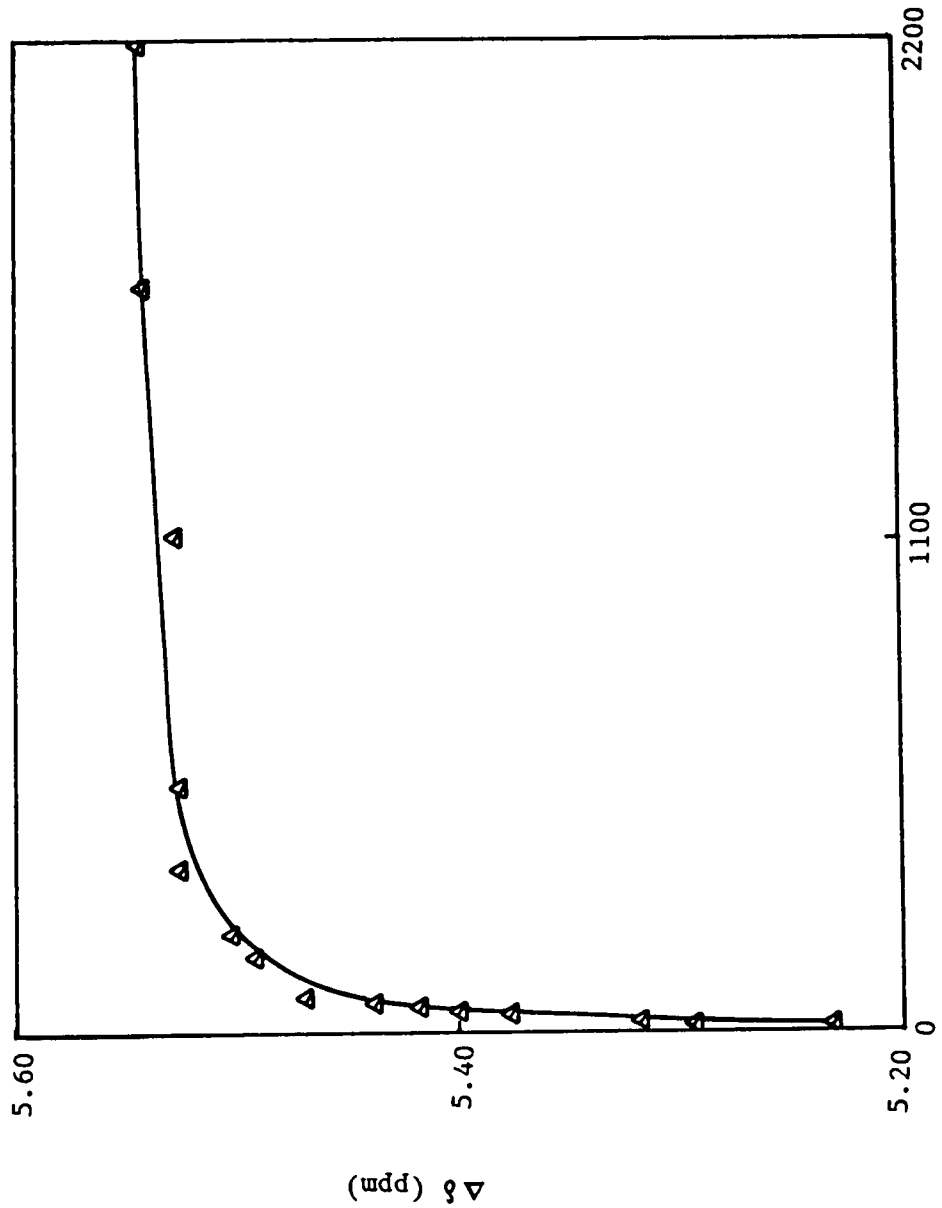

Figure 14. Concentration dependence of ^{23}Na chemical shifts: C_7SS.

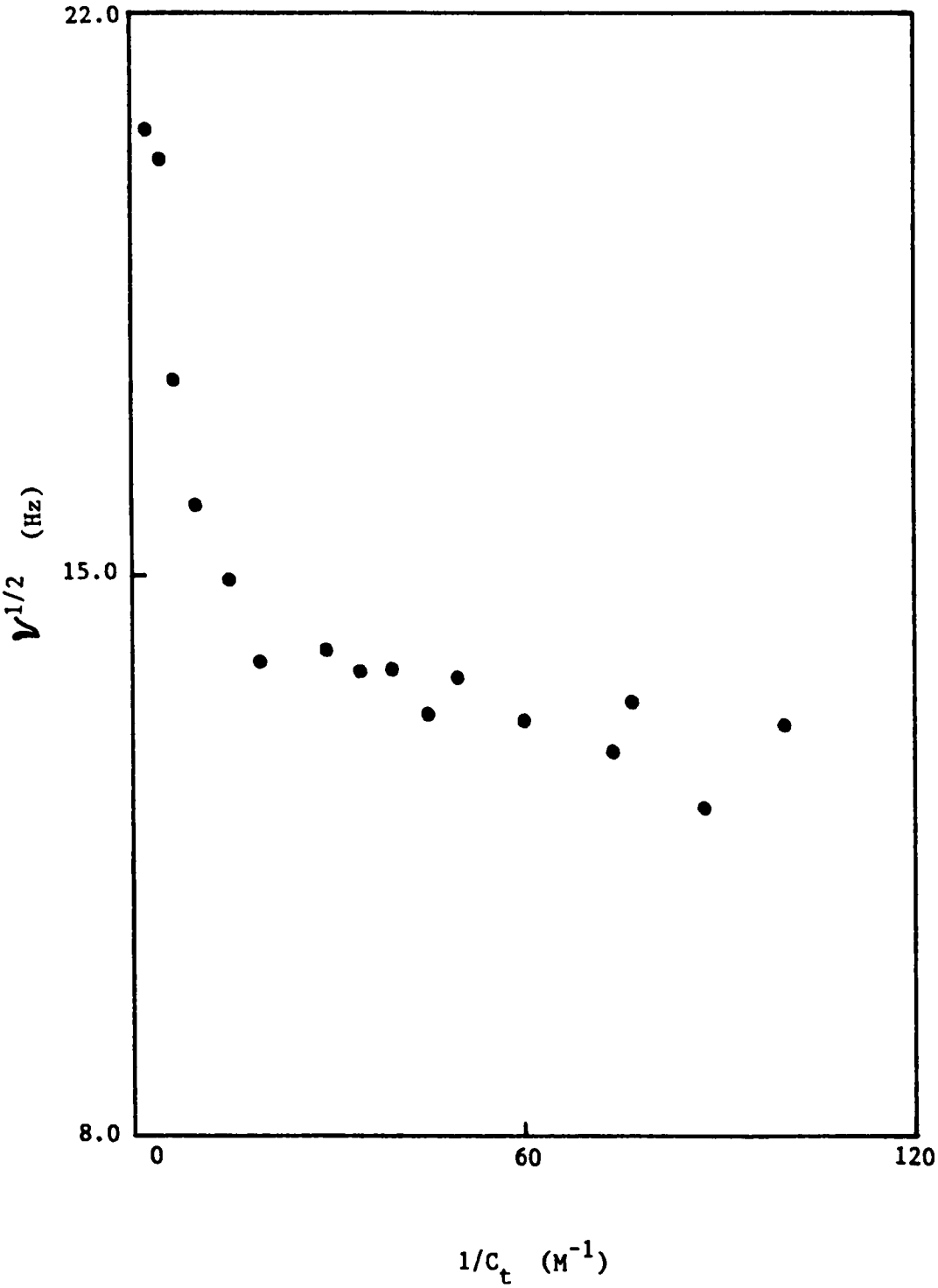

Figure 15. Concentration dependence of ^{23}Na linewidths: C_6SS.

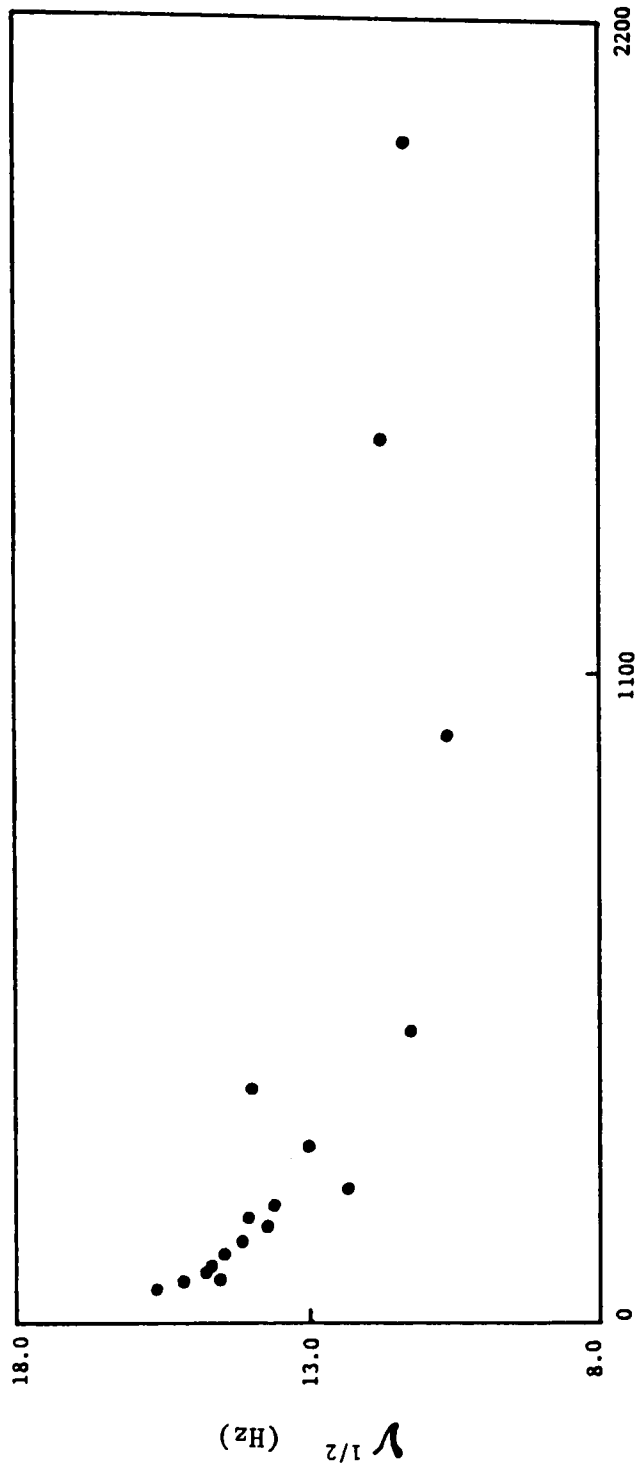

Figure 16. Concentration dependence of ^{23}Na linewidths: C_7SS.

$$S_1 + S_1 \rightleftharpoons S_2 \qquad K_2 = C_2/C_1^2 \tag{32a}$$

$$\vdots \qquad \vdots$$

$$S_1 + S_2 \rightleftharpoons S_3 \qquad K_3 = C_3/K_2 \cdot C_1^3 \tag{32b}$$

$$\vdots \qquad \vdots$$

$$S_1 + S_{n-1} \rightleftharpoons S_n \qquad K_n = C_n/K_{n-1} \ldots K_2 C_1^n \tag{32c}$$

For micellization, this model predicts a peak in the aggregate size distribution; i.e., a maximum value for K(n) exists. The K(n) distribution was modelled as a Gaussian distribution:

$$K(n) = K_o \exp(-a(n-n_o)^2) \tag{33}$$

K_o has no effect on the cooperativity of micellization: it affects only the concentration range over which aggregation takes place. The parameter a controls the degree of cooperativity and variance of aggregate size distribution, whereas n_o determines the aggregation number for the most numerous micelle.

From the K(n) distribution and the total surfactant concentration, the monomer concentration can be calculated from the following n^{th} order polynomial using the Newton iteration method

$$c_t = c_1 + \sum_{i=2}^{N} \pi_{j=2}^{i} i K_j C_1^i \tag{34}$$

The range for N was limited to values of N for which nonnegligible amounts of aggregates existed. Once c_1 was determined, this value was

then used as the initial guess for the c_1 of the next higher concentration.

From the K(n) distribution and β, which was modelled as a constant surface charge density having the form = $1 - a/n^3$, the chemical shifts of the free and micelle-bound counterions were found by linear extrapolation of the experimental NMR data at high and low concentrations. The chemical shifts were computed by finding the fraction of bound and unbound counterions and then assuming that the observed chemical shift is a number-weighted average of the two populations:

$$\delta_{obs} = \frac{c_1 + \sum_{i=2}^{N} i(1-\beta(i))c_i}{c_t}\delta_f + \frac{\sum_{i=2}^{N} i\beta(i)c_i}{c_t}\delta_b \qquad (35)$$

Therefore, to calculate the chemical shifts for the C_6SS and C_7SS data, values for n_o, δ_b and δ_f are needed. By extrapolation of the data at low concentration (to c = 0), a value of 5.542 ppm for δ_f was found. The product $\beta \cdot \delta_b$ was obtained from extrapolation of the data at high concentration; using a limiting value of 0.78 for β (from SANS of 0.20 M C_7SS); $\delta_b = 4.755$. Therefore, $\delta_f - \delta_b = 0.785$ ppm which is in excellent agreement with $\Delta\delta$ of 0.78 found for AOT.[78]

Kilpatrick et al.[78] selected a value of 50 for n_o for SDS and 35 for AOT; in the sulfosuccinate modelling, n_o was 40 for C_7SS and 30 for C_6SS. The next step was to find a value for $\underline{a}$ such that the curvature at the cmc for the experimental curve was matched by the calculated curve. Then, K_o was varied until the calculated curve agreed with the

experimental curve within the error limits. The calculated curve is represented by a smooth line; the agreement between the calculated and experimental curves is seen to be quite good. The value of K_o, n_o and a used in the analysis are shown in Table V.

The chemical shift data for both C_6SS and C_7SS are consistent with cooperative association. The K_o values obtained for these surfactants suggest that micellization occurs over a fairly narrow distribution of micelle sizes which are peaked at a substantial n. A smaller value of K_o was expected for C_6SS; however, a K_o of 250 *vs.* 1000 for C_7SS is a little surprising. This low value reflects the higher cmc of C_6SS when compared to the cmc of C_7SS.

TABLE V

PARAMETERS OBTAINED FROM ^{23}Na NMR FITS

Surfactant	K_o	a	n_o
C_6SS	250	8.0×10^{-4}	30
C_7SS	1000	1.0×10^{-4}	40

CHAPTER III

SMALL-ANGLE NEUTRON SCATTERING

The popularity of small-angle neutron scattering (SANS) as a technique to elucidate micellar structure has grown tremendously over the past several years. Several excellent review articles on SANS are available.[79-84] Since SANS is a relatively new technique, this chapter will develop the background necessary to understand the sections of this dissertation dealing with SANS. Advantages over other scattering techniques will be presented, as well as the variety of experiments that are possible.

A. Background

1. Small-Angle Neutron Scattering Theory

Two forms of interaction are possible between neutrons and matter: a nuclear interaction that arises from interaction with the nuclei of the sample and a magnetic interaction resulting from interaction between the magnetic moment of the neutron and that of any unpaired electrons present in the sample. The focus in this dissertation will be solely on the first type of interaction. The neutron scattering to be considered is quasielastic, i.e., the energy transferred will be small in comparison to the incident energy.

The incident neutron wave is best described by the wavefunction

$$\psi_i = \exp(i\underline{k}_i \cdot \underline{r}) \qquad (36)$$

The initial wave vector is represented by $\underline{k}_i$ where $/k_i/ = 2\pi/\lambda$. The wavelength of the incident neutrons is represented by λ. A spherical wavefunction is used to describe the scattered wave

$$\psi_f = (\frac{b}{r})\exp(i\underline{k}_f \cdot \underline{r}) \tag{37}$$

where b, termed the scattering length, expresses the amplitude of the scattered wave and $\underline{k}_f$ is the final wavevector. One can denote the momentum transfer in the scattering experiment as $\underline{Q}$ where

$$\underline{Q} = \underline{k}_i - \underline{k}_f \tag{38a}$$

and

$$|\underline{Q}| = Q = (4\pi/\lambda)\sin\theta \tag{38b}$$

in which scattering occurs through an angle 2θ. Figure 17 illustrates $\underline{Q}$ for the scattering process.

The cross-section of the scattering process, or the ratio of the scattered flux of neutrons compared to the incident flux, includes both coherent and incoherent parts. Thus, $\sigma = \sigma_{inc} + \sigma_{coh}$. The interferences resulting from σ_{inc} leads to isotropic scattering which produces the background contribution. The distribution of the atoms in the sample defines the scattering associated with the coherent cross-section. Any information concerning intraparticle structure and interparticle correlations is present in σ_{coh}.

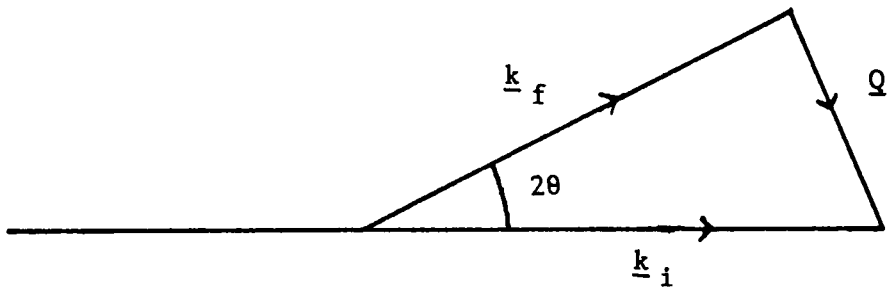

Figure 17. Definition of $\underline{Q}$.

The scattering cross-section is associated with b by $\sigma = 4\pi|b|^2$. Values of b, σ_{inc} and the absorption cross-section, σ_{abs}, have been tabulated.[83] Representative values are shown in Table VI where one sees the large difference in b between ^1H and ^2H. This isotopic difference allows easy overall visualization for normal micelles (which are ^1H-rich) in aqueous solutions by using D_2O; also, experiments investigating specific regions of a micelle are easily designed. This aspect of neutron scattering will be looked at in detail in a later section.

The partial differential coherent cross-section may be defined as:

$$\left(\frac{d\sigma}{d\Omega}\right)_{coh} = \left\langle \sum_{i,j} b_i b_j \exp[i\underline{Q} \cdot (\underline{r}_i - \underline{r}_j)] \right\rangle \qquad (39)$$

where b represents b_{coh}. The summation is over all relative positions of atoms with scattering lengths b_i, b_j and with positions $\underline{r}_i$, $\underline{r}_j$. The atomic positions are relative to an arbitrary origin in the sample. The above equation may be rewritten as

$$\left(\frac{d\sigma}{d\Omega}\right)_{coh} = \left\langle \sum_{p,q} \sum_{i(p)}^{n_p} \sum_{j(q)}^{n_q} b_i b_j \exp(i\underline{Q} \cdot \underline{r}_{i,j}) \right\rangle \qquad (40)$$

The relative separation of the two atoms, $\underline{R}_j - \underline{R}_i$, is given by $\underline{r}_{i,j}$. Figure 18 shows that the atoms i and j may be located within the same particle or in two different particles (in which the centers of mass are located at p and q, respectively). Equation 40 is the general scattering equation; it can be used for light scattering (LS) and

TABLE VI

SCATTERING LENGTHS AND INCOHERENT AND ABSORPTION CROSS SECTIONS OF SOME ISOTOPES AND ELEMENTS[a]

Element or Isotope	Scattering Length (b_{coh})	Incoherent Cross Section (σ_{inc})	Absorption Cross Section (σ_{abs})
^{1}H	-0.3740×10^{-12} cm	79.7 barn	0.33 barn
^{2}H	0.6674×10^{-12}	2.0	0.00046
C	0.665×10^{-12}	<0.018	755.
N	0.936×10^{-12}	0.46	0.0033
O	0.5803×10^{-12}	<0.015	<0.0002
Na	0.363×10^{-12}	1.75	0.505
S	0.2847×10^{-12}	0.012	0.52

[a]Values taken from Kostorz.[83]

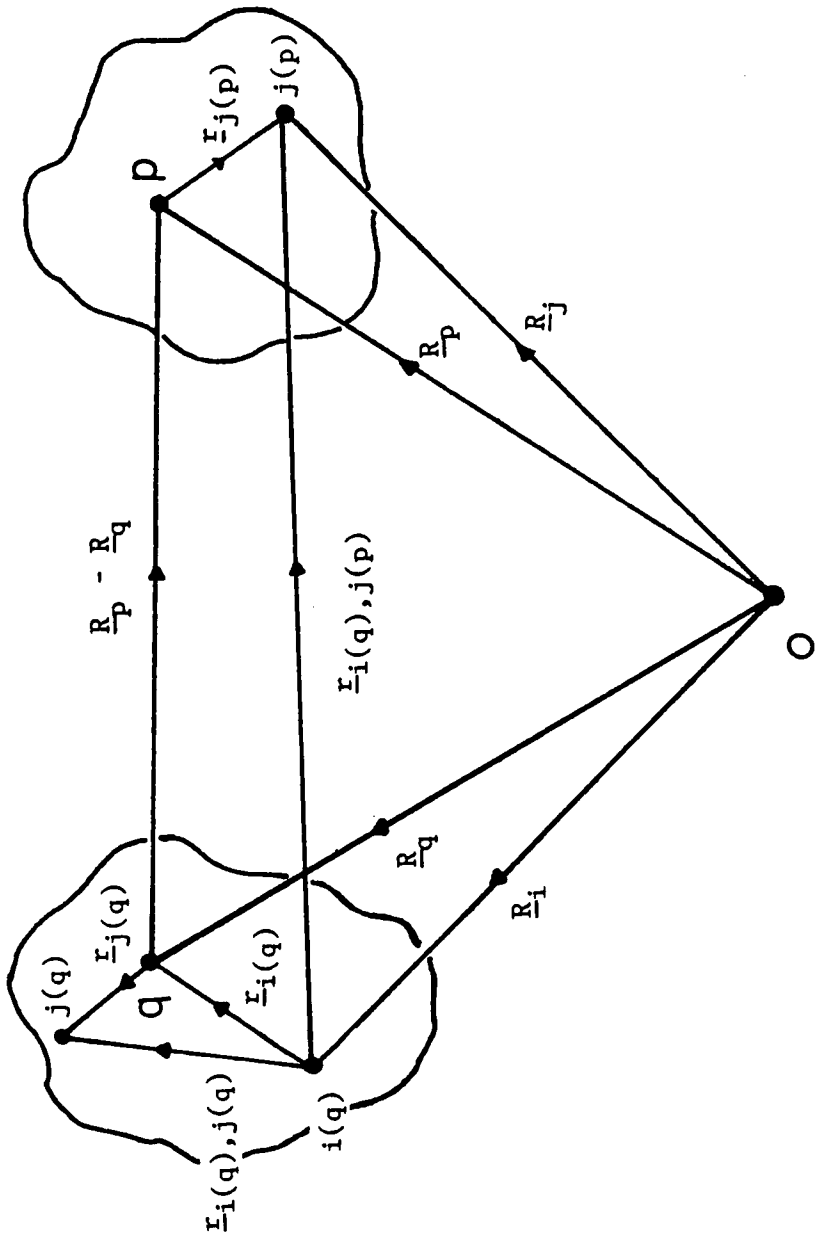

Figure 18. Intra- and interparticle interactions.

small-angle x-ray scattering (SAXS) when the appropriate substitution for b is made.

Separation of equation 40 into intraparticle (p=q) and interparticle (p≠q) terms yields

$$\left(\frac{d\sigma}{d\Omega}\right)_{coh} = \left\langle \sum_{i(p)}^{n_p} \sum_{j(q)}^{n_q} b_i b_j \exp(i\underline{Q} \cdot (\underline{r}_j - \underline{r}_i)) \right\rangle + \left\langle \sum_{p\neq q=1}^{N} \exp[i\underline{Q} \cdot (\underline{R}_p - \underline{R}_q)] \cdot \sum_{i(p)}^{n_p} \sum_{j(q)}^{n_q} b_i b_j \exp[i\underline{Q} \cdot (\underline{r}_j - \underline{r}_i)] \right\rangle \quad (41)$$

N is the number of particles, $\underline{R}_p - \underline{R}_q$ represents the center-to-center distance for a pair of particles p,q and $\underline{r}_{i(q),j(p)}$ is equivalent to $\underline{R}_p - \underline{R}_q + \underline{r}_{j(p)} - \underline{r}_{i(q)}$. If the single-particle form factor, $F(\underline{Q})$, is defined in the following manner,

$$F(\underline{Q}) = \sum_{j(q)} b_j \exp(i\underline{Q} \cdot \underline{r}_j) \quad (42)$$

(where the sum is over all the atoms present in the sample), then N times the square of $F(\underline{Q})$ yields the intraparticle term in equation 41.

Currently no exact solution for the second term in equation 42 exists for any type of interparticle interaction. Nonetheless, the second term may be solved if the assumption that little correlation exists between particle size and orientation and interparticle distance

holds.[84-86] Making this assumption, the second term may be averaged separately to give

$$\frac{d\sigma}{d\Omega} = N \langle |F(\underline{Q})|^2 \rangle + \langle \sum_{p \neq q} \exp[i\underline{Q} \cdot (\underline{R}_p - \underline{R}_q)] \rangle$$

$$\cdot \langle \sum_{i(p)}^{n_p} \sum_{j(q)}^{n_q} b_i b_j \exp[i\underline{Q} \cdot (\underline{r}_j - \underline{r}_i)] \rangle \qquad (43)$$

In the case of ionic micelles interacting through a screened Coulombic repulsive potential, contact between neighboring particles is not probable and the above assumption works well.

Now the average structure factor, $S(\underline{Q})$, may be defined as

$$S(\underline{Q}) = 1 + N^{-1} \langle \sum_{p \neq q} \exp[i\underline{Q} \cdot (\underline{R}_p - \underline{R}_q)] \rangle \qquad (44)$$

where the averages are over all positions and orientations. Because S(Q) describes the interactions between the particles, for dilute solutions the averaged term equals zero and S(Q) is one (i.e., interferences of neutrons scattered by nuclei located on different particles are averaged out by the ability of the particles to take random positions in the solution).

If $\underline{r}_{i(p)}$ and $\underline{r}_{j(q)}$ are statistically independent, then equation 43 can be rewritten

$$\left(\frac{d\sigma}{d\Omega}\right)_{coh} = N \langle |F(\underline{Q})|^2 \rangle_Q + N [S(\underline{Q}) - 1] \cdot \langle \sum_{j(q)} b_j \exp(i\underline{Q} \cdot \underline{r}) \rangle_Q^2 \qquad (45a)$$

which can, in turn, be rewritten as

$$\left(\frac{d\sigma}{d\Omega}\right)_{coh} = N \langle|F(\underline{Q})|^2\rangle + N\,[S(\underline{Q}) - 1] \cdot |\langle F(\underline{Q})\rangle|^2_Q \qquad (45b)$$

$$= N\,[\langle|F(\underline{Q})|^2\rangle_Q - |\langle F(\underline{Q})\rangle|^2_Q] + N \cdot S(\underline{Q}) \cdot |\langle F(\underline{Q})\rangle|^2_Q \qquad (45c)$$

where $\langle F(\underline{Q})\rangle$ is the Fourier transform of the scattering length's radial distribution within one particle; $\langle|F(\underline{Q})|^2\rangle$ corresponds to the Fourier transform of the average distribution of distances P(r) within one particle; S(Q) is the Fourier transform of the radial distribution function, g(r), for the centers of mass of the particles.

2. Comparison to Other Techniques

Earlier it was noted that equation 40 can be applied to LS and SAXS if an appropriate substitution for b is made. For light scattering b is related to the changes in polarizabilities or refractive indices of the particles with respect to the medium, and for small-angle x-ray scattering b is related to the atomic number and therefore to the number of electrons per atom. The characteristic size in real space, R, can be shown to be reciprocally related to the characteristic width of the intensity distribution in Q space;[87] thus, for aggregates of size R, the Q range should be such that it spans an order of magnitude on both sides of the value $Q_o = 2\pi/R$.[79] For micelles with R = 20 Å, x-rays or neutrons having wavelengths = 1 Å to 20 Å should be used whereas LS, with wavelengths in the range 4000 Å to 8000 Å, is more suitable for the study of larger particles.

Why, then, use SANS instead of SAXS, which is of reasonable availability and cost? Since the scattering length is SAXS is directly related to the number of electrons per atom, contrast between hydrogen-rich micelles and water is very small. The addition of a probe molecule containing atoms of heavy elements will reduce the counting time; however, the potential for perturbation of the micellar structure is greatly increased due to the presence of such a large molecule. For SANS contrast is made with the smallest perturbation possible, the substitution of ^{2}H for ^{1}H.

3. Single-Particle Form Factors

The form factor may be rewritten for particles in solution as shown below:

$$F_p(\underline{Q}) = \int [\rho_p(\underline{r}) - \rho_{solv}]\exp[i\underline{Q} \cdot \underline{r}]d^3r \qquad (46)$$

The scattering length density ($\rho = \Sigma b_i/V$) in excess of the scattering length density of the solvent (ρ_{solv}) is the contrast term of interest. Form factors are available for different particle shapes.[88] The simplest shape is a homogeneous sphere whose form factor was derived by Rayleigh;[89] the expression is

$$F_p(\underline{Q}) = \int_o^R \frac{\sin Qr}{Qr} 4\pi r^2 dr \qquad (47a)$$

$$= \Delta\rho \cdot \frac{4}{3}\pi R^3 \cdot \phi(QR) \qquad (47b)$$

where $\Delta\rho = \bar{\rho} - \rho_{solv}$. The mean scattering length density of the volume-excluded particle is $\bar{\rho}$ and $(4\pi/3)R^3$ also corresponds to the volume-excluded particle. $\phi(x)$ is defined as $3(\sin x - x\cos x)/x^3$. For monodisperse spheres equation 45c can be simplified since $\langle|F(\underline{Q})|^2\rangle = |\langle F(\underline{Q})\rangle|^2$. The intraparticle term is usually expressed as $P(Q) = \langle|F(\underline{Q})|^2\rangle$. Equation 45c now has the following form:

$$\left(\frac{d\sigma}{d\Omega}\right)_{coh} = I(\underline{Q}) = N_p \cdot S(\underline{Q}) \cdot P(\underline{Q}) \tag{48}$$

where N_p denotes the number particle density.

Micelles can be modeled as consisting of a set of n centrosymmetric shells in which each shell has its own characteristic scattering length density (see Figure 19). For monodisperse spheres, the form factor may be rewritten in terms of the centrosymmetric scattering length density inhomogenieties:

$$F_p(\underline{Q}) = (\rho_1 - \rho_2)V_1\phi(QR_1) + (\rho_2 - \rho_3)V_2\phi(QR) \ldots + (\rho_N - \rho_{solv})V_N\phi(QR_N) \tag{49}$$

The focus of this dissertation will be upon particles which consist of a core-plus-shell; for this model equation 49 rearranges to

$$F_p(\underline{Q}) = (\rho_1 - \rho_{solv})V_1\phi(QR_1) + (\rho_2 - \rho_{solv})[V_2 \cdot \phi(QR_2) - V_1 \cdot \phi(QR_1)] \tag{50}$$

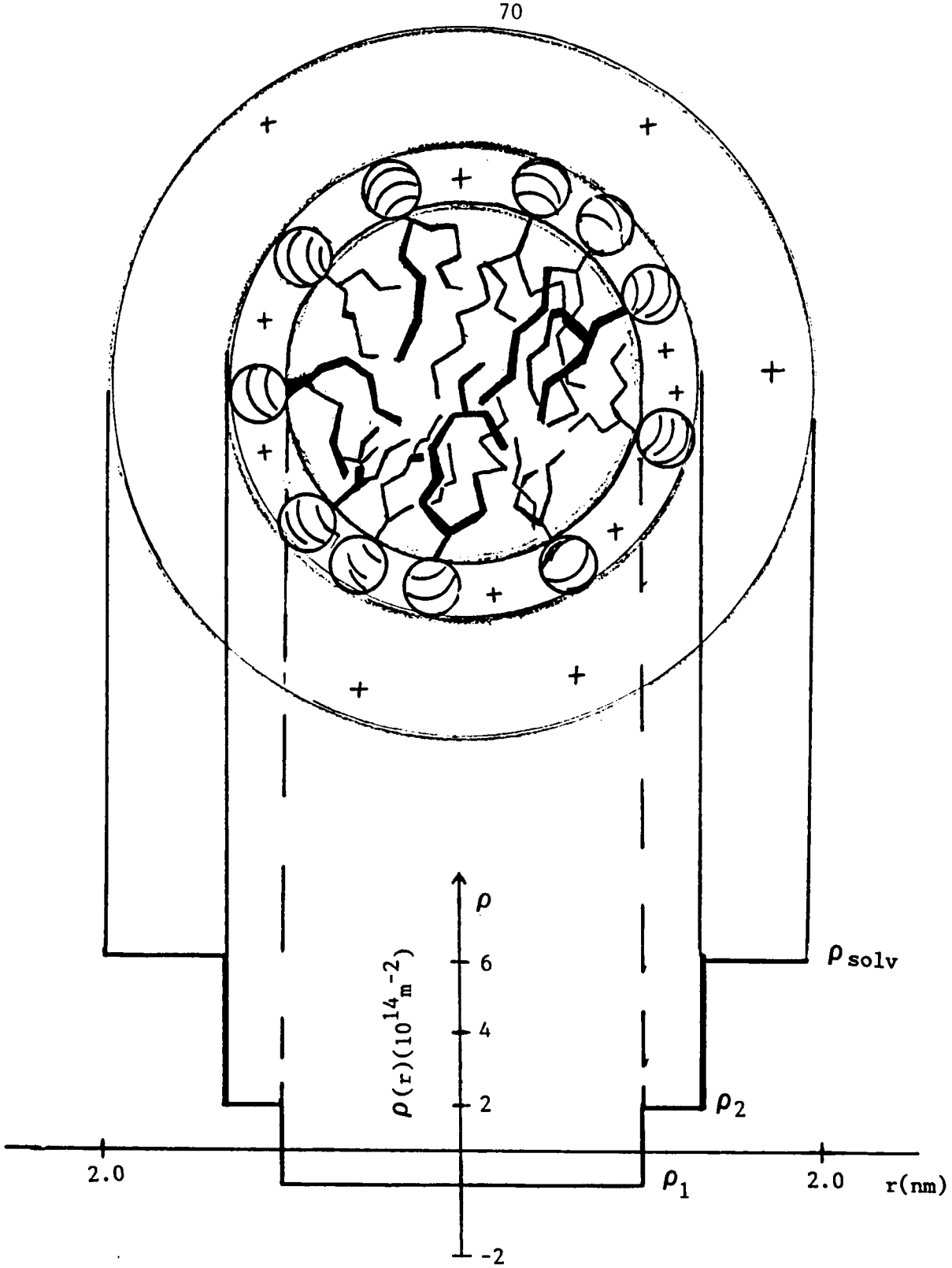

Figure 19. Scattering length density inhomogenieties for a core plus shell model.

where $V_2 - V_1$ is the volume of the surrounding shell.

4. Form Factors for Polydisperse Spheres and Ellipsoids

For the cases of polydisperse spheres or ellipsoids, the inequality $\langle|F(\underline{Q})|^2\rangle \neq |\langle F(\underline{Q})\rangle|^2$ holds. In the case of polydisperse spheres, it is necessary to average over the distribution of particle sizes. The following equations give the form of the size-averaged functions.

$$\langle|F(\underline{Q})|^2\rangle = \int_0^\infty |F_p(Q,R)|^2 f(R)dR \qquad (51a)$$

$$|\langle F(\underline{Q})\rangle|^2 = \left| \int_0^\infty F_p(Q,R)f(R)dR \right|^2 \qquad (51b)$$

The above integrals have been solved using a number of distributions; the Shulz distribution is one of the more frequently used:[84,86]

$$f(R) = \frac{Z+1}{\bar{R}}^{Z+1} R^Z \exp[-\frac{Z+1}{\bar{R}} R]/\Gamma(Z+1),\ Z > -1 \qquad (52)$$

Here R is the number-average particle radius, and Z denotes the width parameter of the distribution.

For the case of ellipsoids, the form factors must now include averages over all the possible orientations of the ellipsoid with respect to $\underline{Q}$; the form factors are calculated by[84,86]

$$\langle|F(Q)|^2\rangle = \int_0^1 |F(Q,a,ECC,t,\mu)|^2 d\mu \qquad (53a)$$

$$|\langle F(Q)\rangle|^2 = \left| \int_0^1 F(Q,a,ECC,t,\mu) d\mu \right|^2 \qquad (53b)$$

and the function F is

$$F(Q,a,ECC,a',ECC',t,\mu) = V_1 \cdot (\rho_1 - \rho_2) \cdot [3j_1(u')/u'] + V_2 \cdot (\rho_2 - \rho_{solv}) \cdot [3j_1(u)/u] \qquad (54)$$

where ECC is the axial ratio of the ellipsoid and t is the thickness of the shell. Then the overall ellipsoid (of volume V_2) has axes a, a and ECC·a (semimajor for prolate, semiminor for oblate) and the ellipsoid core (of volume V_1) has axes a', a' and ECC a'. The expression u(a,ECC) is $Q[(ECC \cdot a \cdot \mu)^2 + a^2(1 - \mu^2)]^{1/2}$.

Unfortunately, scattering from monodisperse ellipsoids with small axial ratios is difficult to distinguish from scattering from polydisperse spheres, and vice versa. The situation occurs because for each orientation of an ellipsoid relative to Q, the form factor is identical to that for a sphere with an equivalent radius, which varies with orientation.[90] Nonspherical shapes and polydispersity in particle size have the effect of dampening the oscillations observed in the form factor of monodisperse spheres.[81]

5. Interparticle Interference

Again the focus of this discussion will be upon monodisperse spheres. Earlier it was noted that the interparticle interference arose from interference of neutrons scattered by nuclei located on different particles. In dilute solutions where the particles would be able to take completely random positions in the solution these interferences would be averaged out and S(Q) would equal one at all values of Q. For most micellar solutions however, the positions of the particles become correlated due to the particles repelling each other; this is especially true for electrostatic repulsions. S(Q) describes these interactions; S(Q) is the Fourier transform of the radial distribution function g(r). This distribution function is given by

$$g(r) = 1 + (1/2\pi^2 Np) \int_0^\infty Q^2[S(Q)-1]\,[(\sin Qr)/Qr]dQ \qquad (55)$$

The probability of finding another particle at a distance r from a reference particle centered at the origin is given by g(r). When r is less than the distance of closest approach of two particles ($r < 2R_{hs}$ where R_{hs} is the hard sphere radius), g(r) is equal to zero; $r \to \infty$ $g(r) = 1$.

The potential of mean force, $\Phi(r)$, between particles consists of two potentials: the pair potential between particles, U(r), and the perturbation potential, $\psi(r)$. The perturbation potential accounts for the many body interactions present in the system.

The total correlation function, given by $h(r) = g(r) - 1$, gives the total correlation between two particles separated by a distance r. Note

that in the limit of r approaching infinity, h(r) is equal to zero. The Ornstein-Zernike equation[91] defines h(r) as being composed of two contributions

$$h(r_{12}) = C(r_{12}) + N_p \int c(\underline{r}_{13})h(\underline{r}_{32})d\underline{r}_3 \qquad (56)$$

The first contribution, $c(r_{12})$, represents the direct influence of particle 1 on particle 2. The second contribution reflects the indirect influence of particle 1 on particle 2 which is transmitted via a third particle situated at a distance $\underline{r}_{13}$ from particle 1 and $\underline{r}_{32}$ from particle 2. The indirect influence is integrated over all possible positions of the third particle.

Since the repulsive screened Coulombic potential is generally larger than thermal energies at small interparticle separations, electrostatic repulsions dominate the particle-particle interactions possible in ionic systems. Consequently the attractive forces rarely come into play.[92]

The repulsive Coulombic potential describes the interaction of the electrical double layers of spherical macroions (of diameter σ).[93] This potential is written as

$$U(r) = \pi\varepsilon_o\varepsilon\sigma\psi_s^2\exp[-\kappa\sigma(x-1)]x^{-1}, \quad x > 1 \qquad (57)$$

ε_o is the permitivity of free space, ε is the dielectric constant of the solvent, ψs is the surface electrostatic potential, x is r/σ where r is the effective particle diameter and κ corresponds to the Debye-Huckel

inverse screening length. The surface potential and the electronic charge, Zm, on the macroion are related through[94]

$$\psi s = Zm/\pi\varepsilon_o\varepsilon\sigma(2 + \kappa\sigma) \qquad (58)$$

where the term $(2 + \kappa\sigma)$ accounts for the mutual exclusion by the macroions of their counterions from each other's volume. At low values of κ (low supporting electrolyte), the electrostatic repulsions are long-ranged whereas at high values of κ these repulsions decay more rapidly.

Analytical solutions for S(Q) and c(r) have been obtained by Hayter and Penfold[94] who solved equation 57 using the Ornstein-Zernike equation with the mean spherical approximation (MSA)[95] closures. For an interaction potential with a hard core, these closure relations are

$$g(r) = 0 \qquad r < 2R_{HS} \qquad (59a)$$

$$c(r) = -U(r)/k_BT, \qquad r > 2R_{HS} \qquad (59b)$$

At low volume fractions a rescaled version of the MSA (RMSA)[92] must be used.

For nonionic systems van der Waals attractions and hydration forces affect S(Q). Several investigators[96,97] have modeled these potentials in the Yukawa form for surfactants containing polyoxyethylene headgroups.

6. SANS Experiments

A typical scattering curve for di-C_6 sulfosuccinate is shown in Figure 20, along with the calculated P(Q), S(Q) and I(Q). Three Q regions are apparent in the scattering curve. In the low Q region, where 1/Q values correspond to distances greater than the average intermicellar distances, the osmotic compressibility of the solution determines the scattering. An interaction peak is present at intermediate Q values; this peak results from the dominance of S(Q) in this region. The position of the peak, Q_{Imax}, is related to the average intermicellar distance. In the high Q region S(Q) becomes one, therefore the intensity is now proportional to P(Q) which contains information concerning the size and shape of the micelles.

a. Guinier region. If noninteracting particles are present in the solution, then the first region can be utilized to obtain information about the radius of gyration, R_g, of the particles. Expanding equation 46 in the limit of small Q yields

$$F_p(\underline{Q}) = \int_{\text{particle p}} [\rho_p(\underline{r}) - \rho_{solv}](1 + i\underline{Q}\cdot\underline{r} - 1/2(\underline{Q}\cdot r)^2 + \ldots)d^3\underline{r} \qquad (60)$$

The center of gravity of ρ ($\underline{r}$) is assumed to correspond to the center of gravity of the particle's volume. One may then write (for noninteracting, monodisperse particles)

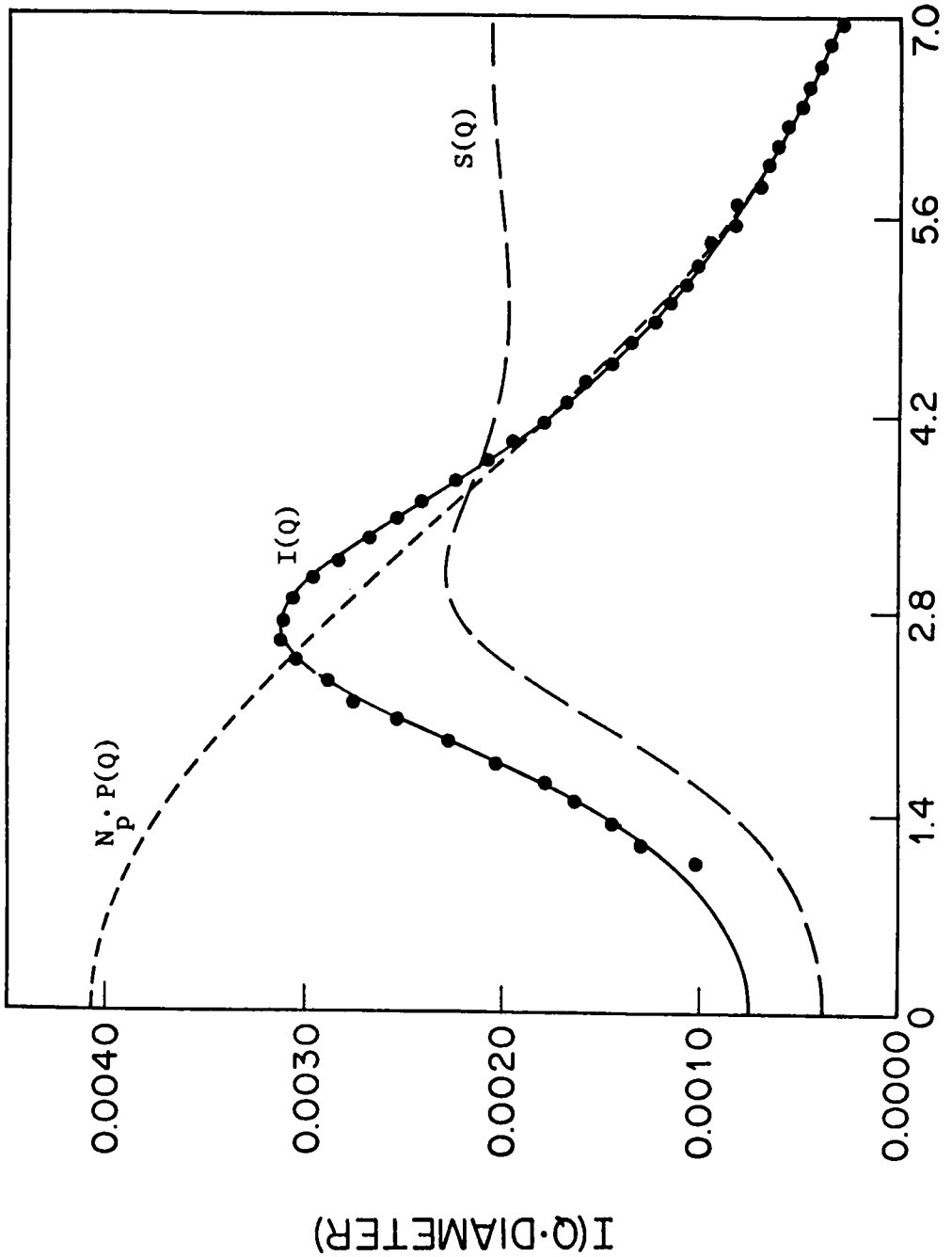

Figure 20. SANS curves for 0.07 M C_6SS.

$$I(Q) = N_p \cdot (\rho V_p)^2 (1 - 1/3 \frac{Q^2}{\bar{\rho} V_p} \int_{V_p} r^2 [\rho(\underline{r}) - \rho_{solv}] d^3 r) \qquad (61)$$

Equation 61 contains the second moment of the scattering length density distribution. The second moment can be defined as the radius of gyration[88,98]

$$R_g^2 = \frac{1}{\Delta\rho V_p} \int_{V_p} r^2 [\rho(\underline{r}) - \rho_{solv}] d^3 r \qquad (62)$$

The above equation may be rewritten as[98]

$$R_g^2 = R_{gv}^2 + \frac{1}{\Delta\rho V_p} \int_{V_p} \rho_F(\underline{r}) r^2 d^3 r \qquad (63)$$

The fluctuation of the average scattering length density around its mean value is given by $\rho_F(\underline{r})$. R_g is the radius of gyration for a particle identical to that under investigation but with an uniform scattering length density. Therefore a particle with a contrast independent R_g possesses a small gradient of scattering length density in it.[98]

One can rewrite equation 61 in the low Q limit to yield

$$I(Q) = I(0) \cdot \exp(-R_g^2 Q^2/3) \qquad (64)$$

The above equation (the Guinier Law) is valid in a Q range which satisfies the relationship $QR < 1$. Plots of ln I(Q) vs Q^2 allow one to determine both R_g and I(0).

b. Contrast variation, As mentioned earlier, SANS is a very valuable technique for studying hydrogen-rich systems because simple substitution of ^1H by ^2H provides excellent contrast. By selective deuteration specific regions of the micelle may be studied; this technique is known as contrast variation. For external contrast variation, the scattering length density of the solvent is varied by employing different H_2O/D_2O compositions in aqueous solutions (or C_nH_{2n+1}/C_nD_{2n+1} composition in hydrocarbon solvents). The scattering length density of the particle itself can be changed by using different protiated/deuterated surfactant compositions. For a micelle consisting of a core-plus-shell, two contrast-matching situations are possible for these sets of experiments (see Figure 21): (1) $\rho_1 = \rho_{solv}$, here only scattering from the shell is seen, and (2) $\rho_2 = \rho_{solv}$, one observes scattering from the core only. For this case equation 50 becomes

$$Fp(\underline{Q}) = (\rho_1 - \rho_{solv})V_1\phi(QR_1) \qquad (65)$$

and the size of the core can be determined from the analysis of the full scattering curve.

Returning to the discussion of the small Q region, one sees that $\Delta\rho$ can be varied by either of the contrast variation methods. For the core-plus-shell structure two radii of gyration are present: $R_{g,1}$ (core) and $R_{g,2}$ (shell). One can then write

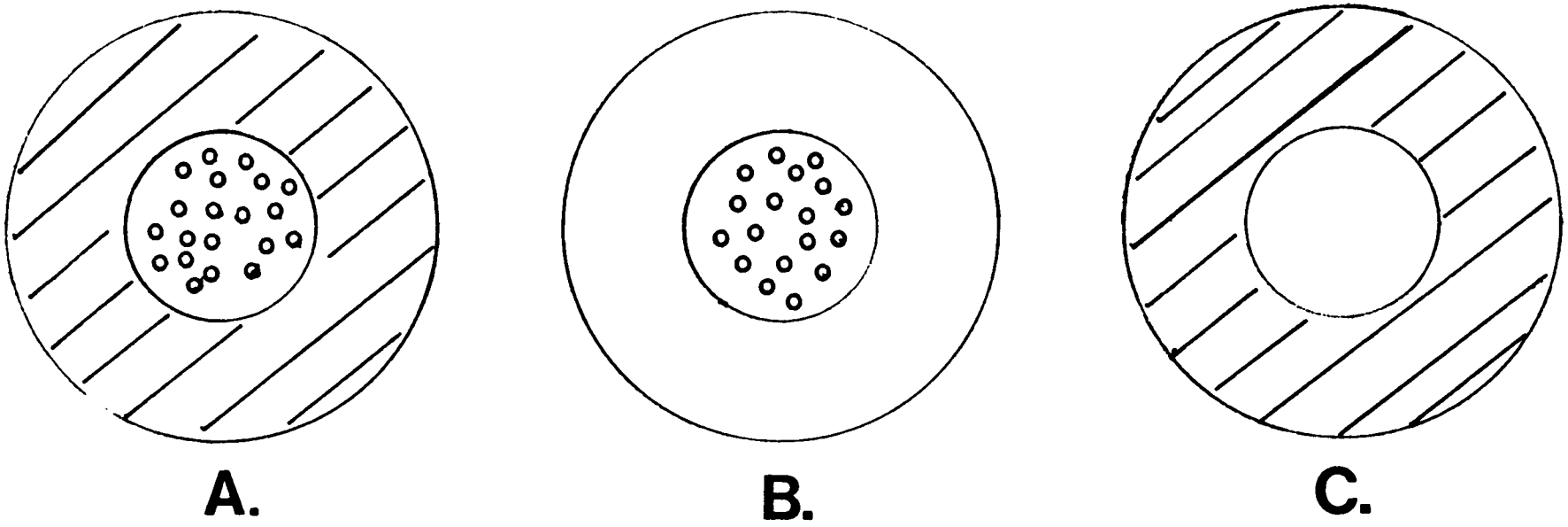

Figure 21. Possible contrast conditions for core plus shell model.

$$R^2 = \frac{C_1(R_{g,1})^2 + C_2(R_{g,2})^2}{C_1 + C_2} \tag{66}$$

C_1 and C_2 are given by

$$C_1 = \int[\rho_1 - \rho_{solv}]d^3r \tag{67a}$$

$$C_2 = \int[\rho_2 - \rho_{solv}]d^3r \tag{67b}$$

and are equivalent to the $\Delta\rho$ Vp term seen for a homogeneous particle. By proper adjustment of ρ_1, ρ_2 or ρ_{solv}, C_1 or C_2 can be set equal to zero.

In the past, the external contrast variation technique has been used to address the issue of water penetration into the micellar core. However, this method is not able to provide information concerning water penetration. Cabane and Zemb[99] have emphasized that I(0) is related only to the mass of the dry particle. Consider the following equation:

$$I(Q\rightarrow O) = N_P \cdot (\bar{\rho} - \rho_{solv})^2 \cdot V_P^2 \tag{68}$$

Inclusion of solvent in the particle results in equal contributions to both εb_i and to the total particle volume. Therefore, only parameters of the dry particle can be obtained. The same argument can be extended to a core-plus-shell particle in which inclusion of solvent in the shell would contribute equally to ρ_2 and $(V_2 - V_1)$.

Two possible routes are available to measure solvent penetration of a few A into the micelle. Since spatial resolution in the scattering experiment is $2\pi/Qmax$, where Qmax is the maximum value of the scattering vector, one possibility is to perform the measurements at large scattering vectors (1 $Å^{-1}$).[100] The other possibility would be to study solutions of strongly interacting micelles where the effective volume fraction depends upon the extent of hydration.[101,102]

B. SANS Experimental Considerations

1. Experimental Set-Up

Figure 22 illustrates the 30 m SANS apparatus located at the National Center for Small-Angle Scattering Research (NCSASR), Oak Ridge National Laboratory (ORNL). The available Q-range of this apparatus is 0.002-0.6 $Å^{-1}$. The thermal neutron beam, which originates in the core of the High Flux Isotope Reactor (HFIR), passes through a beryllium filter and then through two sets of graphite monochromator crystals. The crystals can be set to select a wavelength of either 4.75 Å or 2.37 Å (with a spread of $\Delta Q/Q$ of 6%). A proportional counter positioned in front of the source slit continuously monitors the incident beam flux, I_o (neutrons per cm^2 per second). The length of the evacuated beam flight path is 7.6 m; three removable two-meter-long beam guides are available for use in the flight path. A second slit is present before the sample. Since cadmium has such a high absorption cross-section for neutrons, all slits are constructed from cadmium. The diameter of the entrance slit, S_1, usually ranges from 0.5 cm to 3.5 cm and that of the

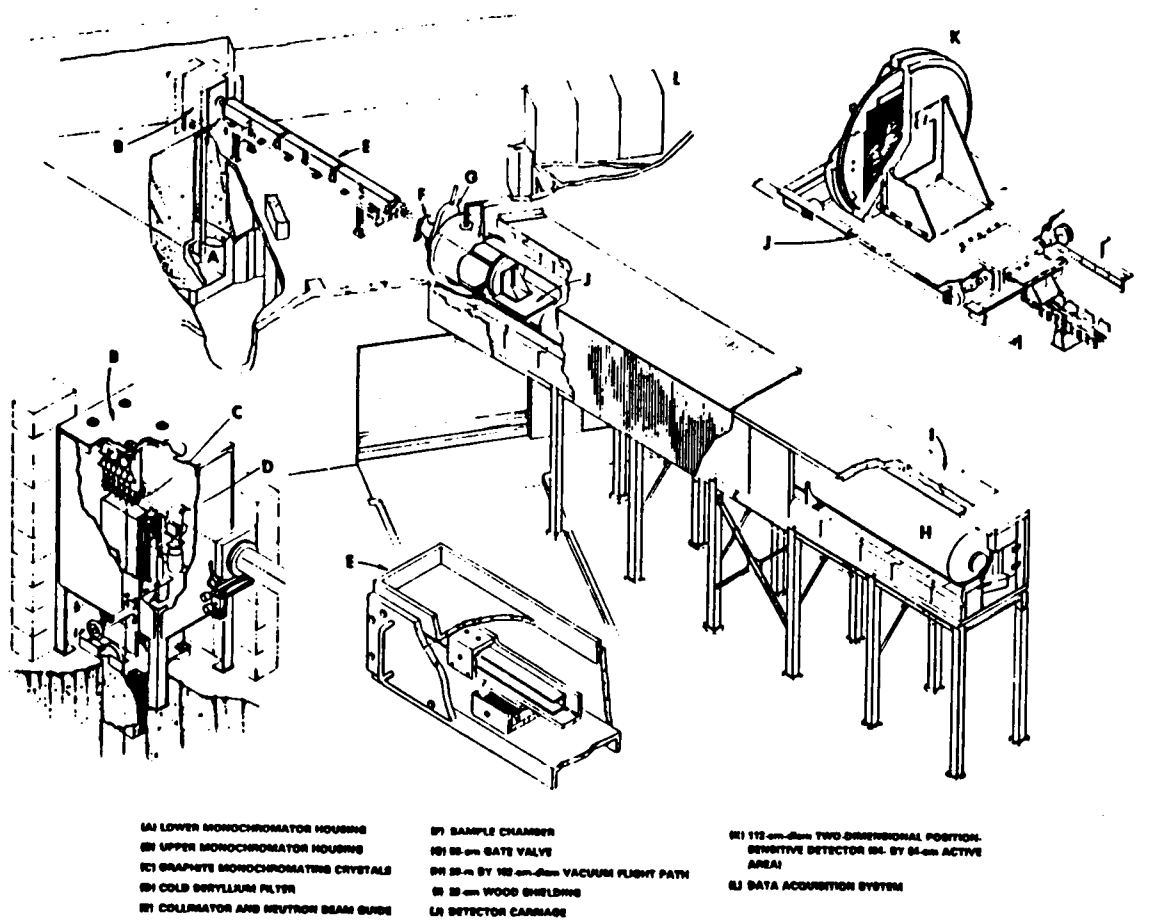

Figure 22. Schematic of 30 M SANS instrument.

sample slit, S_2, is in the range 0.4 cm to 2.0 cm. A cadmium beamstop of diameter 4 or 8 cm is located at the center of the detector to intercept the unscattered beam which is focused (onto the beamstop) by the two-slit geometry. The scattered neutron intensity, I_s, is detected for many scattering angles at once by a helium-filled two-dimensional position-sensitive proportional counter designed by Borowski and Kopp.[103] This detector contains 4096 detector elements (64 x 64 cm^2).

The spectrophotometric cells for liquid samples are constructed from quartz because boron (in borosilicate glass) is a very efficient neutron absorber. The cylindrical cells used had pathlengths of one or two mm. Up to six sample cells can be placed on a motor-driven slide which is lowered into the sample chamber. The samples are thermostatted via a removable well inserted through the top portion of the permanent sample chamber.

2. Choice of Scattering Geometry

Several factors should be considered in choosing the appropriate scattering geometry:

1. For constant S_2, the flux at the sample is proportional to the area of the first slit. However, a large S_1 can only be used in conjunction with a small sample-to-detector distance (SDD) because of the finite size of the beamstop.

2. The experimental Q range needs to be kept as large as possible in order to keep the value for the Q resolution, $\Delta Q/Q$, as small as possible. Therefore, the compromise must be made to make measurements over as large a Q range as possible, as dictated by the size of the

particle (i.e., $0.5 < QR < 5.0$) while keeping S_1 at a maximum and SDD at a minimum. Generally, the scattering geometry is chosen such that the transmitted beam is completely intercepted by the beamstop and that the size of S_2 is approximately half the size of the source slit, S_1.

The sample-to-detector distance has a range of 1.4 m to 19 m; at large SDD Q is estimated by

$$Q = \frac{2\pi}{\lambda} \tan\theta = \frac{2\pi}{\lambda} \cdot \frac{d}{SDD} \qquad (69)$$

where d is defined as shown in Figure 23. A typical intensity map, or contour plot, for a micellar solution is shown in Figure 24. The typical scattering curve, I(Q) vs. Q where I(Q) is corrected as illustrated below, is obtained from the one-dimensional radial average.

3. Data Correction

The total scattering detected includes scattering from: (1) the solute; (2) the solvent, I_{so}; (3) the empty cell, I_e; and (4) the background, I_b, which is determined with a sheet of Cd blocking the beam. Transmission coefficients (I_t/I_o) are determined for each sample so that the attenuation of the neutrons, resulting from their passage through the sample, can be corrected.

Since variations in sensitivity exist among the detector elements, this was the first correction to be made. A water calibration run which was taken at long enough counting times to give ca. 10^3 counts per second was typically used for this correction. The counting probability of an element was then determined as the number of neutrons recorded in

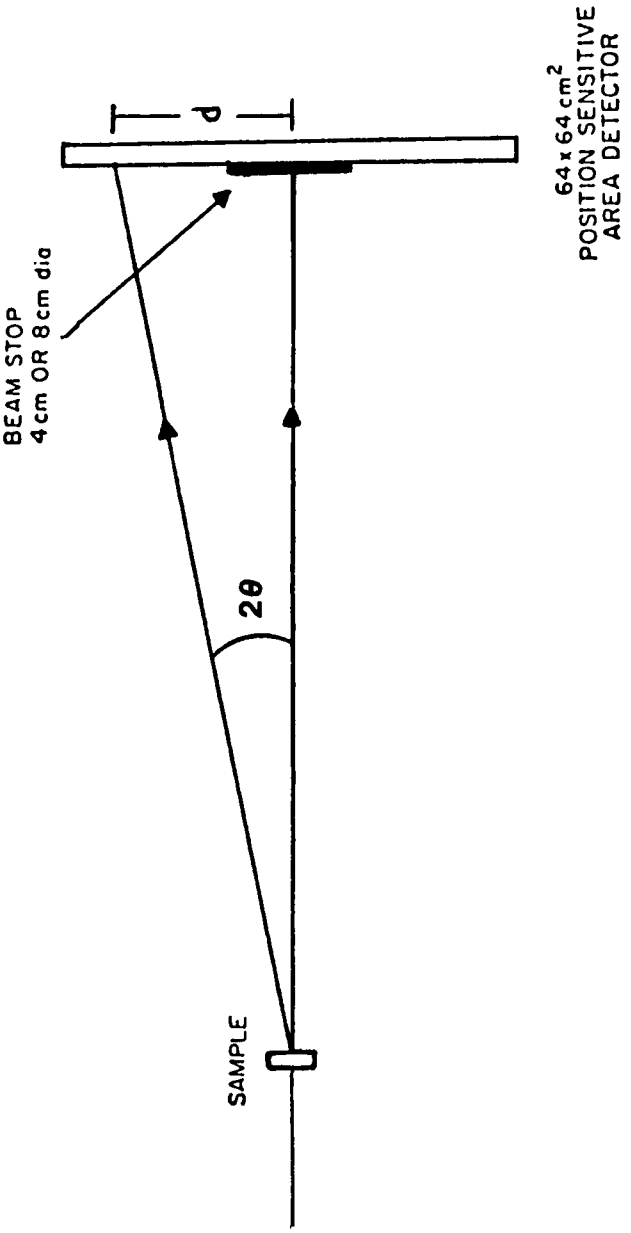

Figure 23. Definition of d.

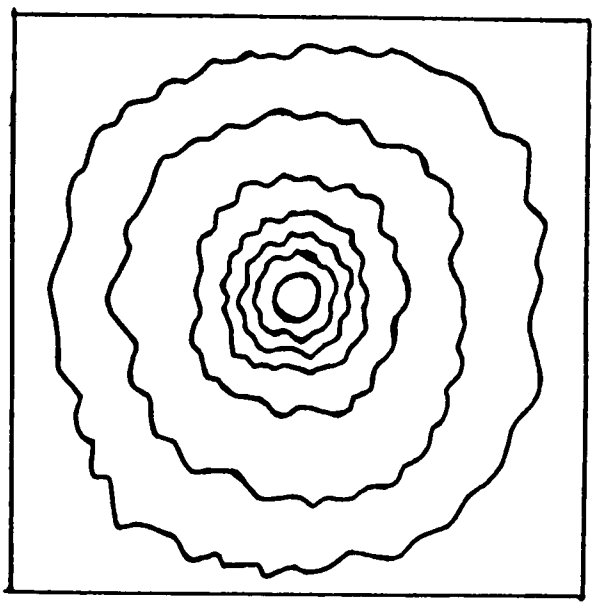

Figure 24. Experimentally obtained contour plot.

that element divided by the average number of neutrons recorded per unit element.

The data is then corrected for the sources of scattering other than that of the sample by a variety of online programs developed by NCSASR's staff members. The raw data (both solution and solvent) is first corrected for background and empty beam scattering (all intensities have been normalized) by

$$I_{s,corr} = (I_{tot} - I_b) - T_s/T_e(I_e - I_b) \qquad (70)$$

T_s and T_e are neutron transmission coefficients. $I_{s,corr}$ is computed for each detector element using the equation above.

An attractive feature of SANS is the ability to put I(Q) in absolute units. This is accomplished by calibrating the detector using a standard scatterer (water at short SDD's, Al-4 at larger SDD's; Al-4 is an irradiated sample containing voids having a well-characterized R_g and I(0).). For water, the neutron calibration constant, K_n, is obtained from

$$I_{inc} = \frac{1-T}{4\pi} \cdot \frac{Kn \cdot A}{SDD} \cdot G \qquad (71)$$

where (1-T)/4 is the fraction of total neutrons scattered into a unit solid angle, A is the area of the limiting slit and G is the Jacrot factor.[104] For λ = 4.75 Å, a Jacrot factor of 1.5 is used. The neutron calibration constant is then used to convert corrected scattered intensities into absolute differential cross-sections by

$$I(Q) = \frac{I_{s,corr}(Q)}{t \cdot T_s} \cdot \frac{SDD^2}{K_N A} \qquad (72)$$

where t is the thickness of the sample. After both the solution and solvent runs have been corrected for background and incoherent scattering, the solvent run is subtracted leaving only the coherent scattering cross-section of equation 39.

CHAPTER IV

ELUCIDATION OF THE STRUCTURE OF SULFOSUCCINATE MICELLES BY SMALL-ANGLE NEUTRON SCATTERING

SANS is a very powerful technique for probing micellar structure; reliable aggregation numbers and micellar charges may be obtained as well as the arrangement of various groups within the micelle. Since the advent of Hayter and co-workers'[92,94] analytical solution for S(Q), many SANS studies of micellar systems have appeared; Table VII lists a portion of these for ionic surfactants. From this limited compendium, one sees that the dodecylsulfate surfactant has been studied extensively; because this surfactant is similar in structure to the sulfosuccinates, the SANS studies of dodecylsulfates will be considered in some detail.

A. Application of SANS to SDS Micelles

The first application of Hayter and co-workers'[92,94] analytical solution for S(Q) was to a SANS study of SDS as a function of surfactant and salt concentration.[105] SDS was determined to form spherical micelles consisting of a hydrocarbon core plus one or two shells (these models could not be distinguished based on spatial resolution); these micelles were found to grow with increasing amphiphile concentration and upon the addition of salt. In a later SANS study, micellar structures formed by SDS and several cationic surfactants were compared. Hayter and Penfold[50] claimed that the surface roughness of SDS micelles increased with increasing surfactant concentration; however, based

TABLE VII

IONIC SURFACTANTS INVESTIGATED BY SANS

Surfactant	Investigators
SDS	Hayter & Penfold[105]
LDS	Bendedouch et al.[106-9]
LDS	Chao et al.[110]
Sodium octanoate	Hayter & Zemb[111]
SDS, $C_{12}TACl$, $C_{12}TABr$, $C_{16}TACl$	Hayter & Penfold[112]
SDS	Cabane et al.[28,113]
Tetramethylammonium DS	Berr et al.[114]
Sodium octylphosphate	Chevalier et al.[115]
CTAB	Quirion & Magid[116-7]
CTA chlorobenzoates	Carver[9]
Texas #1, $6PhC_{12}SNa$	Magid et al.[57,118]
$6PhC_{12}SNa$	Triolo et al.[119]
$6PhC_{12}SNa$, $nC_{12}PhSNa$	Caponetti et al.[120]
$C_8C_{16}N(CH_3)_2Br$	Magid et al.[121]

upon their spatial resolution, such a claim in fact cannot be sustained. However, from comparisons with the cationic surfactants studied, SDS micelles appear to have a less well-defined core/polar surface than do the cationics.

Unlike SDS, lithium dodecylsulfate (LDS) exhibits little growth and/or polydispersity over a wide range of concentrations; for these reasons, Bendedouch and co-workers[106-110] chose to investigate LDS by SANS. From internal and external contrast variation studies, water was determined to penetrate only to the level of the first two methylene groups at most; however, this result came from a misinterpretation of the contrast variation technique, as was stressed by Cabane and Zemb.[28] Also, the reported methyl distribution in the core was erroneous because the distribution was simply the image of their experimental resolution.

The definitive determination of the micellar structure of SDS comes from Cabane et al.'s[28,113] SANS study; scattering was measured to Q = 0.6 $Å^{-1}$ which corresponds to a spatial resolution of 5 Å. This resolution is more than adequate to address the issues of water penetration and methyl group distribution in the core. By appropriate contrast studies, Cabane et al.[28,113] found SDS micelles to be spherical at a concentration of 0.07 M with an aggregation number of 74. The hydrocarbon/water boundary was determined to be limited to the surface of the core (see p. 8 for details) and the methyl groups were found to be randomly distributed in the core; i.e., distribution of distances between $-CD_3$ groups was close to that of the whole core. Since the γ-CD_2 groups

were found to be distributed between the core and the thin spherical shell, shape fluctuations were proposed to exist.

The SANS literature on double-tailed surfactants is not as extensive as that of single-tailed surfactants. Magid et al.[58] resolved the issue concerning the presence of micelles in aqueous solutions of Texas #1 through SANS; small spherical micelles were found which had a radius of gyration of 16.9 Å. Triolo et al.[119] used SANS to determine the micellar structure of 6-$PhC_{12}SNa$; these spherical micelles were found to have considerable amounts of methylene groups in the shell. Upon comparing the scattering of $6PhC_{12}SNa$ to its straight-chain analog, $n\text{-}C_{12}PhSNa$, Caponetti et al.[120] suggested that the planar phenyl group acted as a supplementary headgroup and resulted in a thicker polar shell.

B. Structural Elucidation for Micelles of Di-n-Alkyl Sulfosuccinates in Water Using SANS

In this work, SANS was employed to address the following aspects of sulfosuccinate micellar behavior: (1) the determination of a realistic model for the micelles, including the hydration of headgroups and volume per monomer; (2) the determination of the rate of micellar growth as a function of surfactant and salt concentration; and (3) the determination of shape changes that occur, if any, as the micellar solubility limit is approached. Each of these areas will be addressed in turn; enabling each study to build upon the previous one(s).

To address (1), a series of internal/external contrast variation experiments were performed for C_7SS at 0.03 M C_7SS in 0.06 M NaCl and at

0.10 M C_7SS without added NaCl. Guinier analysis of the data obtained in the salt study will be treated first; then the data obtained at 0.10 M C_7SS will be presented. Next, SANS data for the concentration and salt studies for C_6SS, C_7SS and C_8SS will be considered; since additional surfactant concentrations were studied, several micellar models will be considered. Finally, the evolution of micellar shape for C_6SS, C_7SS and C_8SS solutions will be discussed as the boundary between L_1 and L_1 + LC is approached.

1. Application of SANS Contrast Variation Technique in the Study of C_7SS Micelles

a. Guinier Analysis. The addition of supporting electrolyte to C_7SS solutions produces non or weakly interacting particles; thus, the Guinier law may be applied for $QR < 1$. For such solutions, the interparticle structure factor is one and the differential cross-section can be written as

$$I(Q) = I_o \cdot P(Q) = (C - cmc) \cdot \bar{n} \cdot (b_m - \rho_s V_m)^2 \cdot P(Q) \qquad (73)$$

Two sets of SANS measurements were made on 0.03 M C_7SS in 0.06 M NaCl: (1) an external contrast variation series in which the solvent scattering length density was changed by varying the volume/volume ratio of D_2O/H_2O, designated as β = 1.00, 0.85, 0.70, 0.55, 0.40 and (2) an internal contrast variation series in which b_m was varied by using appropriate ratios, denoted by γ, of deuterated C_7SS (alkyl chains deuterated to the extent of 85%, see Chapter VII for details) and

protiated C_7SS; the ratios used were 0.0, 0.20, 0.40, 0.62, 0.85. Figure 25 displays typical scattering curves; the absence of the interaction peak supports the assumption that S(Q) is approximately one and that the scattered intensity can be described by equation 73. Guinier plots were made for the appropriate Q range and the values obtained for I(0) and R_g are shown in Table VIII. The R_g values obtained from the external contrast data decrease as the % H_2O increases. This decrease occurs as the scattering length density of the solvent approaches that of the shell, and the weights (see eqns. 67a, 67b) that determine R_g are shifted to the core. This trend in radii of gyration indicates that the C_7SS headgroup lies, on the average, farther from the center of the micelle than do the hydrocarbon tails. Chen et al.[146] found a similar trend in R_g values for the micelles formed by dihexanoylphosphatidylcholine (diC_6PC); at 100% H_2O, an increase in R_g was noted. This increase occurs because the scattering length density of the solvent now begins to approach the value of the core, and the weights that determine R_g are shifted to the shell region. For the C_7 sulfosuccinate, the radii of gyration obtained for the internal contrast data appeared scattershot; no trend in the R_g values was found. The I_o values obtained will be used in a latter analysis.

Aggregation numbers and the volume of the <u>dry</u> surfactant monomer, V_m, were obtained from the intensity at zero Q, I_o. The solvent scattering length density can be expressed as

$$\rho(\beta) = (1 - \beta)\rho_{H_2O} + \beta \cdot \rho_{D_2O} \qquad (74)$$

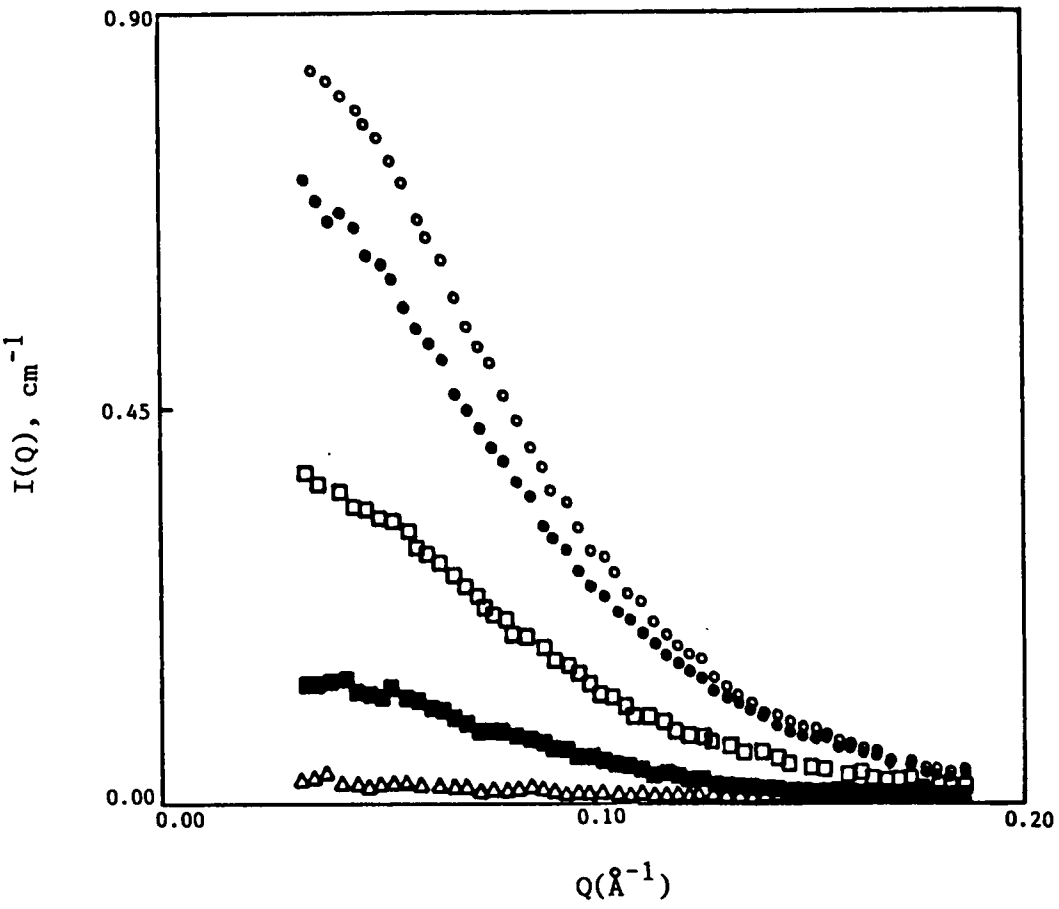

Figure 25. SANS curves for 0.03 M C_7SS with 0.06 M NaCl.

TABLE VIII

RESULTS FROM GUINIER ANALYSIS FOR 0.03 M C_7SS IN 0.06 M NaCl

	I_o, cm^{-1}	R_g, Å
External Contrast Variation		
β		
1.00	0.9940 ± 0.0074	19.00 ± 0.07
0.85	0.8720 ± 0.0057	18.96 ± 0.08
0.70	0.5215 ± 0.0080	17.74 ± 0.18
0.55	0.2585 ± 0.0042	17.09 ± 0.23
0.40	0.0972 ± 0.0063	13.66 ± 1.06
Internal Contrast Variation		
Y		
0.0	0.9940 ± 0.0074	19.00 ± 0.07
0.20	0.8607 ± 0.0062	18.43 ± 0.08
0.40	0.4390 ± 0.0032	18.40 ± 0.08
0.62	0.1663 ± 0.0018	19.21 ± 0.13
0.85	0.0247 ± 0.0010	17.84 ± 0.50

Combination of this equation with equation 73 yields

$$I_o = (C - cmc)\,\bar{n}\,\{b_m - [\rho_{D_2O} - (1-\beta)(\rho_{D_2O} - \rho_{H_2O})]V_m\}^2 \qquad (75)$$

or

$$(I_o)^{1/2} = [(C-cmc)\bar{n}]^{1/2}\{b_m - [\rho_{D_2O} - (1-\beta)\Delta\rho]V_m\} \qquad (76)$$

V_m and $\bar{n}$ were determined from the plot of $(I_o)^{1/2}$ vs. $(1 - \beta)$ for the external contrast variation measurements; the result is shown in Figure 26. For C_7SS, $V_m = 277$ Å^3 and $\bar{n} = 350$. For a C_7SS micelle at this surfactant and salt concentration, both these values are unreasonable. The calculated volume of the surfactant without the CH_2-$CH(SO_3^-Na^+)$ moiety is 505 Å^3. The aggregation number for 0.04 M C_7SS in 0.04 M NaCl will be seen to be 70.8.

$(I_o)^{1/2}$ can be written as a function of the scattering length density of the monomer in the following way

$$(I_o)^{1/2} = [(C-cmc)\bar{n}]^{1/2}\{[\gamma b_m^D + (1-\gamma)b_m^H] - \rho_{D_2O}\cdot V_m\} \qquad (77)$$

For the protiated surfactant $b_m = 1.948 \times 10^{-12}$ cm and for the deuterated surfactant $b_m = 33.187 \times 10^{-12}$ cm. (Note that these values for b_m do not contain the sulfonate headgroup or counterion.) A plot of $(I_o)^{1/2}$ vs. γ yielded a straight line (see Figure 27) from which V_m and $\bar{n}$ were determined to be 508 Å^3 and 79. These values are much more realistic for the C_7SS micelles under these conditions.

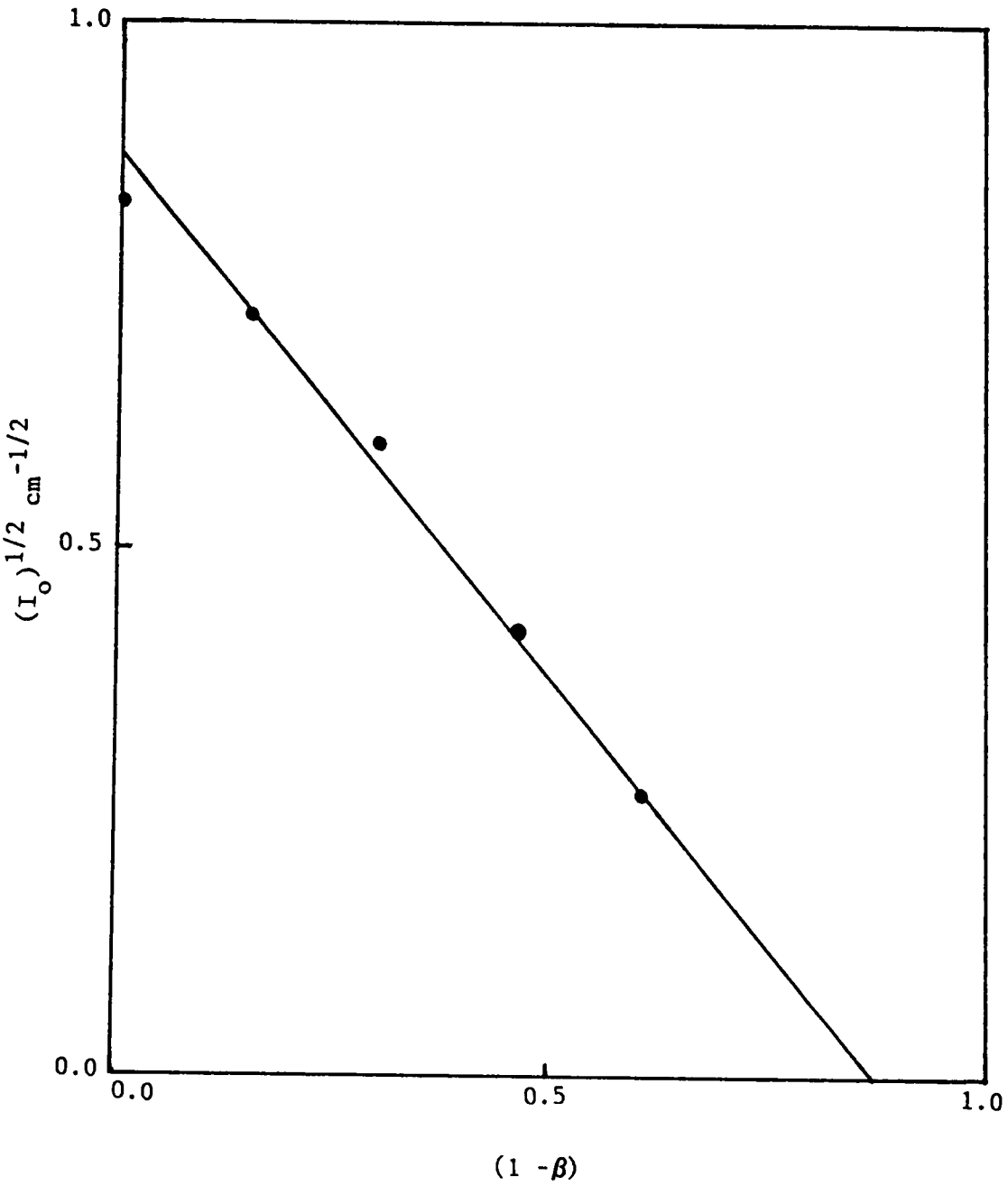

Figure 26. Plot of $(I_o)^{1/2}$ versus (1 -β) for 0.03 M C_7SS with 0.06 M NaCl.

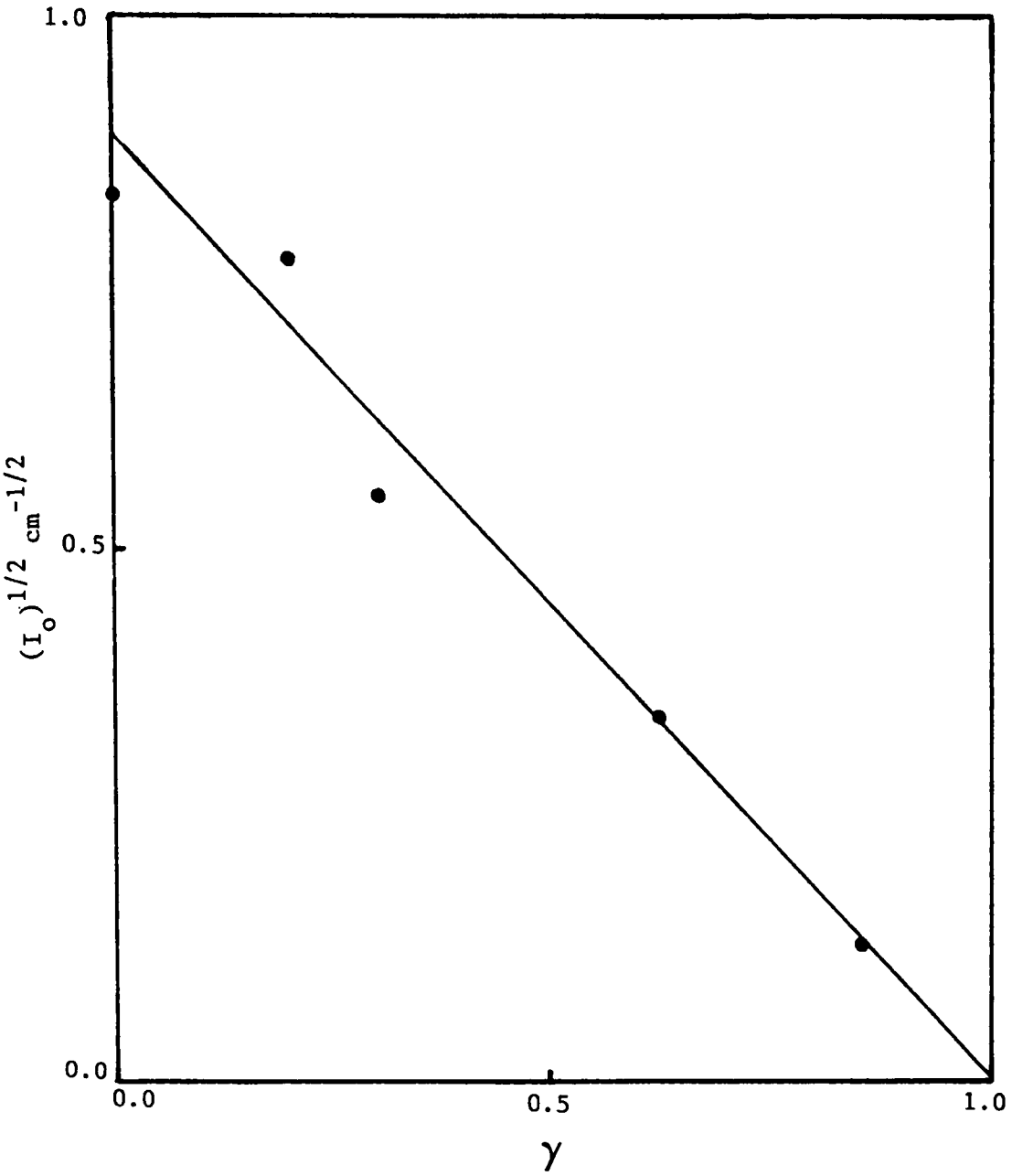

Figure 27. Plot of $(I_o)^{1/2}$ versus γ for 0.03 M C_7SS with 0.06 M NaCl.

For a micelle consisting of a core plus shell, two radii of gyration can be identified: $R_{g,1}$ which is associated with the core and $R_{g,2}$ which is associated with the shell. The variation of R_g with the scattering length density suggests that the C_7SS micelles possess scattering length density inhomogeneities. The R_g values obtained from the Guinier analyses can be used to validate a model for the micelles.

As a first try, a core plus shell model was used in which the alkyl tails were placed in the core and the remainder of the surfactant monomer, including the ester moieties, were placed in the shell. A uniform distribution of these groups in their respective regions was assumed. (This requirement of uniformity is applied due to the limitations of SANS spatial resolution.) Assuming that the core plus shell model is valid for these micelles, then all the R_g values should be able to be calculated through equation with the weighting factors given by equations 67a & b. The weighting factors can be rewritten as

$$C_1 = \bar{n} [b_t(\gamma) - \rho_s(\beta) V_t] \quad (78a)$$

$$C_2 = \bar{n} [b_h(\gamma) - \rho_s(\beta) V_h] \quad (78b)$$

The volume of the two heptyl tails, V_t, was calculated to be 431.4 $Å^3$ using the equation of Tanford.[33] The "headgroup" volume, V_h, was obtained from the difference between V_m and V_t: $V_h = 76.6$ $Å^3$. The scattering length of the head, b_h, and of the tail, b_t are: $b_h = 3.858 \times 10^{-12}$ cm and $b_t = \gamma(29.329 \times 10^{-12}\text{cm}) + (1 - \gamma)(-1.910 \times 10^{-12}$ cm).

The measured values of R_g were reproduced by using $R_{g,1}$ = 16.0 Å and $R_{g,2}$ = 32.0 Å. The calculated values agreed fairly well with the R_g values from the external contrast data but not with those from the internal contrast data, see Table IX. Several other models were considered which placed a fraction of the alkyl tails in the shell and/or counted the ester moieties as part of the core; however, all of these models failed to reproduce the experimentally obtained R_g values for either the internal contrast or external contrast data. The remainder of this discussion will focus upon the external contrast data.

A C_7SS micelle with an aggregation number of 79 is probably no longer spherical; therefore, the model of choice is an ellipsoid. The model should have the correct $R_{g,1}$ and $R_{g,2}$ values and must be able to reproduce the whole scattering curve.

The core semiminor axis, A_1, and semimajor axis, B_1, are related to $R_{g,1}$ through

$$R_{g,1}^2 = 1/5\ (B_1^2 + 2A_1^2) \tag{79}$$

If A_1 = 10.4 Å (the extended length of the alkyl tail), then B_1 = 32.61 Å.

The volume of the shell is determined by its semiminor thickness, THIKA, and semimajor thickness, THIKB, which are related to $R_{g,2}$ through

$$R_{g,2}^2 = \frac{[(B_1+THIKB)+2(A_1+THIKA)^2](B_1+THIKB)(A_1+THIKA)^2}{5[(B_1+THIKB)(A1+THIKA)^2-B_1A_1^2}$$

$$- 2B_1A_1^2/5[9B_1+THIKB)(A1+THIKA)^2-B_1A_1^2] \tag{80}$$

TABLE IX

COMPARISON OF CALCULATED AND EXPERIMENTAL RADII OF GYRATION

	$\frac{C_1}{C_1+C_2}$	$\frac{C_2}{C_1+C_2}$	R_g(exp, Å)	R_g(calc, Å)
External Contrast Variation ($\gamma = 0$)				
β				
1.0	0.843	0.157	19.00 ± 0.06	19.40
0.85	0.866	0.134	18.96 ± 0.08	18.95
0.70	0.902	0.098	17.74 ± 0.18	18.20
0.55	0.962	0.038	17.09 ± 0.23	16.89
0.40	1.092	-0.092	13.66 ± 1.06	13.61
Internal Contrast Variation ($\beta = 1$)				
γ				
0.0	0.843	0.156	19.00 ± 0.06	19.40
0.20	0.776	0.224	18.43 ± 0.08	20.69
0.40	0.698	0.302	18.40 ± 0.08	22.09
0.62	0.512	0.488	19.21 ± 0.13	25.12
0.85	0.210	0.790	17.84 ± 0.50	29.35

In order to calculate I(Q), a normalized P(Q) was computed by

$$P_o = [(C_1 - C_2(V_1/V_2))/C_1 + C_2 \cdot 3\phi(U_1) + (C_2 + C_2(V_1/V_2))/V_1 + V_2 \cdot 3\phi(U_2) \quad (81)$$

where $V_1 = (4\pi/3)\ A_1^2\ B_1$ and $V_2 = (4\pi/3)\ [(A_1 + \text{THIKA})^2\ (B_1 + \text{THIKB}) - A_1^2\ B_1)$.

Numerous attempts to fit the scattering curves using this model failed even though several different combinations for THIKA and THIKB were used. Several other values for A_1 and B_1 were also used, but to no avail. Fits to the scattering curves were only obtained when the volume of the shell was reduced (by decreasing the value of $R_{g,2}$) and b_h and b_t were used as adjustable parameters. The value of b_t obtained in this manner was positive, which is in conflict with the calculated value using scattering length tables. This suggests that the micellar model predicted by the R_g values is unrealistic; however, as is illustrated by the sample calculation outlined above, it is $R_{g,2}$ that is unrealistic, not $R_{g,1}$. Possible modifications of the model would include removing the restriction of the alkyl tails to the core and counting the ester moieties as part of the alkyl tails.

Two conclusions can be drawn from these studies: (1) The C_7SS micelles contain scattering length density inhomogenieties which may be explained by a core plus shell model; however, the model predicted from the Guinier analysis fails to reproduce the scattering curves. (2) The incomplete deuteration of the di-n-heptylsulfosuccinate may be responsible for the erroneous values obtained for the radii of gyration.

b. Study of Sulfosuccinate Micelles in the Absence of Salt. The external contrast variation method has been used by a number of workers for the determination of micellar structure both in the presence of supporting electrolyte[109] and in its absence.[112,119,120,128] Since S(Q) for all the solvent compositions is the same, the external contrast experiment depends only on the detailed geometry of the micelle, i.e., changing ρ_s will modify P(Q) without otherwise altering the charge or geometry of the micelles. If, for some reason, an unrealistic model gives agreement at one D_2O/H_2O ratio, then the model should not be able to fit the data for any of the other D_2O/H_2O ratios. Also, for a realistic model, the adjustable parameters should agree within experimental error from one composition to the next.

In this section, a different approach will be used to obtain structural information. Whereas in the previous section, the radii were obtained from Guinier analysis and an attempt was made to derive self-consistent R_g's through weighting factors obtained for the core plus shell model, here the full Q range will be fit using full form factors.

Recently, Sheu et al.[147] presented a new application of the external contrast variation technique for their determination of the structure of sodium orthoxylenesulfonate micelles. They analyzed their scattering curves using V_m, V_t along with the charge and aggregation number as variable parameters. Sheu et al.[147] found V_m to be 610 $Å^3$ and V_t to be equivalent to the volume of the dodecyl tail.

In order to determine a realistic model for the sulfosuccinate micelles, the method of Sheu and co-workers[147] was employed in the

analysis of the SANS data for 0.1 M C_7SS. Information gained from this analysis included the basic structural parameters, V_m and V_t, which are independent of concentration, and the number of solvent molecules associated with the surfactant monomer. Usually, solvent is introduced into the shell via hydration numbers that are, in the case of the sulfosuccinate surfactants, associated with the charged headgroup and counterion. However, this method does not allow for any additional water in the shell that may be associated with the ester moieties. In the model used here, the number of water molecules present in the shell are computed from geometrical considerations, i.e., from the difference between the overall volume and the product of the total dry surfactant and the aggregation number.

SANS measurements were performed on 0.1 M C_7SS solutions of varying D_2O/H_2O ratios (β = 1.00, 0.85, 0.70, 0.55) and of varying deuterated C_7SS/protiated C_7SS mixtures (γ = 0.0, 0.20, 0.40, 0.62, 0.85) in which, as before, only the tails were deuterated. Figure 28 shows the scattering obtained for the internal contrast measurements at 45°C

A core plus shell model was employed for the analysis of the scattering data, since this is consistent with the Guinier analysis in which the R_g values suggested scattering length inhomogenieties. The model was fashioned after the model of Sheu et al.[147] for the sodium ortho-xylene sulfonate micelles.

The micelles were modelled as spheres consisting of a hydrocarbon core surrounded by a hydrated outer shell. Three micellar models were used; the first model will be described in detail and then the

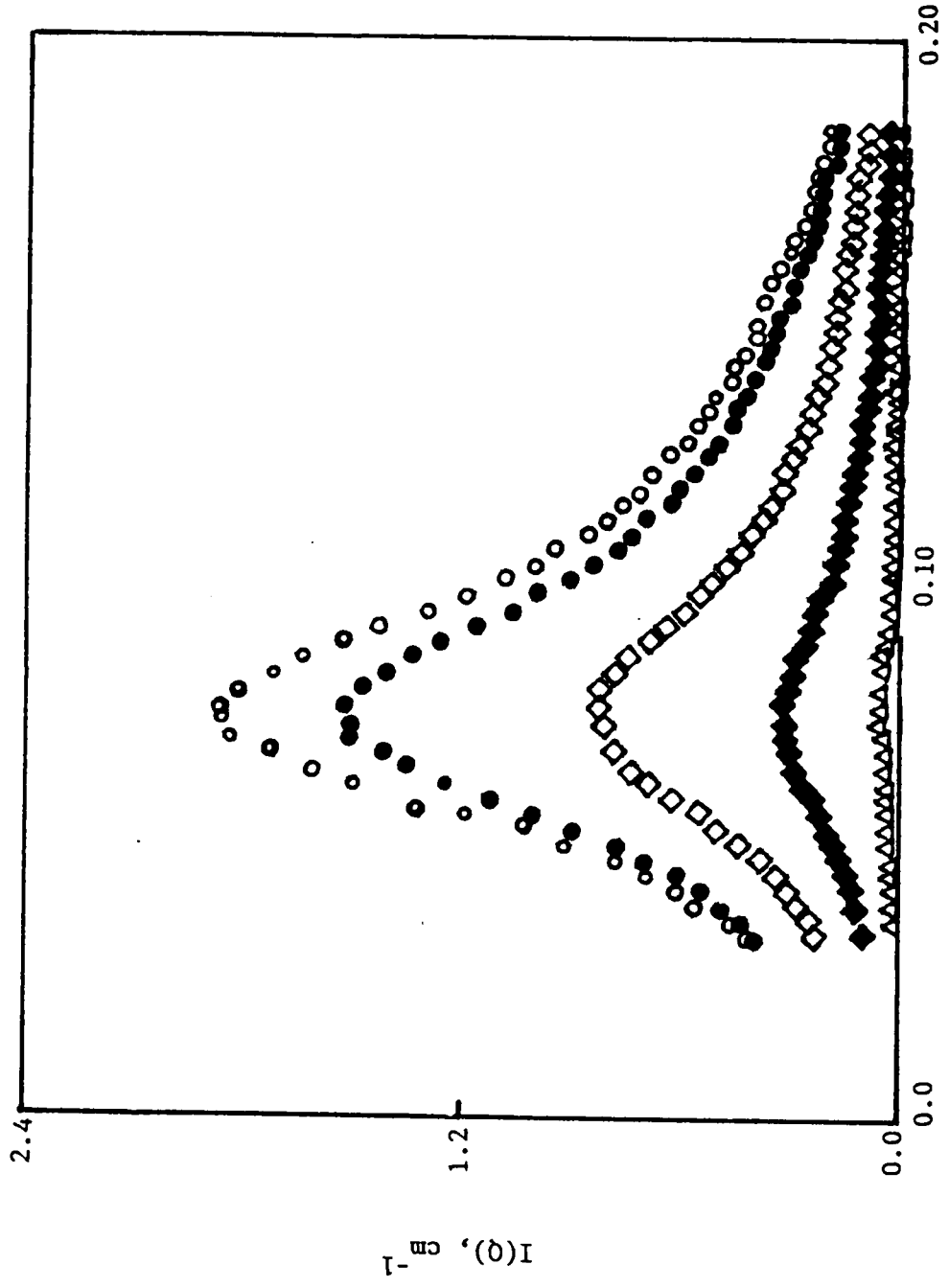

Figure 28. SANS data for 0.1 M as a function of γ.

differences between this model and the others will be outlined. In the first model, the outer shell contained a fraction of the alkyl groups, the headgroups, associated counterions and solvent; the remainder of the alkyl groups were placed in the core. V_t was set equal to the volume of the alkyl tails, in which the ester moieties were included as part of the alkyl tail; volumes used[122] along with hydration numbers are tabulated in Table X. This choice for V_t seemed reasonable in view of Sheu et al.'s results for the volume of the alkyl tail of the sodium ortho-xylenesulfonate micelles. The volume of the core was derived from $V_1 = \bar{n} \cdot V_t \cdot alf$ where alf represents the fraction of alkyl tails in the core. A range of values for alf was tested; an alf of 0.7 appeared to provide the best fits. R_1 was computed from $(3\ V_1/4\pi)^{1/3}$. The effective headgroup volume, V_h, came from $V_m - V_t$ where V_m was an adjustable parameter. The thickness of the shell, THIK, was then calculated from $(6.0*V_h/\pi)^{1/3}$. The overall radius was computed from $R_2 = R_1 + THIK$ and thus the overall volume of the micelle was known, $V_2 = (4/3)\cdot\pi\cdot R_2^3$. From the volume of the shell, $VV = V_2 - V_1$, the number of solvent molecules associated with the surfactant monomer, N_s, was determined from the volume that remained after accounting for the volume of the alkyl tails present, the headgroups and bound counterions. The scattering length density of the core comes from $\rho_1 = \Sigma ib_i/V_1$ and of the shell, $\rho_2 = \Sigma ib_i/(V_2 - V_1)$ where the summation extends to all the nuclei contained in the core and shell, respectively.

The other models differed from the first only by the manner in which R_1, V_1 and V_t were determined. For the second model, R_1 was set

TABLE X

GROUP VOLUMES AND HYDRATION NUMBERS

Group	Volume, $Å^3$	Hydration Number
CH_3	54.3	
CH_2	26.9	
CH	20.6	
CO_2	37.0	
OSO_3^-	70.2	4
SO_3^-	60.6	4
Na^+	-11.0*	6
$C222:Na^+$	567.0	0
D_2O	30.2	

*Electrostrictive volume used.

equal to 10.4, the extended length of the heptyl tail, and V_1 was computed from $V_1 = (4\pi/3)R_1^3$. V_t was then set equal to $V_1/\bar{n}\cdot alf$. For the third model, the core radius was calculated from the relationship $4\pi R_1^2 = 2\cdot\bar{n}\cdot 21.3\ \text{Å}^2$ where $21.3\ \text{Å}^2$ is the cross-sectional area per alkyl tail and the factor two accounts for the presence of the two alkyl tails. V_1 and V_t were calculated as in the second model.

A nonlinear least squares fitting routine was used in which $\bar{n}$, Z, V_m, A and B were adjustable parameters and the Hayter, Penfold and Hansen[92,94] analytical solution was used for S(Q). The factors A and B were necessary due to errors present in the calculated intensity, for example due to lack of precision in the calculated scattering length density, as well as in the experimental intensity. The scaling factor, A, corrected for uncertainty in the calibration for absolute intensity; A has no effect on the shape of the curve, only on its height. The value of this scaling factor can be used to assess the validity of the structural model; however, if A lies in the range $1.2 < A < 0.8$, the models cannot be distinguished. B is added to the equation to account for residual incoherent scattering.

Based on the spatial resolution of this SANS experiment, one model could not be chosen over the others; for example, the spatial resolution is not high enough to determine the exact location of the ester moieties. Since the first model gave consistently better CHI values (and values of A closer to one), this model will be used for the remainder of the discussion in this section. The results obtained using the first model are shown in Table XI. The values obtained from the

TABLE XI

MICELLAR PARAMETERS FOR 0.10 M C_7SS

	V_m	$\bar{n}$	Z	NS	ρ_2 x 10^{10}	ρ_s cm^{-2}
External Contrast Variation						
%β						
100	648.7 ±8.2	49.93 ±0.33	21.62 ±0.33	10.28	3.894	6.340
85	657.2 ±11.0	49.06 ±0.41	21.25 ±0.40	10.76	3.346	5.305
70	633.1 ±13.1	48.73 ±0.50	21.18 ±0.49	9.81	2.834	4.270
55	612.1 ±19.2	48.58 ±0.77	21.63 ±0.76	8.77	2.316	3.235
Internal Contrast Variation						
%γ						
20	648.4 ±8.0	50.29 ±0.39	20.17 ±0.33	10.19	1.797	4.295
40	648.9 ±8.5	49.60 ±0.46	19.41 ±0.36	10.33	2.816	4.583
62	642.2 ±7.1	49.40 ±0.49	18.65 ±0.36	10.09	4.194	4.999
85	651.9 ±23.5	48.22 ±1.90	17.12 ±1.16	10.69	5.640	5.344

$\rho_1 = 0.3108 \times 10^{10}$ cm^{-2}.

$\rho_s = 6.34 \times 10^{10}$ cm^{-2}.

external contrast series showed more scatter than did the values from the internal contrast series. For the external contrast series, V_m = 638 $Å^3$ and $\bar{n}$ = 49 and for the internal contrast series, V_m = 648 $Å^3$ and $\bar{n}$ = 49. This value of $\bar{n}$ is expected because micelles are smaller in the absence of salt than in the presence of salt.

The consistency of this model with the experimental data can be checked through a Q dependent quantity, A(Q) which is defined as

$$A(Q) = [I(Q)/P(Q)/S(Q)]^{1/2} \tag{82a}$$

$$= [(C - cmc)\bar{n}]^{1/2}(\Sigma b_i - V_m\rho_s) \tag{82b}$$

$$= A_o\cdot(\bar{n})^{1/2} \; |\Sigma b_i - V_m\rho_s| \tag{82c}$$

These equations show that A(Q) is a linear function of b_i and ρ_s. Plots of A(Q) vs. β for the external contrast data and of A(Q) vs. γ for the internal contrast data should yield straight lines if the proposed model is consistent with the experimental data. From the slope and intercept, values for V_m and $\bar{n}$ can be obtained.

For this analysis, I(Q) must be rewritten in the following manner:

$$I(Q) = (C\text{-}cmc)\bar{n}[\Sigma b_i - V_m\rho_s]^2 \; F(Q)^2 \; S(Q) \tag{82d}$$

where F(Q) is defined as

$$F(Q) = f\cdot 3\phi(QR_1) + (1 - f)\cdot 3\phi(QR_2) \tag{82e}$$

and

$$f = V_t (\rho_1 - \rho_2)/(\Sigma b_i - V_m \rho_s) \qquad (82f)$$

Values of A(Q) were computed; a plot of A(Q) vs. $(1 - \beta)$ and vs. γ is presented in Figure 29.

The values of V_m obtained from the analysis of A(Q) agree fairly well with the V_m from the fits for the internal contrast series: V_m obtained by this method was 658 $Å^3$ and $\bar{n}$ was 53. The agreement was not as good for the external contrast series: V_m obtained in this manner was 479 $Å^3$ and $\bar{n}$ was 94. These values were not surprising since the V_m values obtained for the external contrast series from fitting the full scattering curves exhibited a trend. This downward trend manifested itself in a lower V_m value from the A(Q) calculations.

On the average, ten water molecules were associated with each surfactant monomer; the hydration number calculated for this surfactant would be 8 (from (1-z/n) x 6.0 + 4.0; see Table X). These numbers are in fairly good agreement based upon the limited spatial resolution of these studies.

The remainder of this chapter will focus on the determination of micellar structure as a function of surfactant and supporting electrolyte concentration. The SANS data will be analyzed by fitting the whole scattering curve as in the previous section. Based upon the spatial resolution of these SANS experiments, several models could describe the micelles equally well. Therefore, in addition to the model outlined above (with $V_1 = \bar{n} \cdot V_t \cdot alf$), several models were used to fit the scattering curves. Each section will focus upon different aspects of the micellar structure; the following section includes models in which the

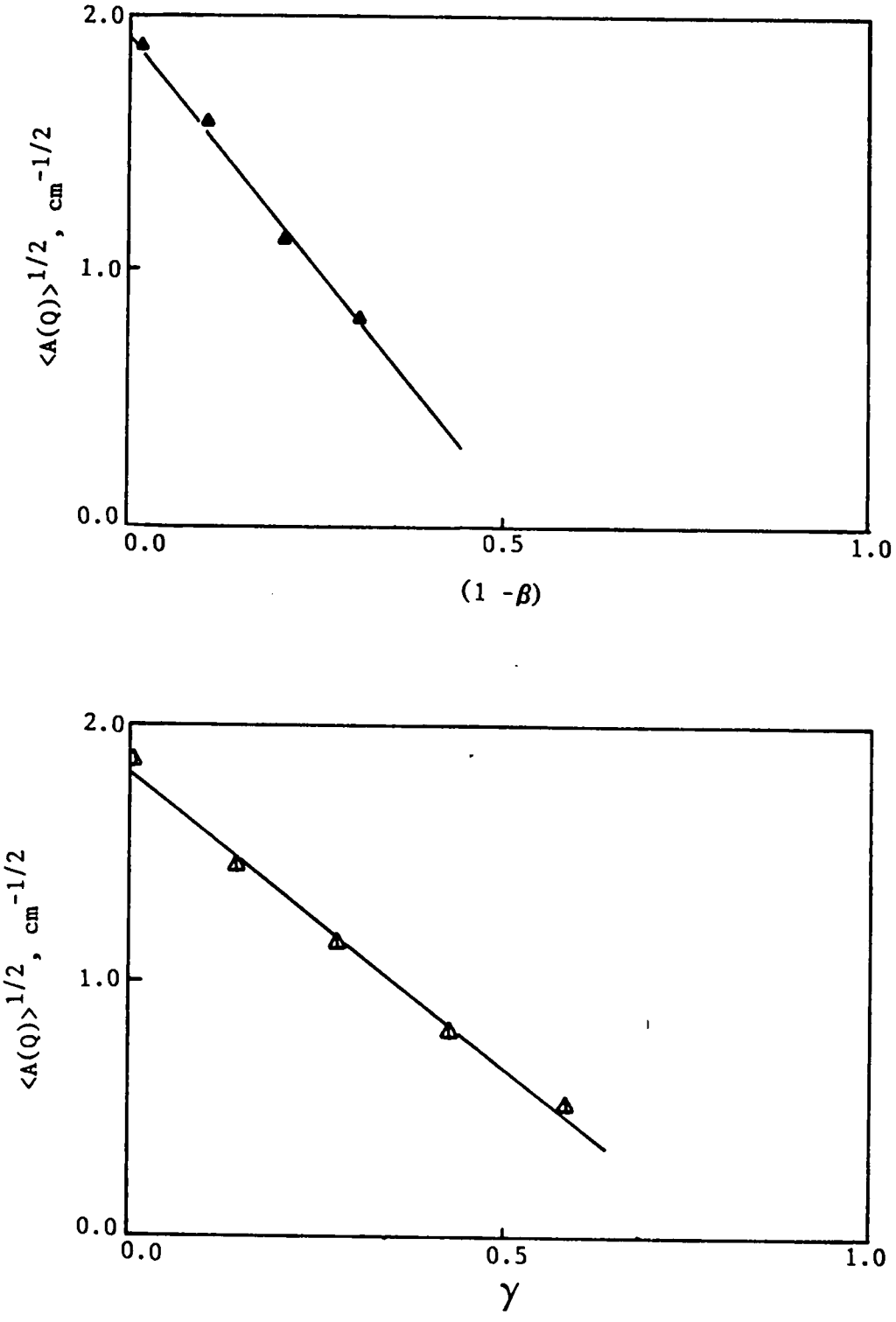

Figure 29. Plot of $\langle A(Q)\rangle^{1/2}$ versus (1 - β) and γ for 0.1 M C_7SS.

ester moieties are restricted to the shell and the last section deals with deviations from sphericity. External contrast measurements were performed to test the models and the results from these measurements will be presented in each section following the model discussions.

2. Concentration and Salt Studies

SANS experiments were performed on C_6SS, C_7SS and C_8SS as a function of surfactant concentration and added electrolyte. Figure 30 shows the scattering curves for the concentration study of C_6SS. As the amphiphile concentration increases, the interaction peak sharpens and moves to higher values of Q. The shift to higher Q values indicates a decrease in intermicellar distance and, therefore, an increase in the number of micelles. Typical scattering curves for C_7SS in the presence of added salt are shown in Figure 31; the main effect of the salt is to decrease the depression of the intensity at low Q.

At the lower concentrations, three additional core plus shell models for spherical micelles were considered in the analysis of the scattering curves (the micellar model derived using V_m as an adjustable parameter will be referred to as model A). Model 1 placed only the headgroups and bound counterions in the shell, thus the core contained the remainder of the surfactant molecule. The core was assumed to have a smooth surface; no water penetrated into the core. The shell contained a substantial amount of solvent; in fact, so much water was present that its scattering length density essentially matched that of the solvent, e.g., $\rho_2 = \rho_s$. The thickness of the shell was set equal to the diameter of the sulfonate headgroup, 4.9 Å. This model is denoted

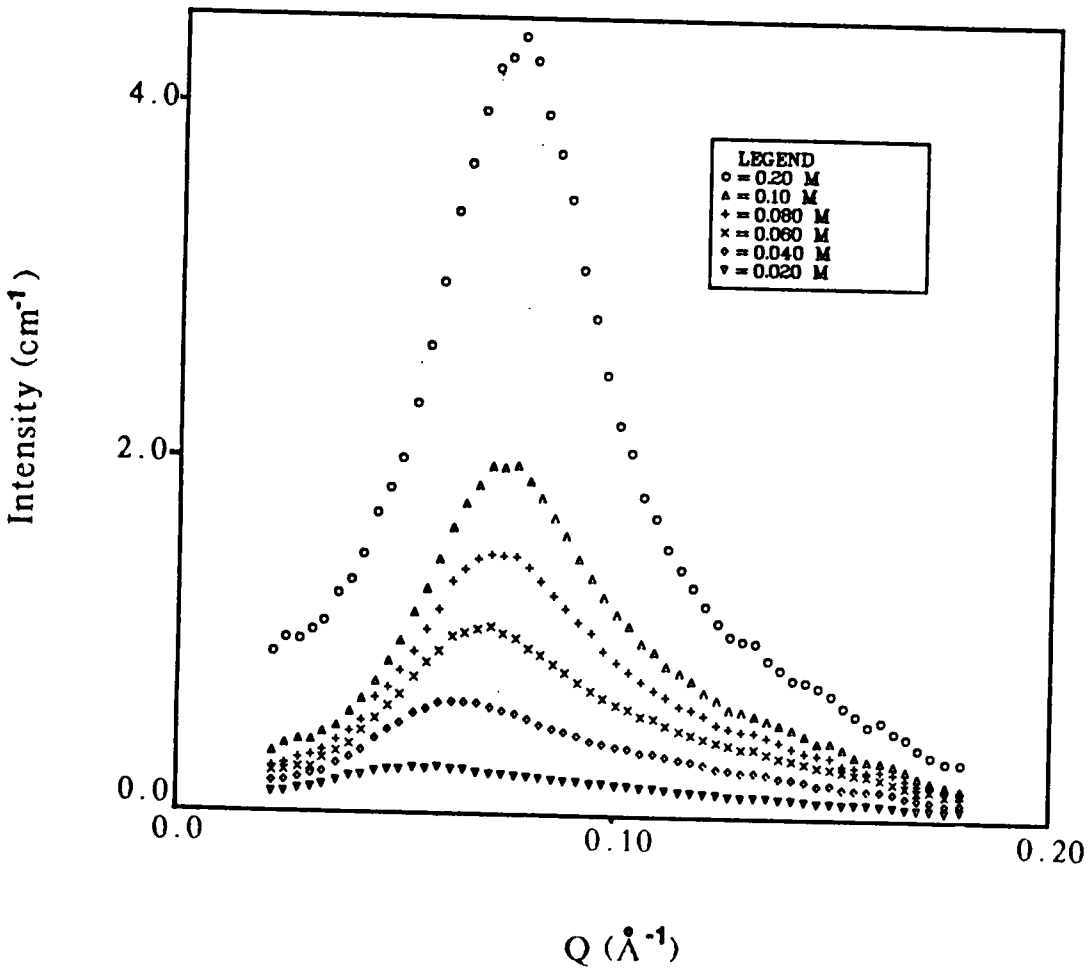

Figure 30. SANS curves for C_6SS as a function of concentration.

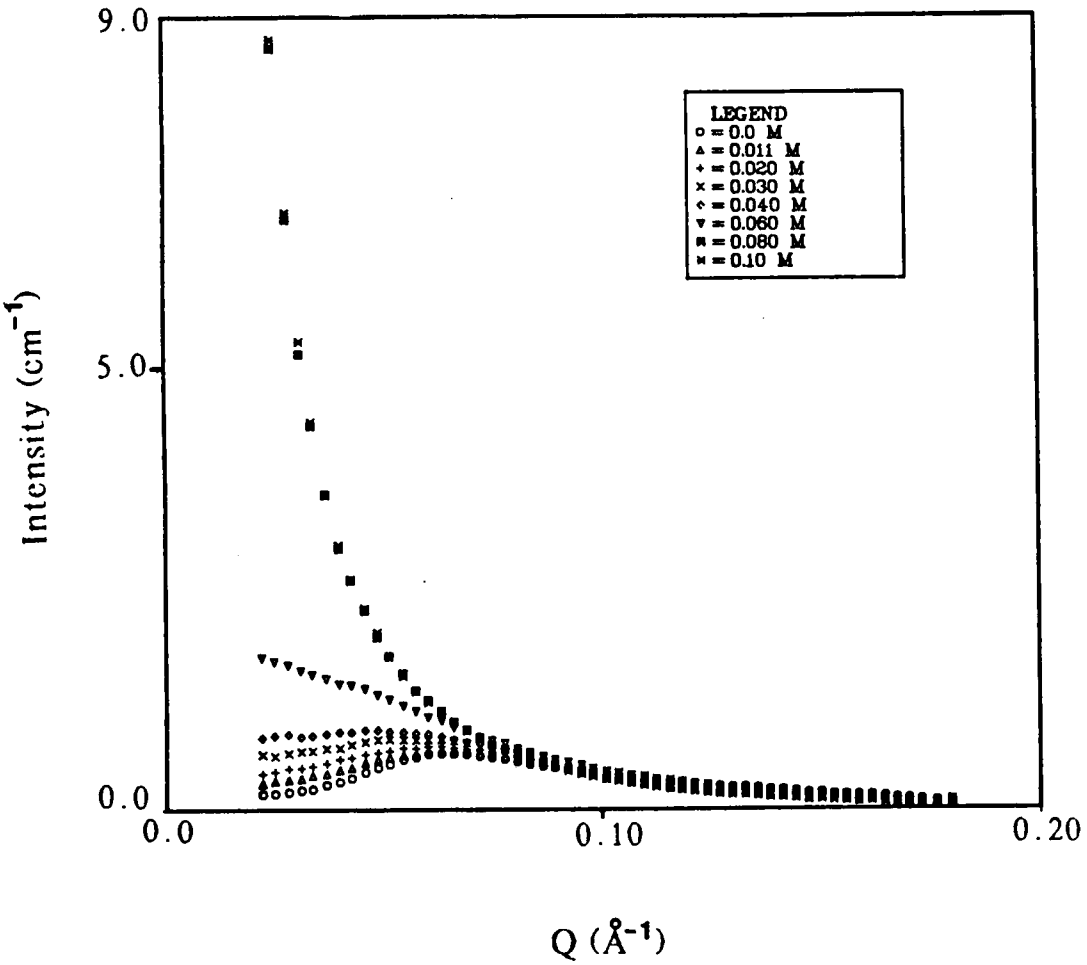

Figure 31. SANS curves for C_7SS as a function of NaCl concentration.

the dry core + "invisible shell" model. Models 2 and 3 placed a fraction of the alkyl groups into the core and the shell contained the remainder of the alkyl groups, the ester group moieties, the CH_2-CH-SO_3^- moiety and any bound counterions. Based on the results of the previous study, the hydration numbers present in Table X were seen as a good approximation for the number of water molecules associated with the surfactant monomer; therefore, these numbers will be used to introduce the solvent into the shell. The differences between models 2 and 3 were due to the determination of the radius of the core, R_1. For model 2, R_1 was set equal to the extended length of the alkyl chain, whereas in model 3, R_1 was calculated from the relationship $4\pi R_1^2 = 2 \cdot \bar{n} \cdot 21.3$ Å^2 where 21.3 Å^2 is the cross-sectional area per alkyl tail and the factor two is included to account for the presence of two tails. From equation 50, one sees that the micellar core is characterized by R_1 and ρ_1, and the shell is characterized by its thickness, $R_2 - R_1$, and its scattering length density, ρ_2. The calculations of these factors will now be presented. Once R_1 has been decided upon, the volume of the core is known from $V_1 = (4/3)\pi R_1^3$. The overall volume, V_2, was determined from group additivities,[57] where $V_2 = \bar{n} \cdot V_{tot}$ and $V_{tot} = V_{alkyl} + V_{CO2} + V_{SO3-} + V_{Na+} + V_{sol}$. β is the fraction of bound counterions (= 1 - Z/n) and hydration was calculated from 4.0 +6.0 (1 - Z/n). R_2 was then obtained from the overall volume ($R_2 = [(3/4\pi)V_2]^{1/3}$). ALFA, the average number of carbons per monomer present in the shell, was computed from geometrical considerations. A nonlinear least squares fitting routine was used in which Z, $\bar{n}$, A and B were adjustable parameters and

the Hayter, Penfold and Hansen[92,94] analytical solution was used for S(Q). It should be noted at this point that the Z obtained from this computation of S(Q) neglects the finite size of the counterion and, therefore, the values of Z presented in this dissertation from analysis of SANS data are only apparent charges.[123]

Tables XII, XIII, XIV list the results for the fits of the three models to 0.20 M C_6SS at various D_2O/H_2O compositions. The CHI values are seen to improve with increasing amounts of H_2O; this is simply a reflection of the poorer statistics obtained at higher % H_2O; due to the incoherent scattering obtained from H_2O, the error bars on the data points are larger for solutions containing larger amounts of H_2O and so the weighted fits appear better. Model 1 gave significantly poorer fits than did models A, 2 and 3 at 90% and 100% (actually 98%) D_2O. Also, more variation in the aggregation numbers were found in fits from model 1. The difference in the quality of fits for models A, 2 and 3 was not sufficient to support one model over the other (i.e., the arrangement of the ester moieties cannot be determined at this spatial resolution); to illustrate this, the fits using model 2 are reported. Figures 32-34 illustrate typical fits for the three surfactants studied. Tables XV, XVI, and XVII contain the tabulated results. For C_8SS, the cmc value suggested by the inflection point (see p. 46) was used in the calculations because fits using a cmc of 0.0011 M failed to converge. The values obtained at the lowest concentration are seen to agree well with the values determined by the EMF and conductivity data. The micelles of these double-tailed surfactants are seen to grow with increasing

TABLE XII

RESULTS OF MODEL 1 FOR 0.20 M C_6SS AT 45°C

% D_2O	R_1, Å	Z	$\bar{n}$	ρ_1 x 10^{10}	ρ_s cm^{-2}	CHI
100	17.8	15.1 ± 3.8	47.5 ± 4.3	0.424	6.20	3.29
90	17.7	15.4 ± 1.2	46.7 ± 1.3	0.424	5.65	2.06
80	17.6	15.3 ± 0.9	45.9 ± 0.9	0.424	4.97	1.69
70	17.6	15.7 ± 0.3	45.4 ± 0.3	0.424	4.28	1.12
55	17.4	16.0 ± 0.9	44.1 ± 0.8	0.424	3.24	1.20

$R_2 = R_1 + 4.9$ Å

TABLE XIII

RESULTS OF MODEL 2 FOR 0.20 M C_6SS AT 45°C

% D_2O	R_1, Å	Z	$\bar{n}$	ALFA	ρ_2 x 10^{10} cm^{-2}	ρ_s	CHI
100	19.94	17.1 ±0.5	42.4 ±0.6	9.71	2.70	6.20	1.65
90	19.86	17.5 ±0.8	42.1 ±0.6	9.69	2.47	5.65	1.72
80	19.77	17.3 ±0.4	41.5 ±0.4	9.66	2.56	4.97	1.31
70	19.75	17.8 ±0.6	41.5 ±0.5	9.66	2.03	4.28	1.33
55	19.63	17.9 ±1.7	40.9 ±1.1	9.63	1.70	3.24	1.38

$\rho_1 = -0.462 \times 10^{10}$ cm^{-2}; $R_1 = 9.0$ Å

TABLE XIV

RESULTS OF MODEL 3 FOR 0.20 M C_6SS AT 45°C

% D_2O	R_1, Å	R_2, Å	Z	$\bar{n}$	ALFA	ρ_2 x 10^{10}	ρ_s cm^{-2}	CHI
100	12.11	20.09	16.9 ± 0.5	43.3 ± 0.4	10.89	2.95	6.20	1.58
90	12.05	20.00	17.3 ± 0.6	42.8 ± 0.5	10.91	2.72	5.65	1.50
80	11.96	19.89	17.2 ± 0.3	42.2 ± 0.3	10.96	2.46	4.97	1.20
70	11.94	19.85	17.6 ± 0.5	42.1 ± 0.4	10.97	2.19	4.28	1.22
55	11.83	19.70	17.9 ± 1.6	41.3 ± 1.2	11.03	1.80	3.24	1.36

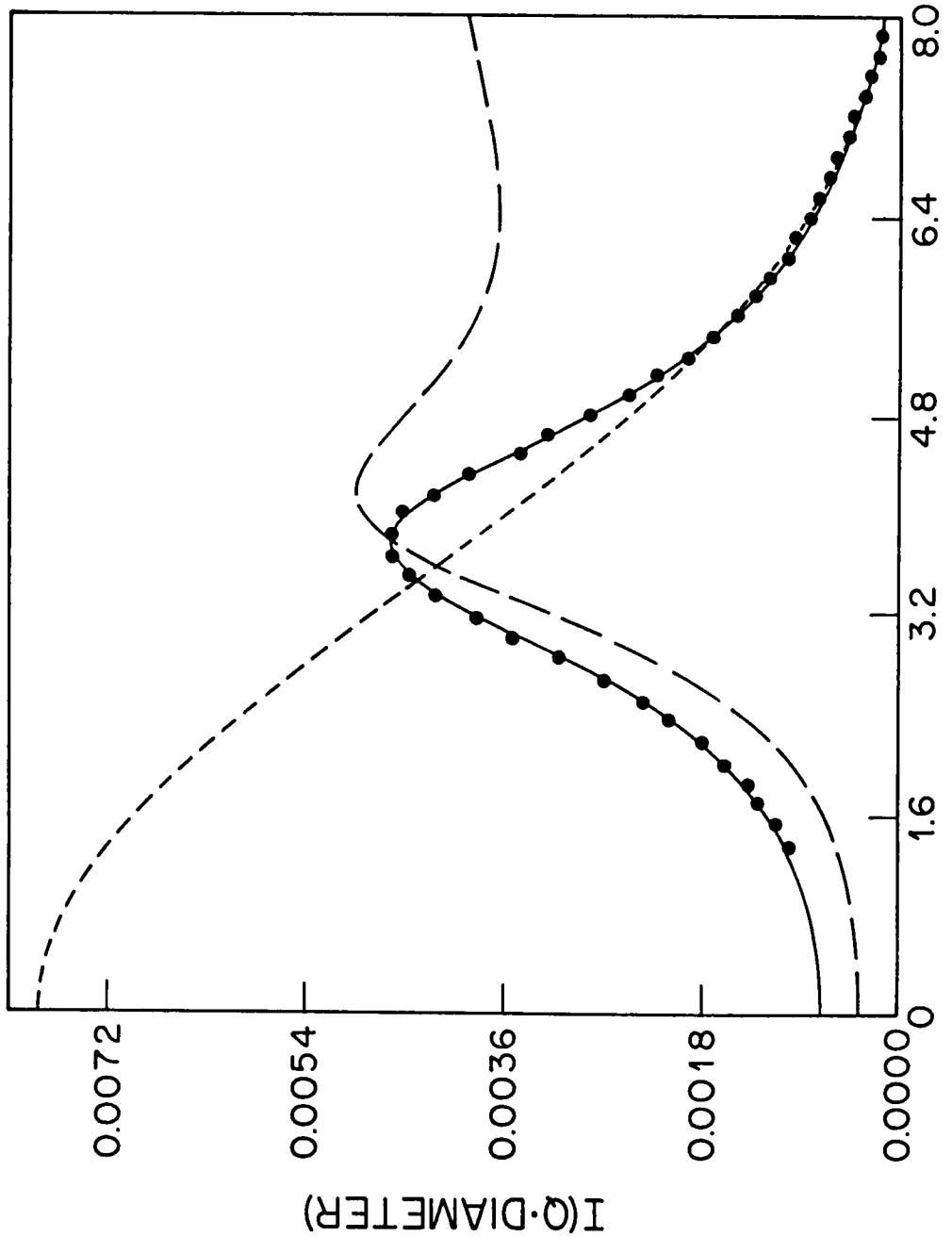

Figure 32. Fit to the experimental scattering curve using model 2 for 0.20 M C_6SS.

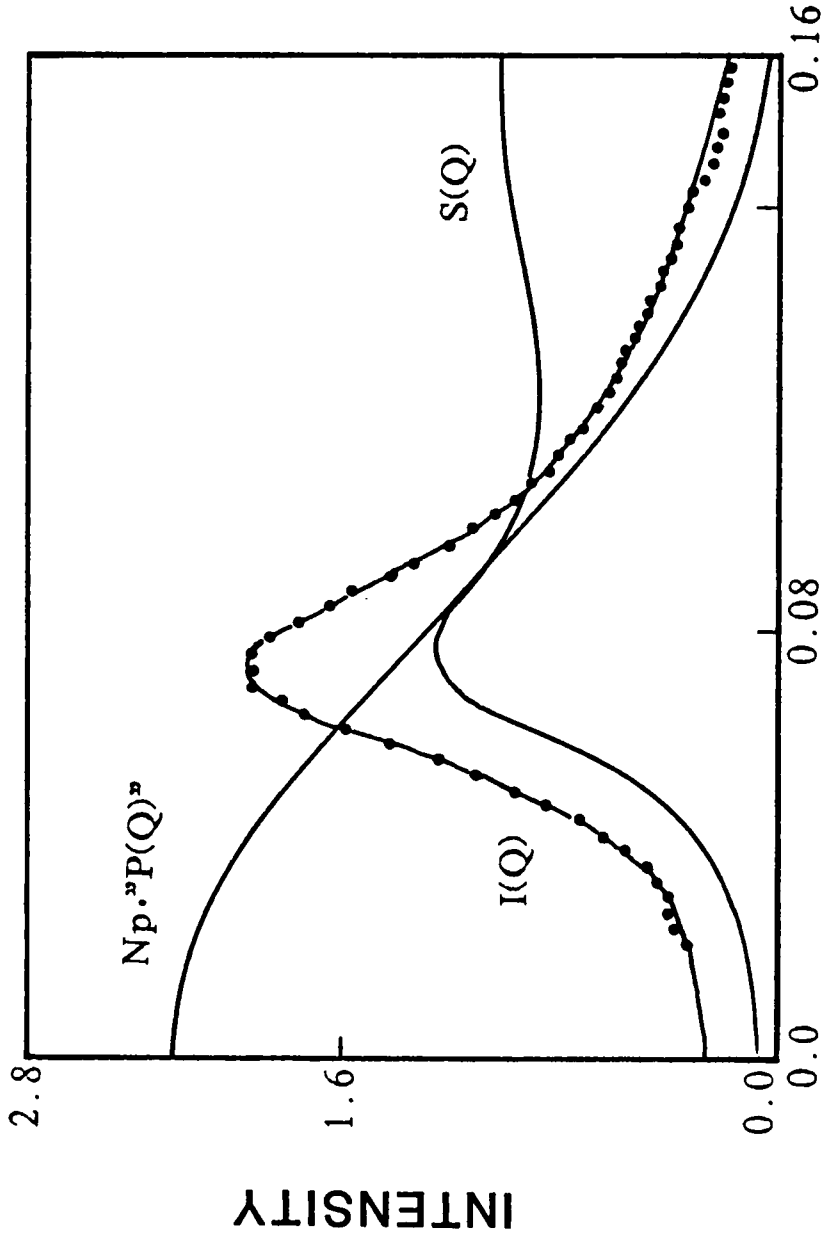

Figure 33. Fit to the experimental scattering curve using model 2 for 0.1 M C_7SS.

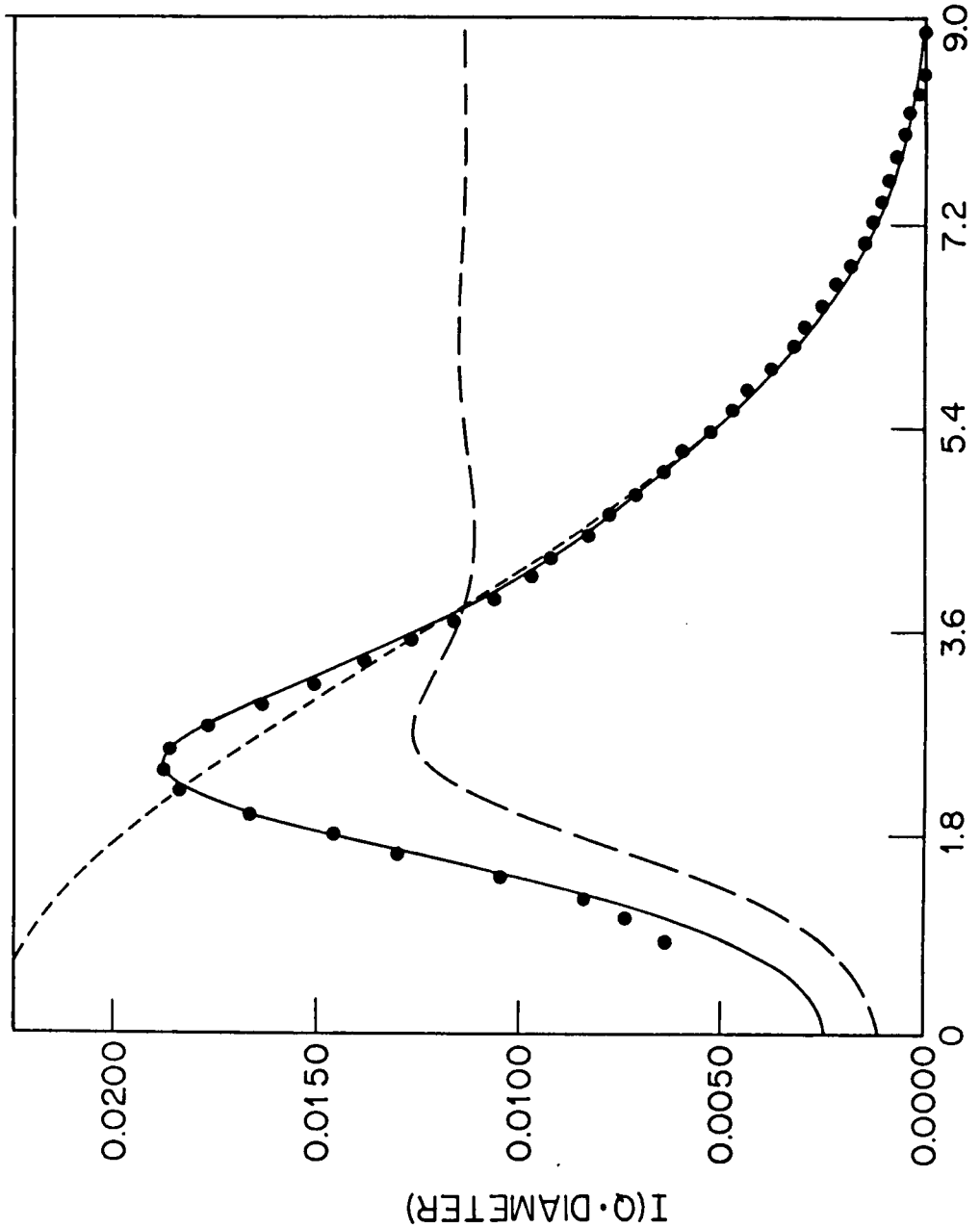

Figure 34. Fit to the experimental scattering curve using model 2 for 0.0343 M C_8SS.

TABLE XV

RESULTS OF MODEL 2 FOR C_6SS AT 45°C

Conc,M	R_2,Å	$\bar{n}$	Z	ALFA	10^{10} ρ_2,cm^{-2}
0.040	17.1	28.3	12.0	7.8	3.02
0.070	18.0	33.4	14.5	8.4	2.92
0.10	18.8	37.9	15.6	8.8	2.89
0.20	20.8	50.4	16.9	9.6	2.85
0.30	22.6	62.6	15.5	10.2	2.87
0.40	23.4	68.6	14.4	10.2	2.88

R_1 = 9.0 Å

TABLE XVI

RESULTS OF MODEL 2 FOR C_7SS AT 45°C

Conc,M	R_2,Å	$\bar{n}$	Z	ALFA	10^{10} $\rho_2 cm^{-2}$
0.020	17.0	25.3	13.9	7.96	1.80
0.040	18.3	32.0	18.4	9.21	2.58
0.060	19.2	37.0	21.3	9.87	2.50
0.080	20.2	42.3	23.1	10.4	2.46
0.10	21.2	48.5	14.9	10.8	2.44
0.20	25.7	83.7	24.4	12.2	2.50

R_1 = 10.4 Å

TABLE XVII

RESULTS OF MODEL 2 FOR C_8SS AT 45°C

Conc,M	R_2,Å	$\bar{n}$	Z	ALFA	10^{10} $\rho_2 cm^{-2}$
0.0110	20.5	41.7	10.7	10.0	2.91
0.0161	21.2	45.6	10.4	10.6	2.87
0.0214	21.9	50.6	11.4	11.0	2.81
0.0305	23.3	60.1	12.2	11.8	2.74
0.0343	24.1	66.5	12.1	12.2	2.72

R_1 = 11.5 Å

amphiphile concentration, as is expected. For 0.20 M C_7SS, the results are reported for fits using the model of a spherical micelle; the doubling of $\bar{n}$ from 0.10 M and the increase in CHI implies that deviations from sphericity are present at this concentration. Figure 35 shows the increase in $\bar{n}$ with increasing concentration for the three surfactants studied.

The effect of added NaCl on the aggregation numbers of 0.10 M C_6SS and 0.040 M C_7SS was determined. The addition of common ion salt screens electrostatic repulsions, causing micellar growth to occur; the rate of growth depends on the structure of the amphiphile. Figure 31 shows the scattering curves for the addition of salt to 0.040 M C_7SS; one sees that the presence of salt increases I(0) and that the interaction peak disappears at high added salt. As the electrostatic repulsions decrease, the system's isothermal compressibility is increased; this result is seen in the increase of S(0).

Tables XVIII and XIX list the results from the fits employing model 2 and Hayter, Penfold and Hansen's[92,94] analytical solution for S(Q) in the analysis. For both C_6SS and C_7SS larger increases in $\bar{n}$ are seen than is the case when salt is added to aqueous solutions of single-tailed surfactants. For 0.040 M C_7SS $\Delta n/\Delta[salt]$ = 970 whereas this value is 350 for SDS at its cmc.[125] The difference in behavior lies in the area per headgroup for these surfactant systems. Double-tailed surfactants, because of their bulky hydrocarbon regions, have larger area per headgroup requirements than do their single-tailed counterparts. The area per headgroup for C_7SS (estimated at the cmc) is 118 $Å^2$

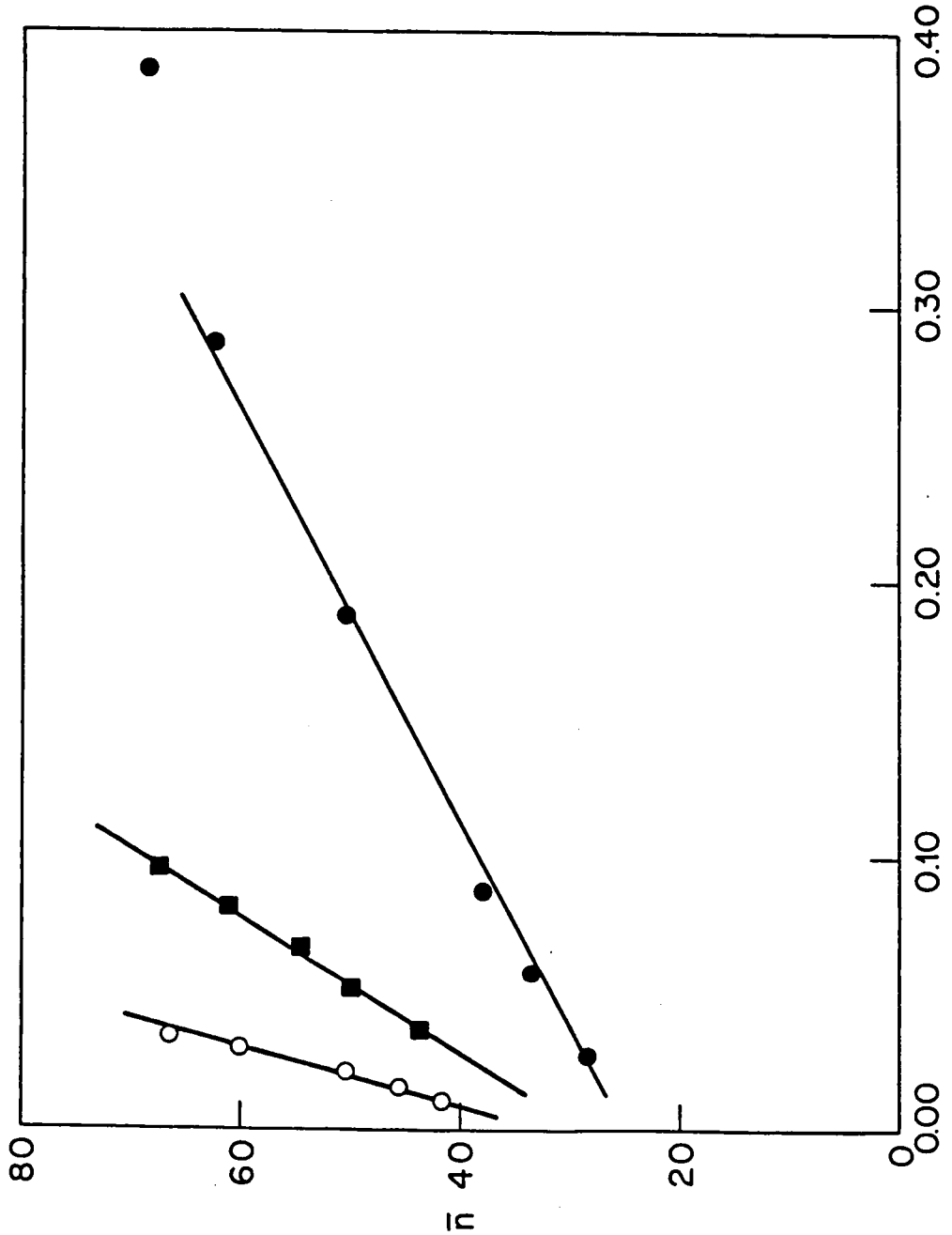

Figure 35. Micellar aggregation numbers versus surfactant concentration.

TABLE XVIII

EFFECT OF ADDED NaCl ON 0.10 M C_6SS AT 45°C

[NaCl],M	R_2,Å	Z	$\bar{n}$	ALFA	ρ_2, x 10^{10} cm^{-2}	CHI
-	18.3	16.6 ± 0.4	33.6 ± 0.3	9.11	2.65	1.15
0.024	19.4	15.4 ± 0.8	38.9 ± 0.8	9.50	2.69	1.51
0.059	21.1	13.8 ± 0.6	49.2 ± 0.9	10.0	2.73	1.35
0.094	22.6	11.4 ± 1.1	59.5 ± 2.3	10.4	2.77	1.69

TABLE XIX

EFFECT OF ADDED NaCl ON 0.040 M C_7SS AT 45°C

[NaCl],M	R_2,Å	Z	$\bar{n}$	ALFA	ρ_2, x 10^{10} cm^{-2}	CHI
-	18.3	18.4 ± 0.6	32.0 ± 0.4	7.96	2.80	0.91
0.011	19.8	15.8 ± 0.6	38.9 ± 0.6	10.1	2.64	1.26
0.020	20.9	15.8 ± 1.0	45.3 ± 1.2	10.6	2.63	1.50
0.030	22.5	15.4 ± 1.5	56.5 ± 2.0	11.3	2.62	1.59
0.040	24.5	12.9 ± 2.2	70.8 ± 3.6	11.8	2.63	1.83

while the area per headgroup for SDS at its cmc in the absence of salt is 62 $Å^2$.[125] A larger area per headgroup for the double-tailed surfactants leads to decreased repulsions and increased counterion dissociation; also an increase in the hydrocarbon-water contact at the micellar surface occurs. The addition of salt results in larger growth seen for the micelles formed from double-tailed surfactants due to the greater reduction of water contact that can result.

3. The Micellar Shape Transition Near the Micellar Solubility Limit

It was noted earlier that the proximate mesophase theory predicts that, as the micellar solubility limit is approached, the micellar shape should undergo a transition to form the precursor to that mesophase, e.g., disks are expected to be present before the lamellar mesophase. Tartar[126] and Tanford[34,127] considered the shape changes that can occur once the spherical micelle has reached its optimum size. In order to incorporate more monomers into the micelles, a distortion of the micellar shape is required. The micellar shapes had to meet the following requirements: (1) the semiminor axis may not exceed l_c and (2) the relationship $V/v = A/a_o = \bar{n}$ must be satisfied, where V is the total hydrocarbon core volume (v is the monomer hydrocarbon core volume) and A is the total surface area. Oblate and prolate ellipsoids satisfied the above requirements; however, the oblate form was slightly favored. Even at small values of the axial ratios, the ellipsoids have substantially larger maximum aggregation numbers than do the corresponding spheres.

Israelachvili et al.[30] have disputed the predictions of a sphereto-ellipsoid transition. The authors argue that the relationship $V/v = A/a_o = \bar{n}$ contains the volume and area of the whole spheroid, which was calculated from averaging the surfactant volumes and surface areas over the whole structure and thus, criterion (2) disguises the fact that the ellipsoidal form is energetically unfavorable almost everywhere. By applying a criterion which would indicate if the packing in a specific region was unfavorable, the authors found that "ellipses of revolution" having smoother edges and ends satisfied all the packing conditions. As the surfactant concentration is increased, the transition sphere→globule→toroid→finite cylinder is predicted for a single-tailed surfactant.

Magid et al.[128] demonstrated by SANS that the double-tailed surfactant $6PhC_{12}SNa$ did undergo a sphere-to-disk transition near its micellar solubility limit. The concentration limit for this surfactant at 45°C is 0.37 M; measurements were made up to 0.32 M. Only modest deviations from sphericity were found and, it was not until concentrations of 0.25 M and 0.32 M were reached, that distinctions could be made between the oblate and prolate form.

The sulfosuccinates, having lamellar liquid crystals as their first liquid crystalline phase, are also predicted to undergo a sphere-to-disk transition as the total concentration increases in the L_1 region, and the micellar solubility limit is approached. The micellar shape changes that occur can be detected through SANS experiments. C_6SS, C_7SS and C_8SS systems were studied to determine if the predicted transition

occurred; here, the surfactant concentrations studied were those at which ellipsoids were definitely present. This study focused upon the C_7SS system for reasons that will be evident shortly. The C_6SS and C_8SS systems will be considered briefly. The scattering curves were analyzed in the same manner as discussed in the previous section with different models being used for the calculation of P(Q). These differences, along the the results, are presented below.

For a direct comparison with the fits at lower concentration in the previous section, an ellipsoidal core plus shell model similar to model 2 for spheres was used to fit the C_6SS and C_8SS systems; the oblate form of this model will be described. Figure 36 illustrates the prolate and oblate ellipsoid forms. For this model, the core and overall semiminor axes were obtained from the molecular dimensions of the surfactant, which, for C_6SS are 9.0 Å and 19.0 Å respectively. The overall semimajor axis and axial ratio (ECC) came from the overall volume, V_2, where V_2 was computed from group volume additivity. The core semimajor axis was obtained from the difference between the overall semimajor axis and the thickness of the shell (10 Å for C_6SS). The solvent in the shell was introduced via hydration numbers and ρ_1 and ρ_2 were calculated in the usual manner. Equations 53a and 53b were employed in the calculation of P(Q) and Z, $\bar{n}$, A and B were used as the adjustable parameters.

In the case of C_6SS, deviations from sphericity were observed at higher concentrations and the results for the oblate fits are presented in Table XX. At 0.40 M C_6SS, the calculated overall ratio is only

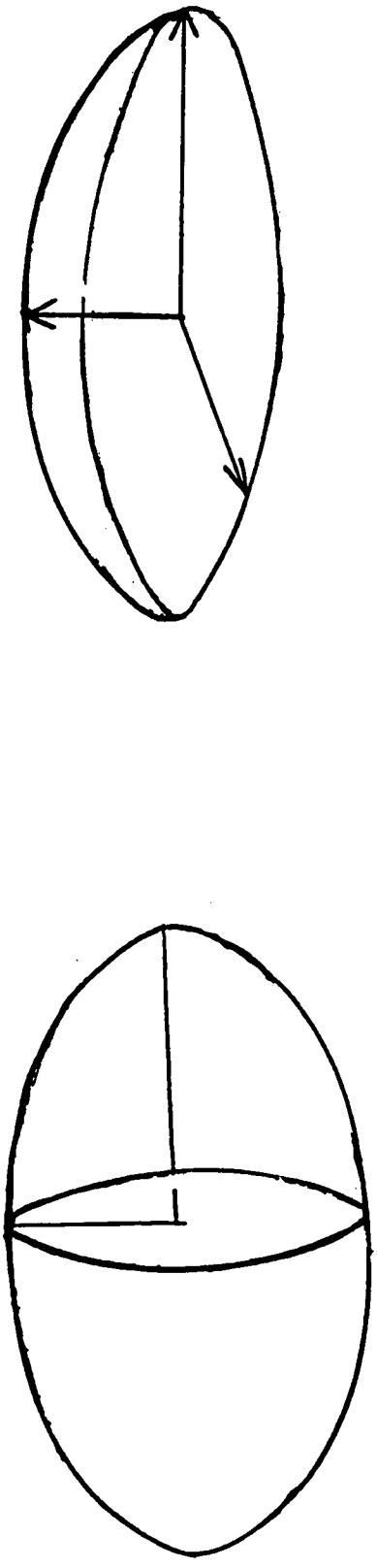

Figure 36. Comparison of prolate and oblate ellipsoids.

TABLE XX

OBLATE ELLIPSOID FITS FOR C_6SS

Conc., M	A_2, Å	A_1, Å	R_2, Å	Z	$\bar{n}$	CHI
0.20	12.4	22.4	21.2	16.4	50.1	1.53
0.30	15.5	25.5	23.1	15.0	63.7	1.02
0.40	17.2	27.2	24.1	14.4	72.0	1.06

0.779. Both oblate and prolate ellipsoids seem to describe the micellar shape equally well; differentiation between the models was impossible. In order to see substantial deviations from sphericity, one would have to go closer to the solubility limit.

The C_8 sulfosuccinate micelles were found to exhibit no deviations from sphericity; even at the highest concentration investigated, 0.041 M (which was quite close to its solubility limit), the fit to the spherical model was quite good (see Figure 33). To double-check for the existence of asphericity, a few fits were repeated for C_8SS using the above oblate model for P(Q); this model resulted in much poorer fits.

Due to the nonconclusive nature of the above studies, an extensive study of the sphere-to-ellipsoid transition was undertaken for C_7SS.

In addition to the model described above, three additional ellipsoid models were developed to analyze the scattering curves obtained for C_7SS. Table XXI outlines the four models which are discussed below for the prolate ellipsoid form. Scattering measurements were performed at three different SDD's for the concentration study in order to cover as large a Q range as possible.

The first model was similar to the dry core plus "invisible shell" model for spheres. In the same manner, the core consisted of all of the surfactant monomer except its headgroup and bound counterions, which resided in the shell. The thickness of the shell is 4.9 Å, e.g., the headgroup diameter, and $\rho_2 = \rho_s$. The parameters obtained for this model are as follows: the radius of the equivalent sphere, R_1, was determined once n had been determined ($R_1 = [(3/4\pi)\ V_1]^{1/3}$), where $V_1 = \bar{n}(V_{mon} +$

TABLE XXI

ELLIPSOID FITS USED FOR SANS ANALYSIS

Designation	Model 1	Model 2	Model 3	Model 4
Type	core + "invisible" shell	core + shell	core + shell	core + shell
Contents of Core	all alkyl groups, ester groups	fxn of alkyl tails (includes ester groups)	same as 2	same as 2
Determination of R_1	from $V_1 = \bar{n}\ (V_{mon}+V_{CH})$	from $V_1 = \frac{4\pi}{3}\cdot A_2^3\cdot ECC2$	from $V_1 = alf\cdot V_{TOT}$	from $V_1 = \frac{4\pi}{3}\cdot A_2\cdot ECC2$
Determination of R_2	R_1 + 4.9 Å	from $V_2 = \bar{n}\cdot V_{overall}$	from $V_2 = \bar{n}\cdot V_{overall}$	from $V_2 = \bar{n}\cdot V_{overall}$
Determination of A1		A1 = 20.4 (prolate) A1 = 20.4/ECC1/oblate)	from V_2	A1 = 20.4
Determination of ECCL		ECCL = $V_2\cdot 3/(4\pi\cdot A_1^3)$ (prolate) ECCL = $[(A_1^3\cdot\frac{4\pi}{3})/V_2]^{1/2}$	adjustable parameter	from $V_2/(4/3\pi\cdot/A_1^3)$
Determination of A2	from $(V_1\cdot 3/4\pi\cdot ECC2)^{1/3}$	from A_1 - THIK	from $(V1\cdot 3/4\pi\cdot/ECC2^{1/3}$	from A1 - THIK
Determination of ECC2	adjustable parameter	from $\frac{ECC1\cdot A1-THIK}{A2}$	adjustable parameter	from (ECCL·A1-THIK)/A2
Determination of THIK		THIK = 4.9 Å	THIK = A_2-A_1; $A_2\cdot ECC2-A_1^2\cdot ECC1$	adjustable parameter

$$V_{TOT} = \bar{n}(\Sigma(V_{CH_3} + V_{CH_2} + V_{CO_2}))$$

$$V_{overall} = \bar{n}\ (\Sigma(V_{CH_3} + V_{CH_2} + V_{CH} + V_{CO_2} + V_{SO_3^-} + \beta\cdot V_{Na^+} + + \delta\cdot V_{H_2O})$$

V_{CH}) and $V_{mon} = V_{CH3} + V_{CH2} + V_{CO2}$. $R_2 = R_1 + 4.9$ Å and V_2 was then derived from R_2: $V_2 = (4\pi/3)R_2^3$. The axial ratio of the core, ECC2, was an adjustable parameter and the semiminor axis, A2, was obtained from $A2 = (3V_1/4\pi\ ECC2)^{1/3}$. Both oblate and prolate forms were used.

Since model 2' corresponds to the model used for the analysis of C_6SS and C_8SS, only changes characteristic of C_7SS will be noted. Here, A1 = 20.4 Å, the extended length of the surfactant molecule and A2 = A1 - THIK, where the thickness of the shell, THIK, is equal to 4.9 Å, the diameter of the sulfonate headgroup. The fraction of the alkyl groups in the core was set equal to either 0.98 or 0.70 for these last three models. The remainder of the model is the same as for model 2.

Model 3' was characterized by an additional adjustable parameter, the axial ratio, which was assumed to be constant, e.g., ECC1 = ECC2. The core radius of the equivalent sphere was computed from the core volume where $V_1 = ALFA\ V_{tot}$ and $V_{tot} = \bar{n}\cdot V_{mon}$ (where $V_{mon} = V_t$). ALFA represents the portion of the hydrocarbon tails in the core; values of 0.70 and 0.98 were typically used for ALFA. R_2 and V_2 were obtained in the same manner as for model 2. Instead of setting A1 and A2 as in model 2', A1 and A2 were computed from ECC1 and ECC2: $A1 = (3V_2/4\cdot\pi\cdot ECC1)^{1/3}$ and $A_2 = (3V_1/4\cdot\pi\cdot ECC2)^{1/3}$. By varying the initial guess for the axial ratio, oblate or prolate forms were available. In addition, a variation on this model was used in which THIK (shell thickness) was constant; however fits using this model were very poor.

The parameters for model 4' are obtained in the same manner as for model 2' except THIK is an adjustable parameter. Model 4' was developed solely for prolate ellipsoids.

The prolate forms of the models were definitely preferred over the oblate forms; in some cases, the CHI values for the oblate fits were twice as large as those obtained for the prolate fits. Again, the spatial resolution did not permit the exclusion of any of the models; however, the prolate form of model 3', with an alf of 0.7, was found to provide the best fit to the scattering curves as based on the values obtained for A and CHI; Figure 37 shows the fit obtained for 0.156 M C_7SS in 70% D_2O, and Table XXII contains the results. The axial ratios obtained, even at this concentration, are quite large. Figure 38 shows the calculated fit using model 3' for 0.25 M C_7SS; deviations between the calculated and experimental curves are apparent at high Q. The results of fitting model 3' in the prolate form are presented in Table XXIII. Substantial growth is seen as the concentration increased from 0.147 M ($\bar{n}$ = 68) to 0.29 M ($\bar{n}$ = 121). The micellar charge is again seen to be constant over the concentration range. As the amphiphile concentration is increased, the values for CHI increase; the inability of the calculated intensity to match the experimental I(Q) at high Q is the source of the large CHI's. Computer simulations were undertaken therefore to arrive at an understanding of the large CHI values obtained using the ellipsoid model; also, a check for whether the data could be fit as well assuming the micelles were polydisperse spheres was in order.

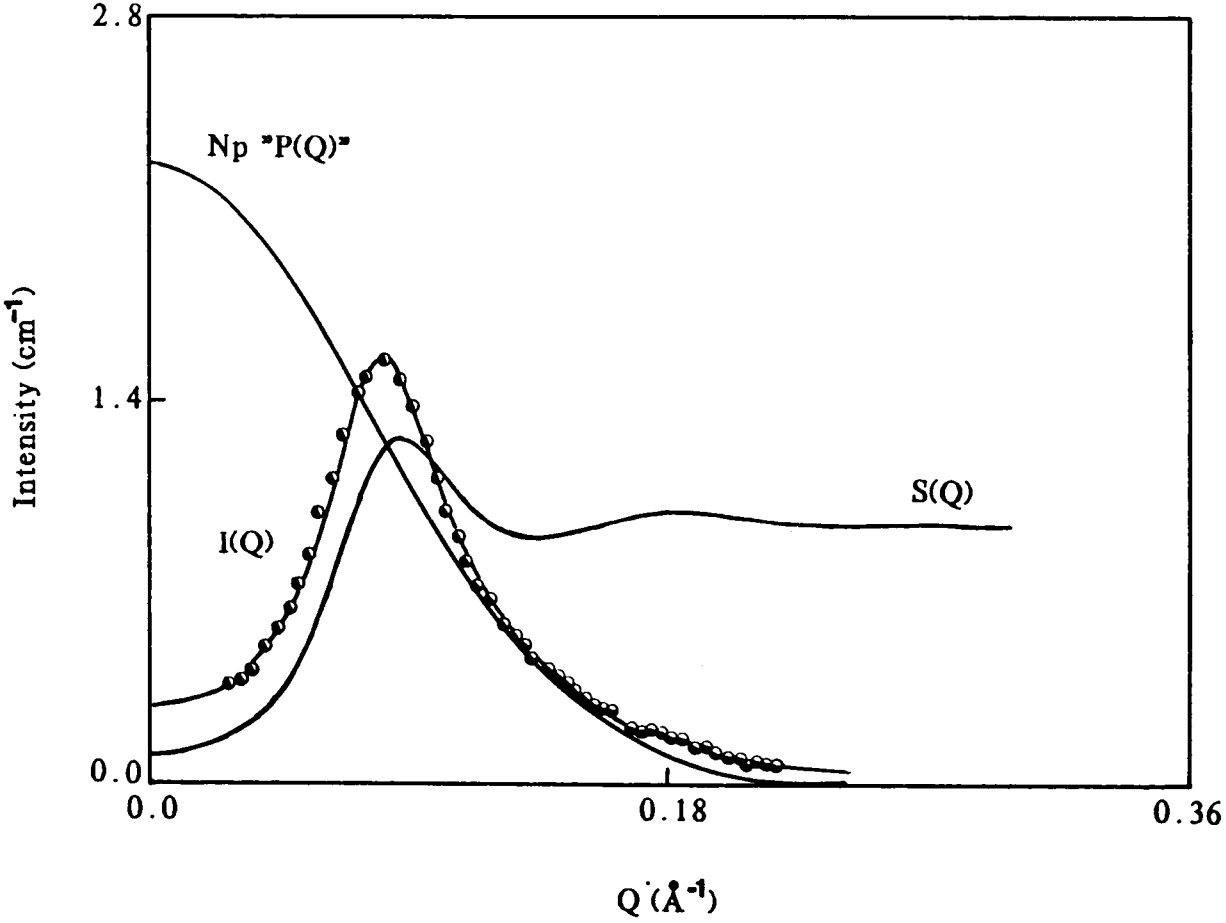

Figure 37. Fit to the experimental scattering curve using model 3' for 0.156 M C_7SS in 70 % D_2O.

TABLE XXII

RESULTS OF CONSTANT ECCENTRICITY MODEL FOR
0.156 M C_7 SULFOSUCCINATE AT 45°C
EXTERNAL CONTRAST

% D_2O	A_2,Å	A_1,Å	ECC,Å	R_2,Å	Z	$\bar{n}$	CHI
100	12.8	17.0	2.34 ± 0.07	22.5	16.0 ± 0.2	55.8 ± 0.3	1.88
85	12.8	16.8	2.34 ± 0.10	22.4	16.3 ± 0.2	54.8 ± 0.3	1.53
70	12.7	16.7	2.36 ± 0.19	22.2	16.2 ± 0.4	54.0 ± 0.6	1.19
55	14.1	16.7	2.34	22.2	16.8 ± 0.5	53.6 ± 0.9	1.02

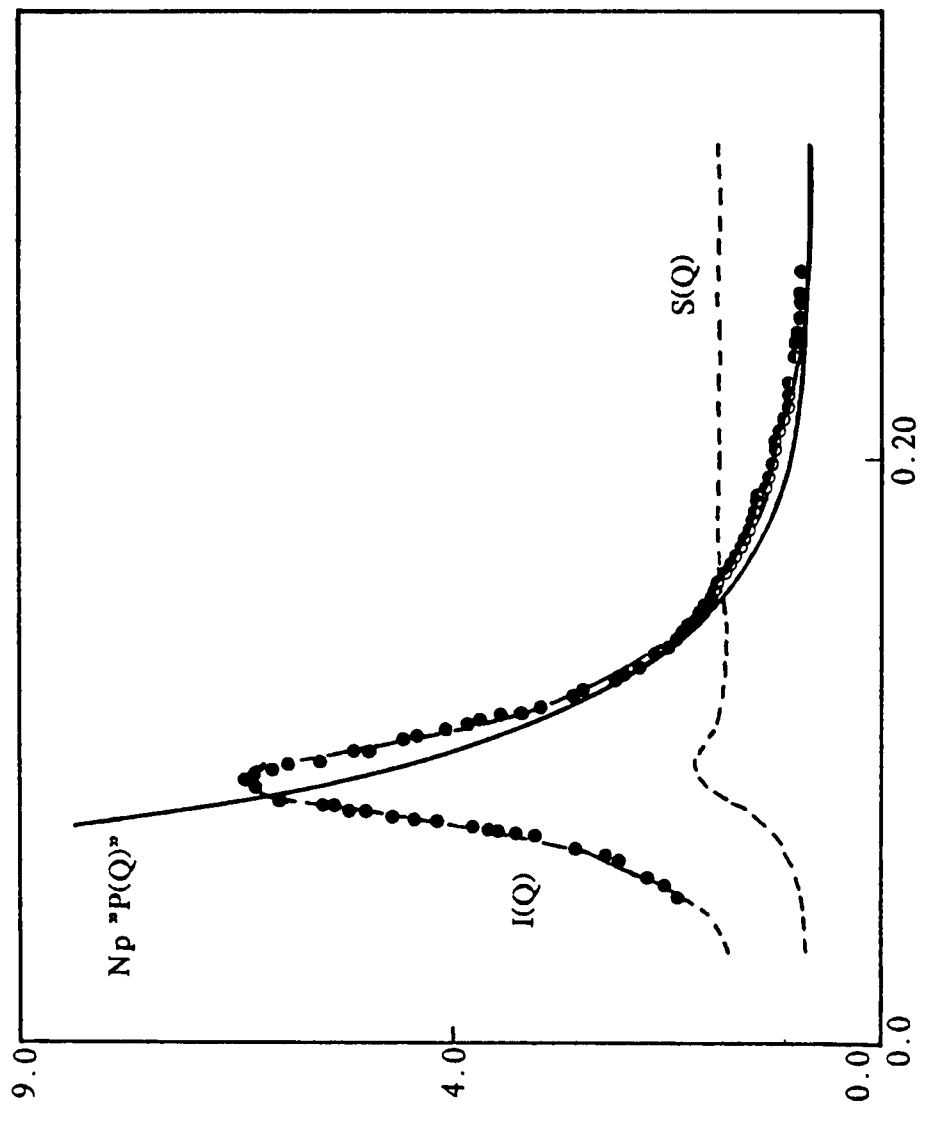

Figure 38. Fit to the experimental scattering curve using model 3' for 0.250 M C_7SS.

TABLE XXIII

RESULTS OF CONSTANT ECCENTRICITY MODEL
FOR C_7 SULFOSUCCINATE AT 45°C

$[C_7]$,M	A_2,A	A_1,A	ECC,A	R_2,A	Z	$\bar{n}$	CHI
0.147	12.5	16.5	3.09 ± 0.08	24.0	19.7 ± 0.5	67.6 ± 0.5	3.55
0.198	13.4	17.8	3.25 ± 0.09	26.4	19.5 ± 0.8	88.8 ± 0.9	5.23
0.250	14.0	18.3	3.40 ± 0.11	27.5	21.1 ± 1.0	104 ± 1	5.73
0.290	14.8	19.8	3.29 ± 0.12	29.4	19.4 ± 1.0	121 ± 1	6.73

Consider first the case of scattering from 0.156 M C_7SS in 70% D_2O. Figure 39 compares the experimental scattering curve with the simulated scattering curves obtained for an equivalent collection of mono- and polydisperse spheres. The curves are plotted as log I(Q) vs. Q in order to emphasize the high Q region. From the low Q region to the right of the interaction peak, all three curves match well; after this point, deviations occur. Oscillations resulting from the form factor for monodisperse spheres are apparent at high Q values, and one sees that the effect of polydispersity is to dampen these oscillations. Figure 40 illustrates the simulated scattering from micelles consisting of an ellipsoidal core plus shell (model 3') and from micelles consisting of an ellipsoidal core plus "invisible shell." These two models appear to match the experimental scattering curve better; however, at this level, one cannot distinguish between the two fits.

Due to the larger Q range covered for 0.25 M C_7SS in D_2O, greater deviations are seen in the tail of this scattering curve and the simulations presented in Figure 41 illustrate this. Obviously, the scattering from this system cannot be described as a collection of mono- or polydisperse spheres. The ellipsoid simulations are presented for 0.25 M C_7SS in Figure 42; the interaction peak appears to be more closely matched by the ellipsoid models, however, deviations are still apparent at high Q.

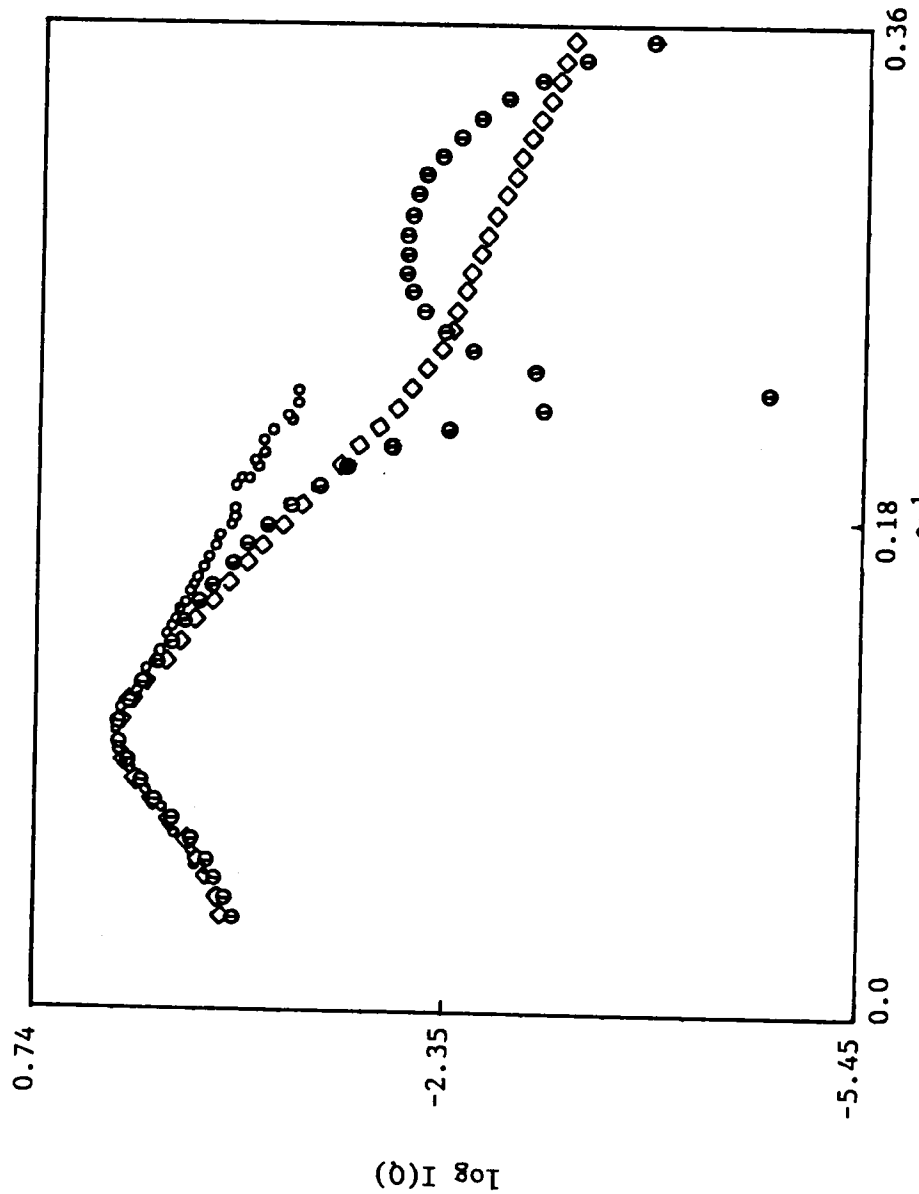

Figure 39. Computer simulations using spherical models for 0.156 M C_7SS.

circles: SANS data
slashed circles: monodisperse spheres
diamonds: polydisperse spheres

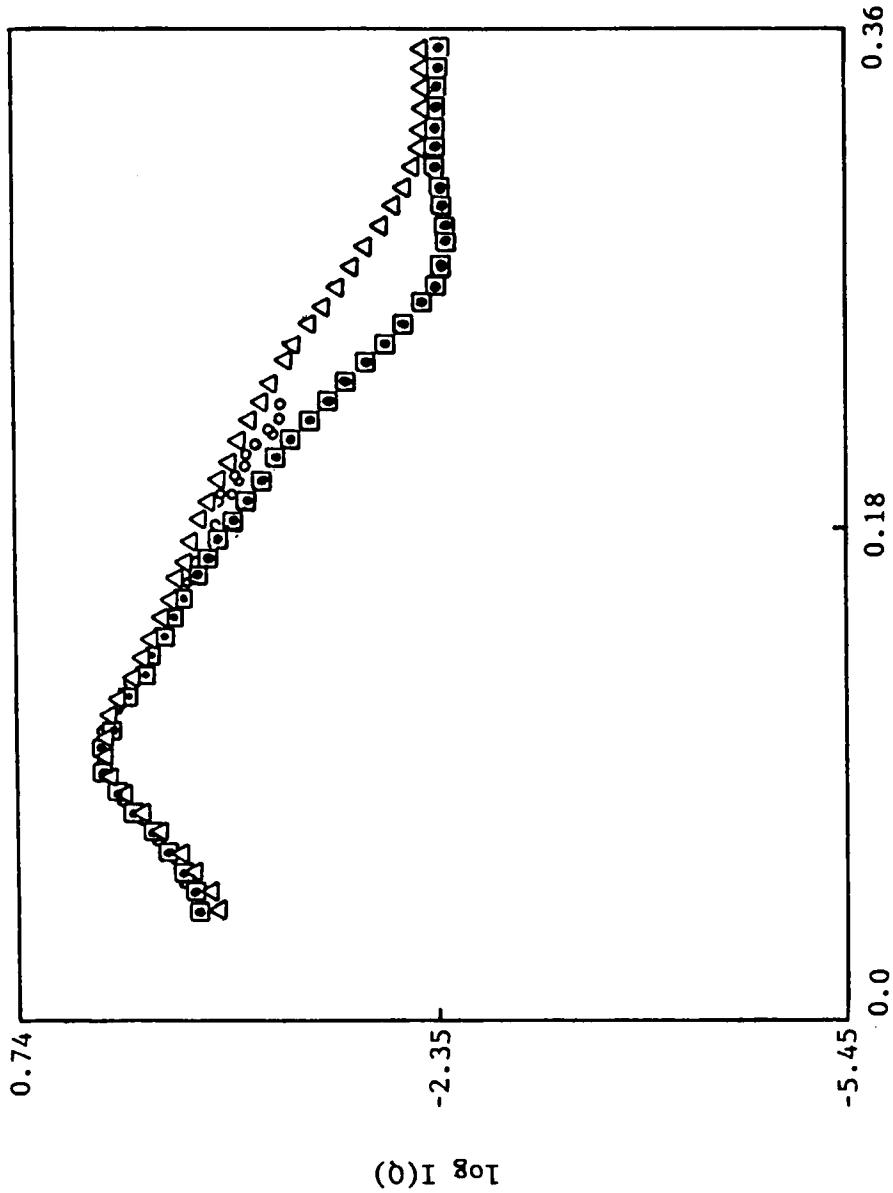

Figure 40. Computer simulations using ellipsoidal models for 0.156 M C_7SS.

circles: SANS data
triangles: ellipsoid core + "invisible" shell
squares: ellipsoid core + shell

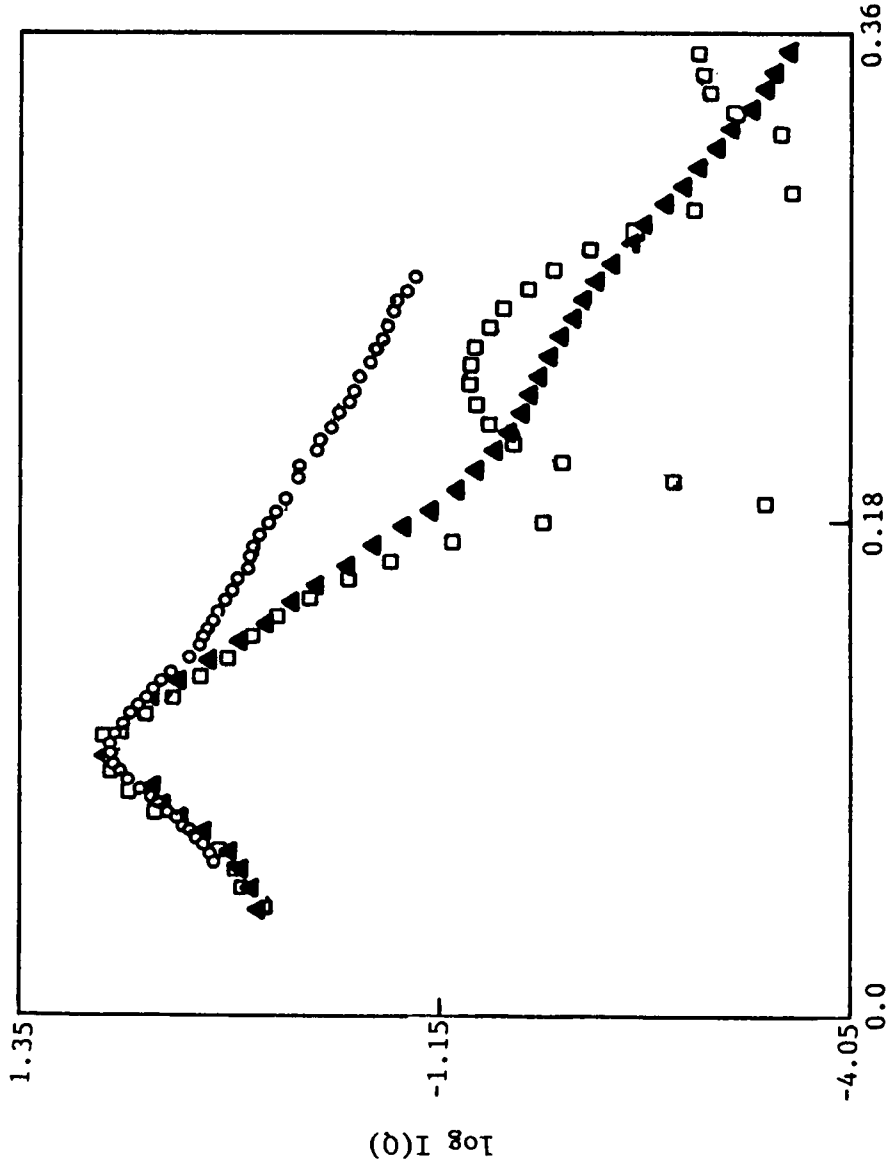

Figure 41. Computer simulations using spherical models for 0.250 M C_7SS.

circles: SANS data
squares: monodisperse spheres
trianges: polydisperse spheres

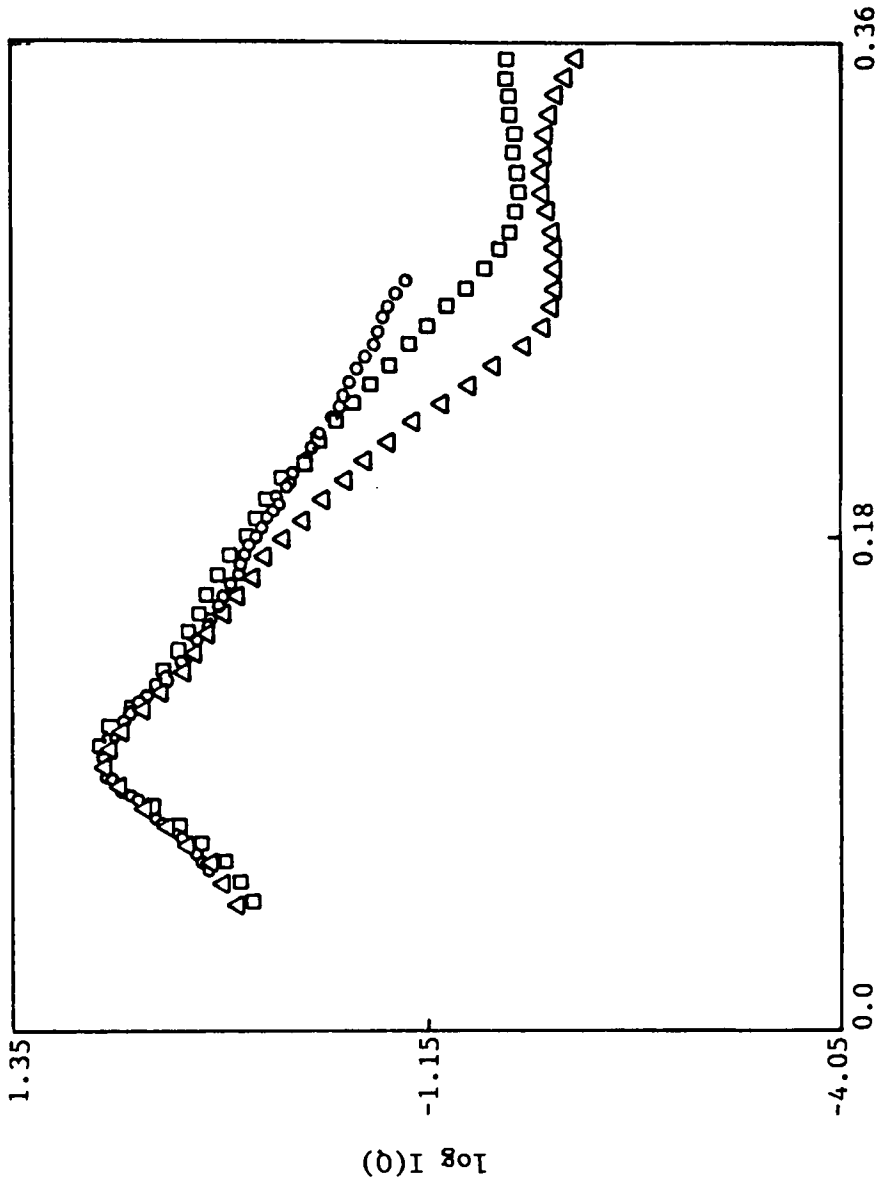

Figure 42. Computer simulations using ellipsoidal models for 0.250 M C_7SS.

circles: SANS data
squares: ellipsoid core + "invisible" shell
triangles: ellipsoid core + shell

CHAPTER V

CHANGES INDUCED IN C_7SS AND SDS MICELLES BY COUNTERION COMPLEXATION

A. Review of Counterion Effects

It is well known that changes in the counterion can alter the micellar structure. By changing the counterion of the dodecylsulfate system, Mukerjee et al.[5] determined the relationship between counterion size and extent of counterion binding. For inorganic counterions, it was determined that the smaller the radius of the hydrated ion, the greater the counterion binding. For hydrophobic counterions such as $(CH_3)_4N^+$, $(C_2H_5)_4N^+$ and $(n\text{-}C_3H_7)_4N^+$, hydrophobic bonding between the micellar surface and hydrocarbon region of the counterion overshadowed the ionic size effect; increased counterion binding resulted for these quaternary ions as the size of the hydrophobic region increased.

In general, micelles formed by cationic surfactants appear more sensitive to the nature of the counterion than do anionics; in fact, changes in micellar structure as well as changes in counterion binding can occur for cationic surfactants as a result of changing its counterion. The effect of the counterion on the micellar structure can manifest itself in one of two ways:

1. The counterion can bind strongly to the micellar surface, thereby reducing repulsions between headgroups effectively. This would result in decreasing the area per headgroup, a, and increasing the

surfactant packing parameter, v/al_c. For a spherical micelle, the resultant structural change would be to form a rod-like micelle.

2. The counterion can bind less tightly to the micellar surface, i.e., the counterion can sit further away from the surface than normal. This situation would lead to increased headgroup repulsions, increases in a and, therefore, a decrease in v/al_c. These increases in area per headgroup requirements mean that a change in aggregation number must occur. For spherical micelles, such a counterion would induce greater curvature and a decrease in micelle size would occur. However, for double-tailed surfactants of limited solubility in water, the effect of such a counterion may be a transition from lamellar liquid crystals to vesicles.

Examples of the first case include cetyltrimethylammonium surfactants with both inorganic and organic counterions. Inorganic ions such as NO_3^-, ClO_4^- and ClO_3^- are all effective at producing a sphere-to-rod transition.[129,130] The ability of these anions to screen charges has been correlated to their position in a lyotropic series for CTA micelles.[129,130] More substantial counterion effects are seen for cationic surfactants having either salicylate (Sal) or Cl-substituted benzoates as counterions. Micelles formed from cetylpyridinium Sal[8] and cetyltrimethylammonium (CTA) mono- and dichlorobenzoates[9] are larger and undergo a sphere-to-rod transition at lower concentrations than CTA micelles with inorganic counterions. In addition, viscoelastic solutions are obtained for cetylpyridinium Sal and for some CTA chlorobenzoates.

Counterions in the second category would include the highly hydrated hydroxide and acetate counterions. Evans and co-workers[132] studied the effect of these counterions on dodecyltrimethylammonium (DTA) surfactants; the cmc values were higher and mean aggregation numbers were lower than for the bromide form. Comparison of the extent of counterion dissociation, α, showed that α is higher for DTA with OH^- or OAc^- as counterions (76% or 69% *vs.* 26% for Br^-). As a result, larger headgroup areas are found for the hydroxide and acetate forms. The difference between the effects of added NaCl or NaBr to aqueous solutions of DTAB *vs.* DTAOH or DTAOAc is striking; only slow increases in aggregation numbers (up to 1 M added salt) are seen for DTAOH or DTAOAc, whereas aqueous solutions of DTAB form gels at 0.5 M added NaBr.

Even more dramatic results are obtained when the counterion of double-tailed cationic surfactants is replaced by hydroxide or acetate. Didodecyldimethylammonium (DDA) bromide is insoluble in water, forming a lamellar liquid crystalline phase which produces vesicles only upon prolonged sonication, whereas DDA surfactants with OH^- or OAc^- counterions are highly soluble in water, forming clear solutions of small micelles and fairly monodisperse vesicles.[133] The formation of a bimodal distribution of micelles and vesicles by DDAOH and DDAOAc solutions has been established by quasi-elastic light scattering (QELS),[133] electron microscopy[134] and video-enhanced differential interference contrast microscopy (VEDICM).[135] Unilamellar vesicles with diameters of 20-100 nm are found in 10^{-4} to 10^{-3} M solutions of DDAOAc; these vesicles collapse to micelles at DDAOAc concentrations between 10^{-2} M and

10^{-1} M.[132] Like the single-tailed surfactants with OH^- or OAc^- as counterions, these systems were relatively insensitive to added salt. Force measurements[132] as well as the micellar properties show that these micellar aggregates are almost fully dissociated. This low extent of counterion binding results in strong repulsive interactions between micellar aggregates as well as strong repulsions between headgroups. Evans et al.[132] showed that the hydroxide counterion is located on the average 4 Å further from the micellar surface than is Br^-.

Counterion effects on the micellar structure of anionic surfactants are normally quite small. Texas #1 in which the sodium counterion has been exchanged by hydronium ion is an exception; dispersions of the partially acidified form contain vesicles and/or small liquid crystalline spherulites.[135] The effect of counterion size on curvature is seen when the acidified form of Texas #1 is titrated with tetraethanolammonium hydroxide. This counterion sits further away from the micellar surface and, as a result, vesicles are produced.[135]

The complexation of counterions offers a unique method for changing the structure of anionic surfactants. Vikingstad and Bakken[136] found that the addition of crown ethers to aqueous solutions of sodium decanoate resulted in lower cmc values and smaller degrees of counterion dissociation. The results were interpreted in terms of complex formation between the crown ether and Na^+ and subsequent association of this complex to the micelle surface which reduced repulsions between headgroups. The decrease noted for the cmc's can also be attributed to the solubility of the hydrophobic molecules in the micelles. Similar

results were obtained for solutions of potassium dodecylsulfate to which crown ethers had been added.[137]

The addition of a cryptand, Kryptofix 2.2.2. (V) (4,7,13,16,21,24-hexaoxa-1,10-diazabicyclo[8.8.8]hexacosane) to aqueous solutions of

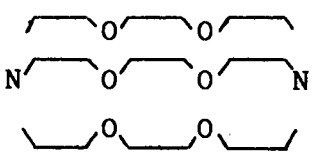

V (C222)

anionic surfactants[6,138] has shown more substantial effects. Evans et al.[6] found that the micellar behavior of aqueous solutions of sodium dodecylsulfate (SDS) containing C222 mimicked that of the didodecyldimethylammonium surfactants with strongly hydrated counterions; i.e., they found an increase in the area per headgroup, an increase in counterion dissociation and insensitivity to the addition of salt for solutions of SDS containing C222. The decrease in the cmc value was attributed to nucleation of the micelles by excess C222.

B. The Effect of Addition of Kryptofix 2.2.2. Upon Structures of SDS and Sodium Di-n-Alkylsulfosuccinate Micelles

A systematic investigation of the effect of addition of a macrocyclic ligand to solutions of double-tailed anionic surfactants, specifically C_7SS, was undertaken. Three techniques were employed to assess the structural changes incurred by counterion complexation: conductivity to determine the effect on the cmc and counterion binding; SANS

to obtain structural information, i.e., micellar shape and size; and fluorescence quenching to obtain a separate determination of aggregation numbers. The question of vesicle formation for $C_{10}SS$:C222 was addressed through the use of VEDICM. SANS provided a thorough characterization of the SDS:C222 micelles formed, and this, in turn, provided a basis upon which to compare results for the C_7SS:C222 micelles.

The importance of the study of these systems by SANS is two-fold. First, the possibility of a constant size for the C_7SS:C222 micelles would give a system which mimics covalent polyelectrolyte solutions. As seen from the SANS results in Chapter IV, C_7SS aggregates are smaller and more highly charged than their single-tailed counterparts. If their behavior parallels that of SDS, then the addition of C222 to C_7SS should draw the counterions further away from the micellar surface, inducing greater curvature which would result in smaller micelles with higher degrees of counterion dissociation. Secondly, since certain properties of micelles formed in the presence of C222 are salt invariant,[6] the assumption can be made that the micellar structures remain the same even upon addition of alkali halides. A salt study of this nature would be an excellent method to check the MSA solution of Hayter and Penfold for a broad range of potentials.

1. Conductivity of C_7SS:C222

Conductivity measurements were performed for C_7SS solutions with and without C222 at 45°C (for details see p. 38); experimental results for C_7SS:C222 system are shown in Figure 43. Kryptofix 2.2.2. was seen to lower the cmc for C_7SS; however the cmc decrease is not as

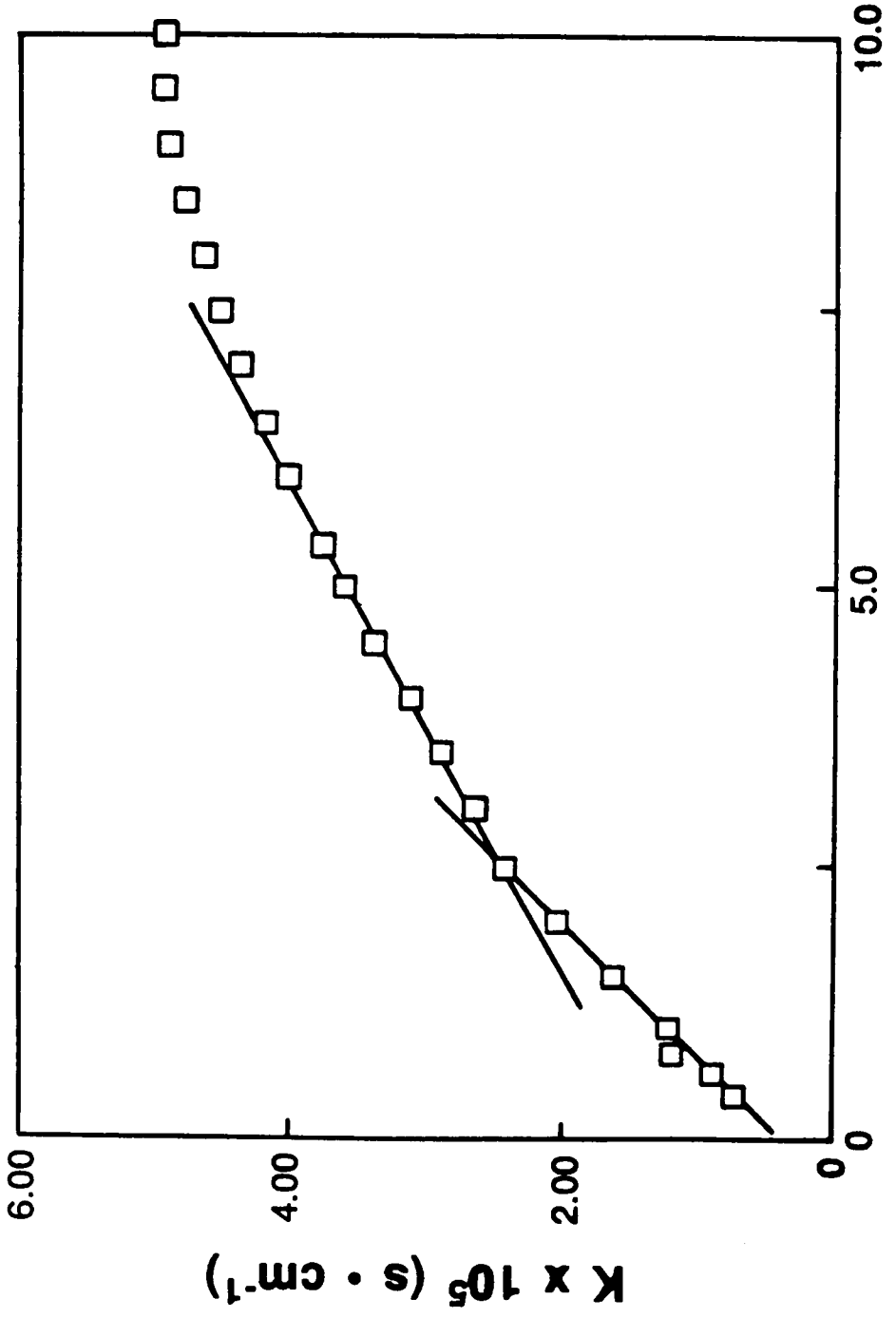

Figure 43. Plot of specific conductivity versus concentration for $C_7SS:C22$.

substantial as that seen for SDS in the presence of macrocyclic ligands.[6,136,137] The degree of counterion dissociation was computed from the Evans equation (p. 46);[61] Table XXIV lists experimental values obtained for C_7SS:C22 solutions along with results for SDS:C222. Opposite effects in are seen for SDS:C222 and C_7SS:C222; β decreases upon addition of C222 to SDS solutions and increases when the cryptate is added to C_7SS solutions. In Figure 43 β is seen to approach values of one for C_7SS:C222 solutions where the concentration is greater than 9.0 x 10^{-3} M.

2. Fluorescence Quenching Measurements

Since this technique was employed primarily as a check for SANS results, a detailed background will not be presented. The method of Turro and Yekta[139] was used; several assumptions must first be made in order to employ their analysis: (1) the fluorescent probe and quencher are associated with the micelle longer than the unquenched lifetime of the probe; (2) the quenching of an excited molecule by a quencher is much faster than the fluorescence decay so that the observed fluorescence is from micelles with no quencher molecules present; (3) a Poisson distribution of the probe and quencher molecules in the micelles is assumed. If these assumptions hold, then the measured intensity in the presence and absence of quencher can be used to determine the mean aggregation number for the micelles. The relationship between the measured intensities and the quencher concentration, [Q], is

$$(I/I^{o}) = \exp\{-[Q]/[M]\} \qquad (85)$$

TABLE XXIV

CMC'S AND DEGREES OF COUNTERION BINDING FOR SOLUTIONS OF SDS AND C_7SS CONTAINING C222

Surfactant	T, °C	cmc, mol/L	β	
SDS	25	0.0080	0.82	Evans[6]
SDS:C222	25	0.0016	0.52	Evans[6]
C_7SS	45	0.0040	0.52	
C_7SS:C222	45	0.0025	0.64	

where I_o and I are the total intensities of fluorescence in the absence and presence of quencher respectively and [M] is the mean concentration of micellar aggregates which is defined as

$$[M] = ([Surf] - [\text{free monomer}])/\bar{n} \quad (86)$$

[free monomer] = cmc. Substitution of equation 86 into equation 85 yields

$$\ln (I^o/I) = [Q]\bar{n}/([Surf] - cmc) \quad (87)$$

Aggregation numbers for C_7SS and C_7SS:C222 solutions were determined by measuring I_o/I as a function of surfactant and salt concentration employing the luminescent probe $Ru(bipy)_3^{2+}$ and the quencher 9-methylanthracene. A typical plot of $\ln I_o/I$ vs. [Q]/([surf]-cmc) is shown in Figure 44 for C_7SS (aggregation numbers are obtained from the slope) and a compilation of the results is presented in Table XXV. Aggregation numbers are observed to increase in the presence of C222 for C_7SS; this effect is opposite to that found with the SDS:C222 systems.

3. Small-Angle Neutron Scattering Measurements

Changes in micellar structure caused by C222 addition to SDS and C_7SS solutions were determined by SANS measurements at several concentrations of surfactant and salt. SDS and C_7SS in D_2O were investigated at 25°C and 45°C respectively, with and without C222. Surfactant and cryptate were present in a 1:1 molar ratio at all times. The concentration range studied for SDS was 0.025 M to 0.50 M and, for C_7SS, 0.05 M to 0.25 M.

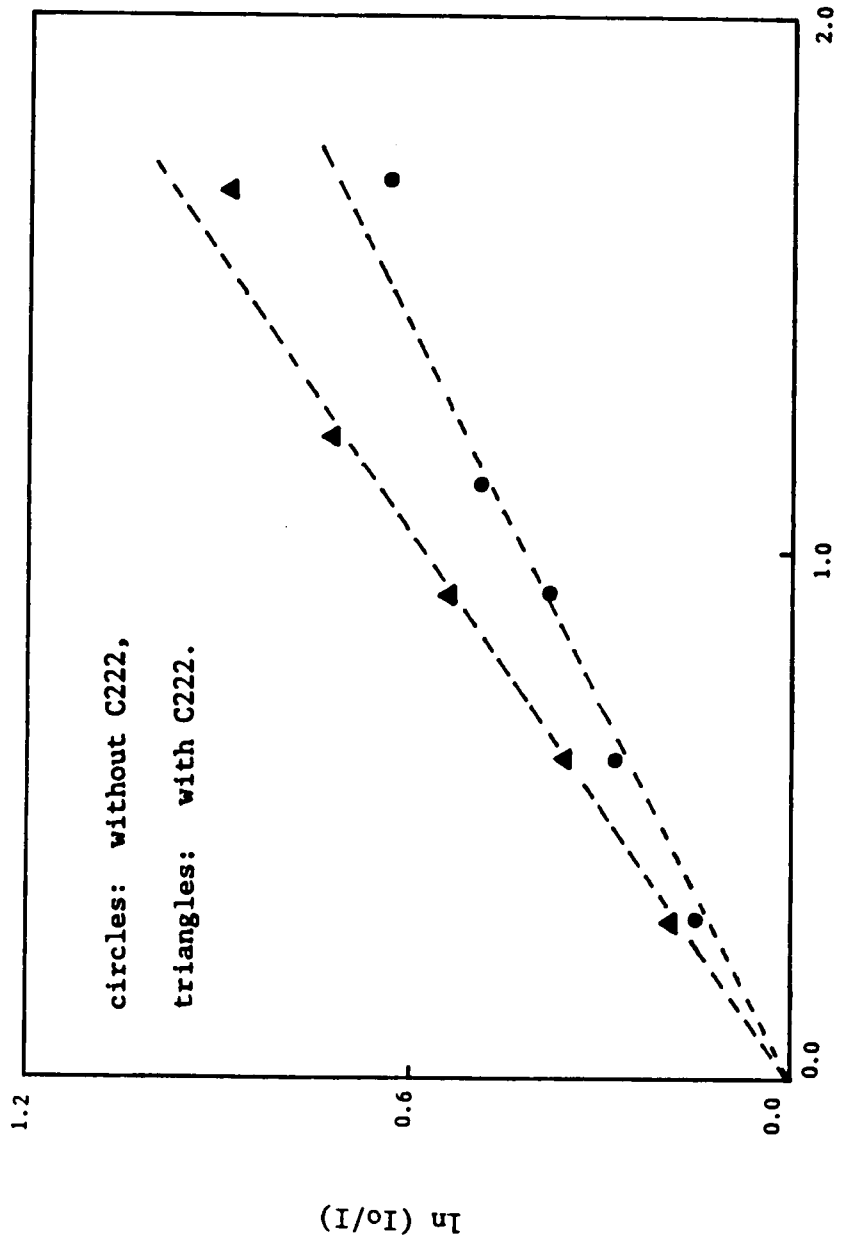

Figure 44. Plot of $\ln(I_o/I)$ versus $[Q]/([surf] - cmc)$ for 0.10 M C_7SS.

TABLE XXV

AGGREGATION NUMBERS OBTAINED FROM FLUORESCENCE QUENCHING MEASUREMENTS

Composition, M	$\bar{n}$	$\bar{n}$ (SANS)
0.10 C_7SS	58.7	50.4
0.05 C_7SS	46.3	35.8
0.03 C_7SS	37.0	30.8
0.20 C_7SS:C222	>117.7	
0.10 C_7SS:C222	78.4	56
0.05 C_7SS:C222	52.1	40
0.03 C_7SS:C222	45.3	
0.03 M C_7SS +		
0.009 NaCl	41.5	
0.017 NaCl	54.4	
0.032 NaCl	53.4	48.9
0.066 NaCl	>105.6	
0.03 M C_7SS:C222 +		
0.017 NaCl	51.3	50.0
0.032 NaCl	54.9	59.5
0.066 NaCl	82.0	
0.111 NaCl	98.9	

The experimental curves were fit as in Chapter IV using a weighted nonlinear least-squares fitting routine using equations 45 and 50 with micellar charge, z, micellar mean aggregation number, $\bar{n}$, A and B as adjustable parameters. Since models used for describing C_7SS micelles have been discussed in detail in Chapter IV, only the models employed for SDS micellar systems will be addressed here. However, before any curve-fitting is attempted and, therefore, before any assumptions concerning the aggregate shape are made, the effect of counterion complexation can be assessed by comparison of how the scattering curves change upon the addition of C222. Figure 45 shows a typical scattering curve for each of the systems investigated. The addition of C222 to SDS solutions increased Q_{max}; since a increase in Q_{max} corresponds to a decrease in intermicellar distance, smaller micelles must be present. For the addition of C222 to C_7SS solutions, a decrease in Q_{max} is seen. This decrease corresponds to a increase in intermicellar distance; therefore, larger micelles are present in solutions containing C222.

For simplicity, SDS in D_2O will be considered first. Hayter and Penfold's[112] model for SDS micelles was determined to provide the best fit for the scattering curves. At SDS concentrations below 0.1 M, a core-plus-shell spherical micellar model was used whereas at higher concentrations better fits were obtained using the prolate ellipsoidal model 3' of Chapter IV. For the spherical micelles, the alkyl tails were present in the core, the diameter of which was equal to the extended length of the C_{12} chains (16.7 Å). The core volume and scattering length density were computed from group volume additivity; a

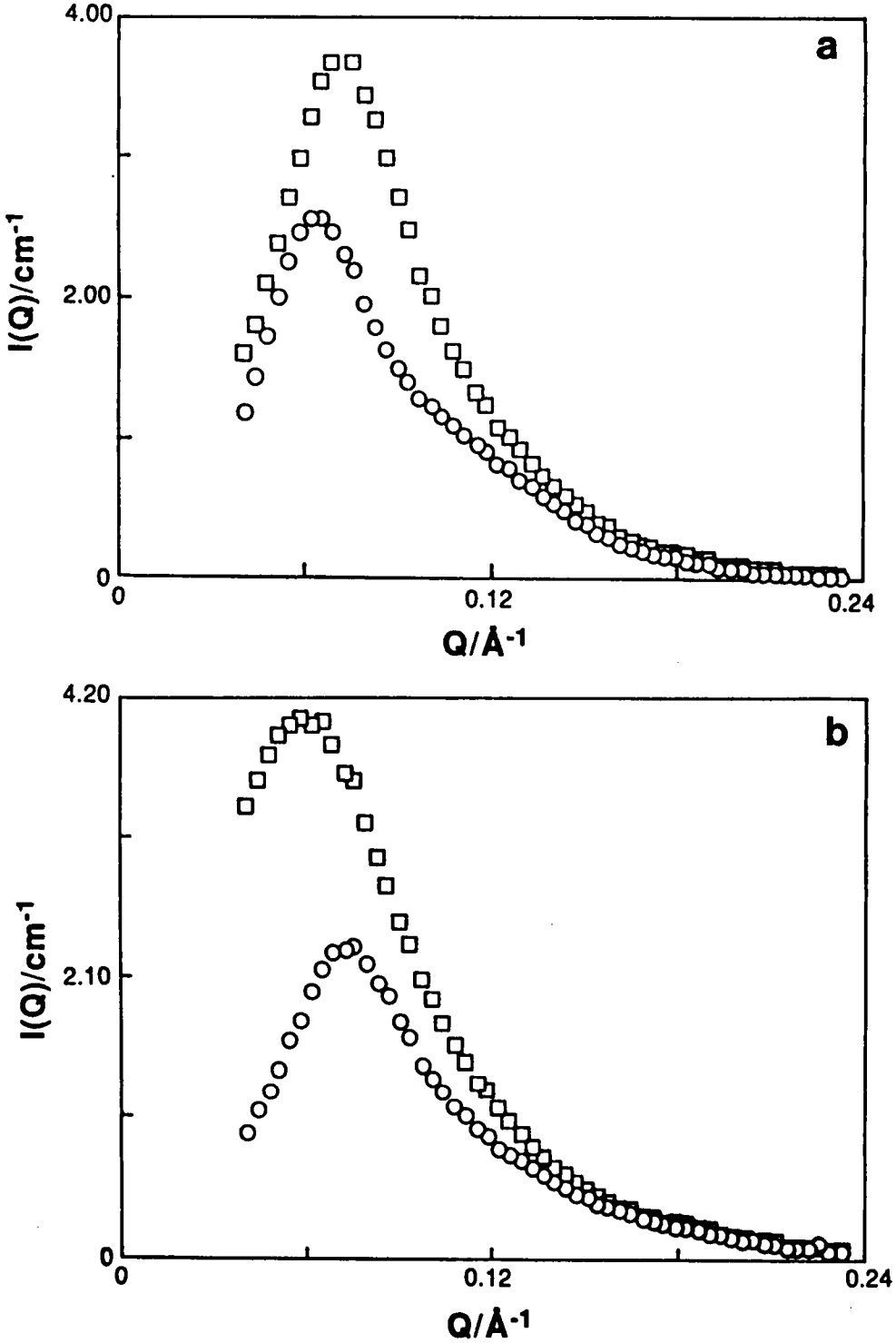

Figure 45. Comparison of scattering curves for (a) SDS and (b) C_7SS with and without C222.

circles: without C222, squares: with C222.

value of -0.39×10^{10} cm^{-2} was obtained for ρ_1. The shell then included the sulfonate headgroups, associated counterions, waters of hydration and a fraction of the alkyl tails once the aggregation number exceeds $(4\pi/3)\ (16.7)^3/V_{c12}$ tail. Table X (p. 135) lists the group volumes and hydration numbers used. Figure 46a shows a representative fit; results are compiled in Table XXVI.

The addition of C222 to SDS micellar solutions is expected to change dramatically the scattering length density of the shell. The scattering curves for SDS:C222 solutions were analyzed first using the above model with $\rho_{Kr} = 0.74 \times 10^{10}$ cm^{-2}. All Na^+ were assumed to exist in C222:Na^+ complexes due to the large complexation constant for Na^+ by C222. The fits obtained in this manner were very poor as evidenced by large deviations of A from 1.0. These fits determined ρ_2 to be 2.2×10^{10} cm^{-2}, a value substantially lower than that of the solvent. It was determined that the large volume of the C222:Na^+ complex placed too much emphasis on z in determining the shell's volume and scattering length density. This discrepancy was corrected by taking z, ρ_2, V_{sh}, A and B as adjustable parameters and fixing $\bar{n}$. The best value for $\bar{n}$ was determined for each concentration. The proportionality constants obtained using this model were close to one, and, as Figure 46b illustrates, the fits obtained were quite good. Table XXVII lists the results determined using this model. The large shell volumes obtained agree with Evans'[6] conclusions that the C222:Na^+ complexes are situated further from the micellar surface than Na^+ normally is.

TABLE XXVI

RESULTS OF FITS TO EXPERIMENTAL CURVES FOR SDS

[SDS],M	$\bar{n}$	Z	ECC	R_2,Å	ρ_2
0.025	69.8±0.7	12.6±1.0	-	22.5	4.8
0.050	74.1±0.5	18.7±0.8	-	22.8	4.5
0.10	80.4±0.5	23.0±0.7	-	23.3	4.3
0.25	94.5±0.4	27.6±0.6	1.3+0.1	24.6	5.2
0.50	106.3±0.4	26.7±0.5	1.2+0.1	25.7	5.2

ρ_2 has units of 10^{10} cm^{-2}.

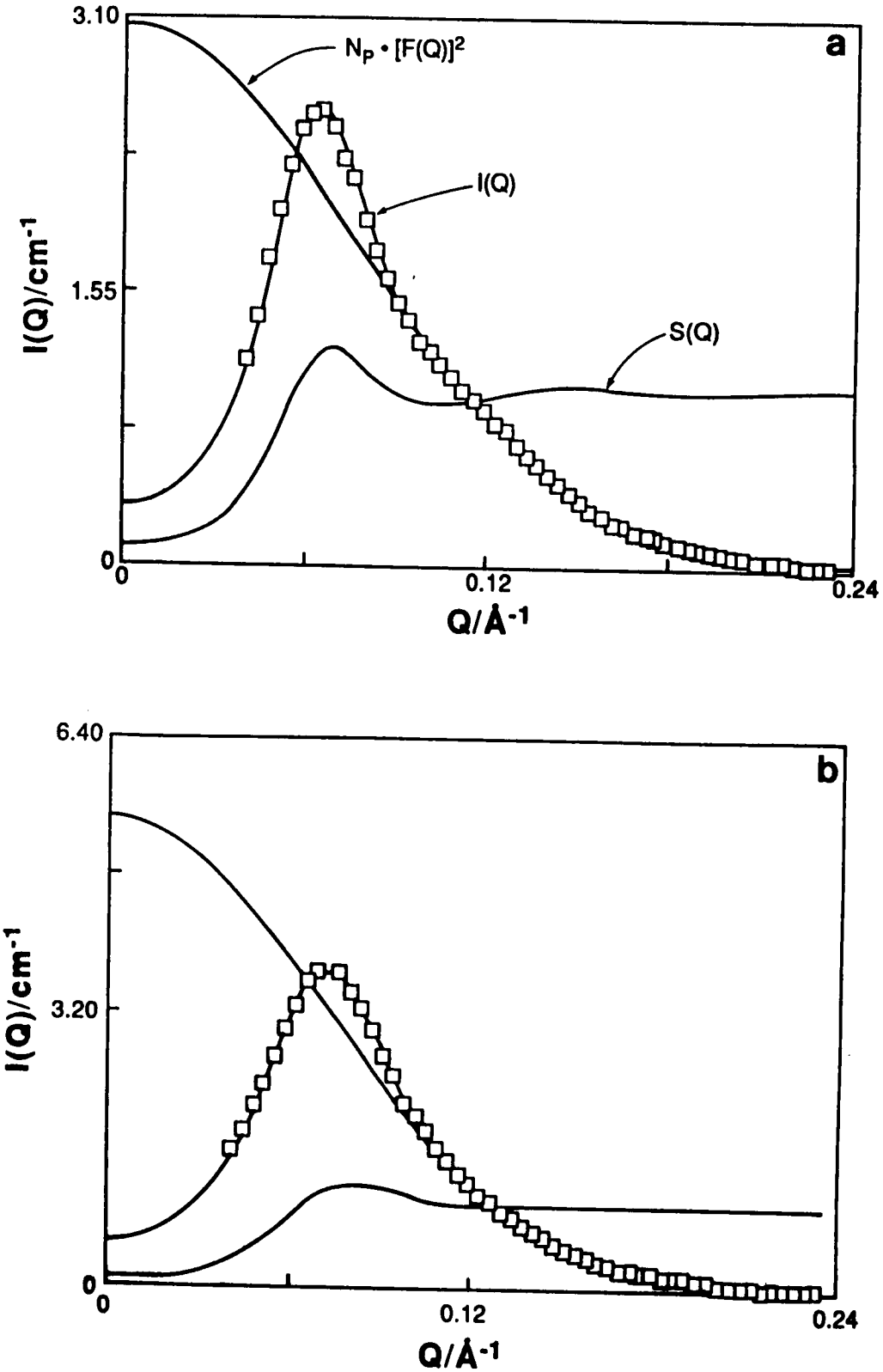

Figure 46. Fit to experimental scattering curves for (a) 0.10 M SDS and (b) 0.10 M SDS:C222.

TABLE XXVII

RESULTS OF FITS TO EXPERIMENTAL CURVES FOR SDS:C222

[SDS],M	$\bar{n}$	Z	R_2, Å	ρ_2, 10^{10} cm^{-2}
0.05	49.5	13.3 ± 0.5	23.4 ± 0.2	3.18 ± 0.08
0.10	53.0	13.0 ± 0.2	25.3 ± 0.1	4.19 ± 0.03
0.25	51.5	12.9 ± 0.2	25.6 ± 0.2	4.09 ± 0.04
0.50	55.5	6.7 ± 0.7	24.8 ± 0.1	4.52 ± 0.03

The scattering curves for C_7SS and C_7SS:C222 were fit employing model 3' (p. 138) in the prolate ellipsoidal form; no changes in the model were necessary to obtain good matches between calculated and experimental curves (recall that due to the presence of 30% of the alkyl tails in the shell, ρ_2 differs substantially from ρ_{solv} even before C222 is added). Table XXVIII contains the results from the curve-fitting. The aggregation numbers in the presence of C222 actually increased for the lower concentrations; it is not until 0.25 M that a slight decrease in $\bar{n}$ occurs for C_7SS:C222 solutions. Low micellar charges and fractional dissociations were found for the C_7SS:C222 micelles, however, these results are consistent with the conductivity data. Figure 47 shows the aggregation numbers obtained from the two surfactants with C222 present.

The effect of added electrolyte was investigated also; Figure 48a illustrates the change in $\bar{n}$ as a function of salt for SDS. The aggregation numbers found for SDS alone agree well with reported values,[112] and the same salt-invariant behavior is noted for SDS:C222 as was reported by Evans.[6] Aggregation numbers *vs.* salt concentration for C_7SS with and without C222 are presented in Figure 48b; a slight increase in $\bar{n}$ is apparent for C_7SS:C222 micelles although the increase in size is smaller than is found for C_7SS in the absence of C222.

4. Vedicm Measurements of $C_{10}SS$:C222 in Water

Upon the addition of C222 to opaque dispersions of $C_{10}SS$ in water, clear solutions were produced at 25°C. Vesicles were observed in the

TABLE XXVIII

RESULTS OF FITS TO EXPERIMENTAL CURVES FOR C_7SS
C_7SS:C222

$[C_7SS]$,M	$\bar{n}$	Z	ECC	R_2,A	ρ_2
without C222:					
0.05	35.8 ± 0.6	13.7 ± 0.4	1.6 ± 0.1	19.3	3.2
0.10	50.4 ± 0.3	15.6 ± 0.2	2.1 ± 0.1	21.7	3.8
0.25	101.7 ± 0.8	15.3 ± 0.4	2.7 ± 0.1	27.7	4.0
with C222:					
0.05	40	7.5 ± 0.2	2.2	23.8 ± 0.2	3.27 ± 0.06
0.10	56	7.4 ± 0.1	2.7	27.0 ± 0.2	3.37 ± 0.05
0.25	75	4.4 ± 0.5	3.3	28.7 ± 0.2	3.59 ± 0.04

ρ_2 has units of 10^{10} cm^{-2}.

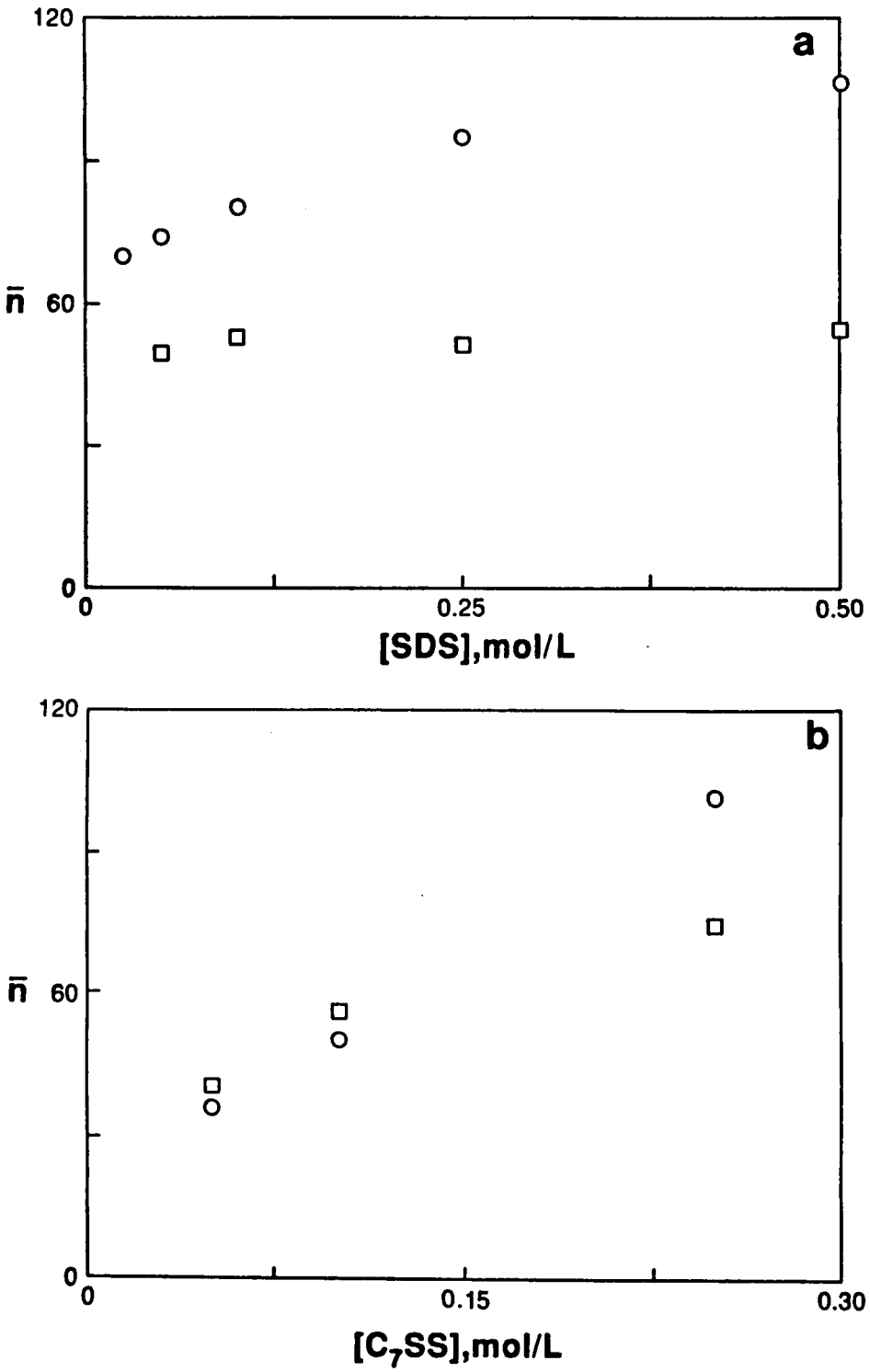

Figure 47. Plot of aggregation numbers versus surfactant concentration for (a) SDS and (b) C_7SS.

circles: without C222, squares: with C222.

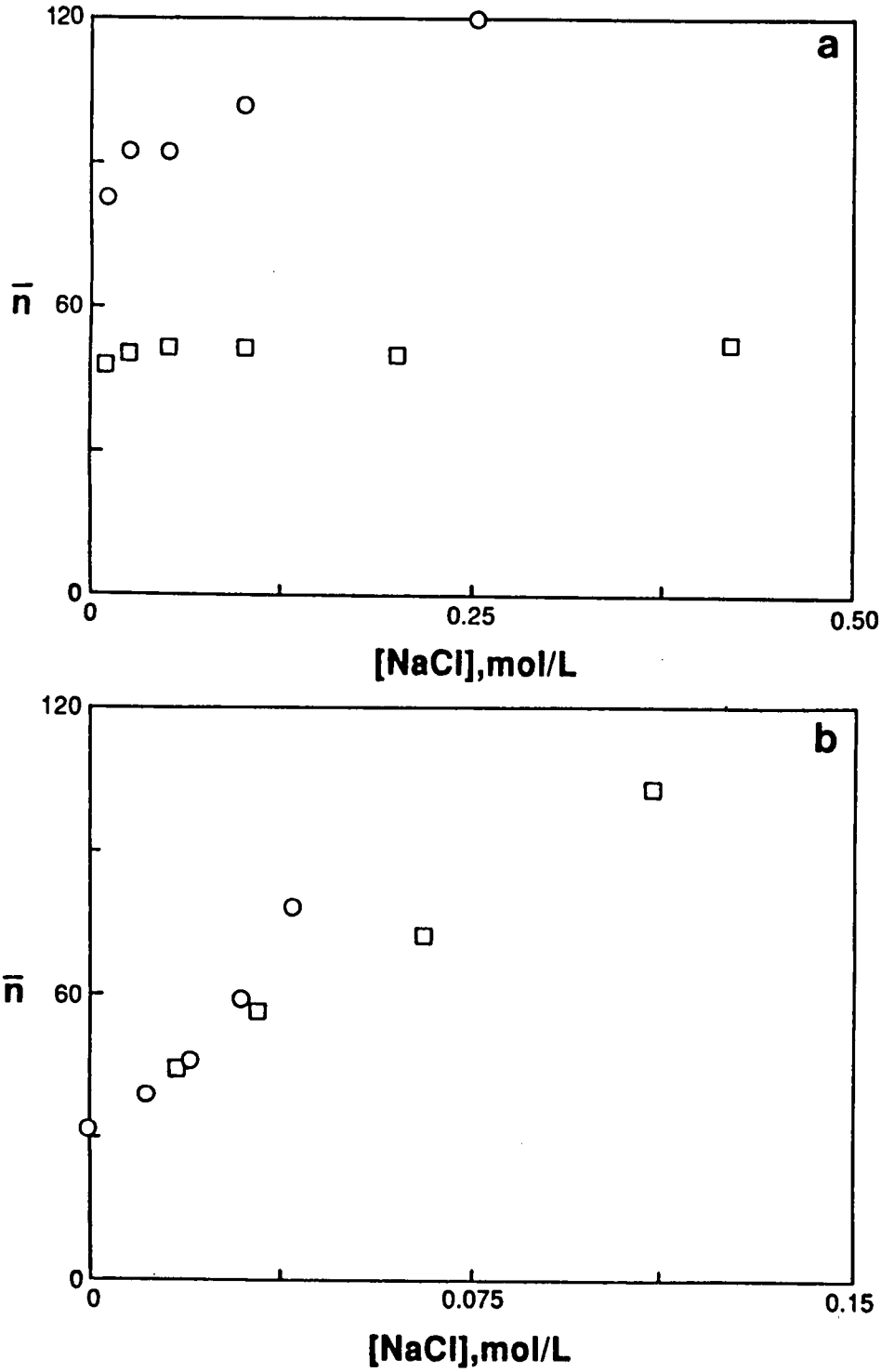

Figure 48. Plot of aggregation numbers versus NaCl concentration for (a) 0.025 M SDS and (b) 0.03 M C_7SS.

circles: without C222, squares: with C222.

concentration range 10^{-4} M to 10^{-2} M C_{10}SS:C222 (1:1 molar ratio) using VEDICM. At 10^{-2} M, the vesicle-to-micelle transition is complete; the transition occurs at a ten-fold lower concentration than the transition of didodecyldimethylammonium acetate. The addition of C222 to Texas #1 has shown similar behavior.[138]

5. Discussion

SDS micelles in the presence of C222 had smaller aggregation numbers and showed no growth with increasing surfactant concentration. The addition of salt to these solutions had very little effect on the values of $\bar{n}$. The SDS:C222 micelles can best be described by a core-plus-shell model where the C222:Na^+ complexes present in the shell result in a voluminous shell having a diameter of several Å. The aggregation numbers obtained by SANS are in agreement with the aggregation numbers obtained by Evans' group[6] using fluorescence quenching.

In contrast, the addition of C222 to C_7SS solutions increased $\bar{n}$ for the lower C_7SS concentrations, while at 0.25 M C_7SS:C222, a slight decrease in $\bar{n}$ is found. The micellar properties of C_7SS:C222 solutions are not salt-invariant; $\bar{n}$'s increase with increasing salt concentration but the increase is not as great as is seen in the case for C_7SS in the absence of C222.

The differences in these systems lie in the area per headgroup available upon the addition of C222. To consider this in detail, the area per headgroups are calculated in the following way. First, model the micelles as smooth spheres having only the headgroups present on the outside (diameter of OSO_3^- is 5.5 Å; SO_3^- is 4.9 Å). Then calculate the

radius of the sphere from n taking into consideration all of the monomer groups except the headgroups and counterions. Finally, add the diameter of the headgroup to the radii and calculate the area per headgroup that is available on the surface of the sphere. Results of the calculations are shown in Figure 49.

The area per molecule at the air-water interface for SDS:C222 was determined[6] to be 136 $Å^2$ at a concentration just below the cmc. For SDS micelles, the headgroup area is not large enough to accommodate one $C222:Na^+$ without some change in the structure occurring, either an increase in α or a decrease in $\bar{n}$. Upon complexation, the C222 molecule pulls the Na^+ away from the micellar surface making it less able to screen charges effectively. The result is an increase in head-group repulsions that is compensated by increasing the area per headgroup. At the idealized surface, the area per headgroup increases to 115 $Å^2$ when Na^+ is complexed.

In the case of 0.05 M and 0.10 M C_7SS, the area per headgroup is already large enough to accommodate one $C222:Na^+$. The hydrophobic nature of the $C222:Na^+$ complex enables this counterion to associate with the micellar surface more strongly than the sodium counterion, resulting in an increase in $\bar{n}$ as well as a substantial increase in β. At 0.25 M C_7SS the area per headgroup is now too small for the presence of one $C222:Na^+$ and consequently $\bar{n}$ decreases and the headgroup area increases. An additional interaction possible in the C_7SS system would be local dipole-dipole interactions between the complex and the ester carbonyls.

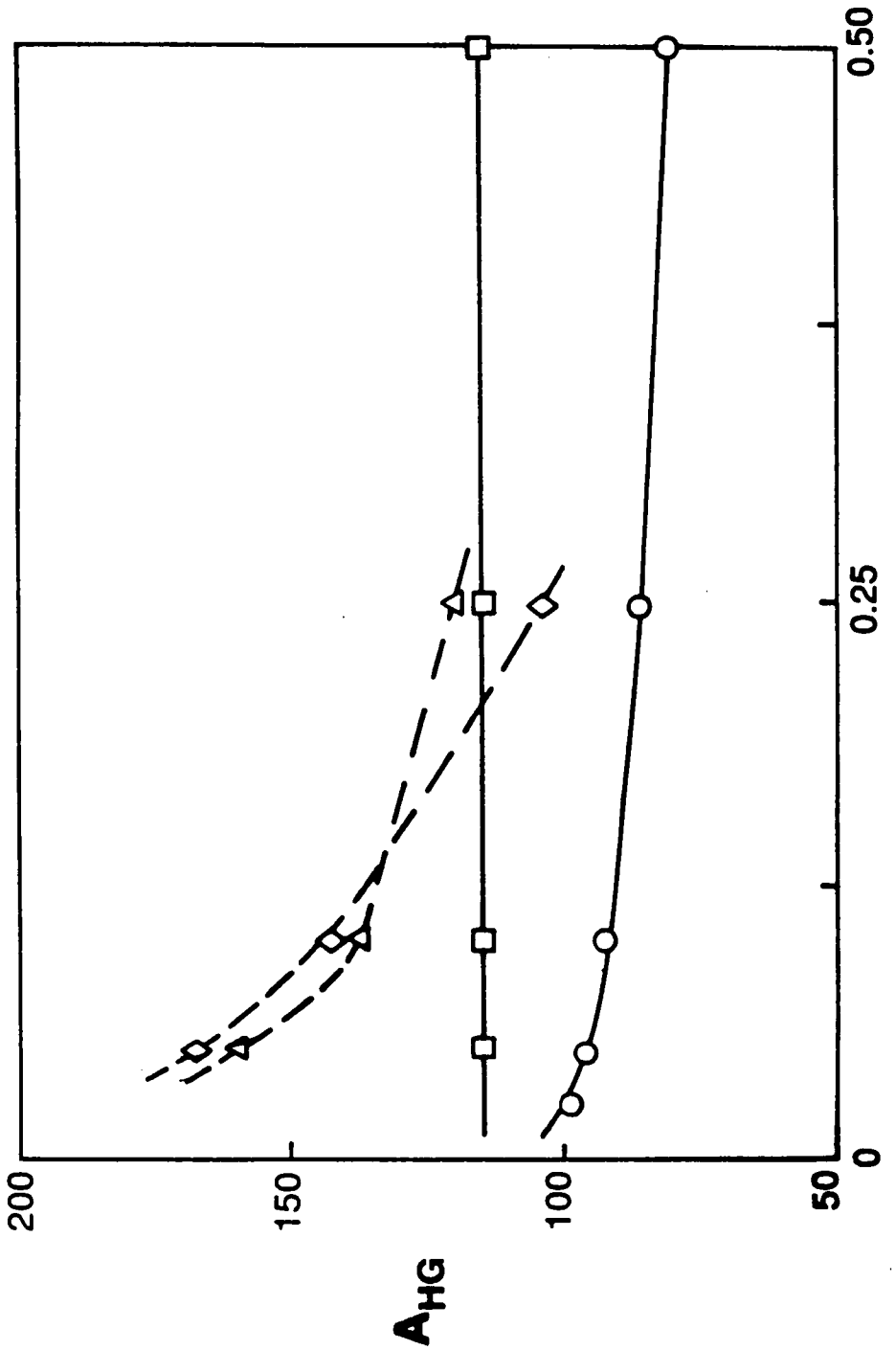

Figure 49. Calculated areas per headgroup.

circles: SDS, squares: SDS:C222, diamonds: C_7SS, triangles: C_7SS:C222.

CHAPTER VI

DISCUSSION

Micellar properties of the sodium di-n-alkylsulfosuccinate surfactants in water were determined using a number of techniques. The phase behavior of these surfactants was characterized first. The Krafft temperatures of the sulfosuccinates were found to exhibit an even/odd alternation; the Krafft temperatures were: C_6SS-16.0°C; C_7SS-31.5°C; C_8SS-32.0°C; C_9SS-45.0°C; and C_{10}SS-49.5°C. As the alkyl chain length of these surfactants increased, the solubility in water decreased. At 45°C, the concentration at which the L_1/L_1 + LC boundary occurs is as follows: C_6SS: 1.2 M; C_7SS: 0.57 M; C_8SS: 0.05 M; C_9SS: 0.020M; and C_{10}SS: 0.0014 M. The surfactants containing alkyl chain lengths of eight carbons and under possessed substantial L_1 regions; for these surfactants the cmc was determined by conductimetry. Two breaks in the plots of specific conductivity versus concentration were noted for C_6SS and C_8SS; the cmc's obtained, along with the value from the second break in parentheses, are as follows: C_6SS: 0.0135 M (0.0178 M); C_7SS: 0.0040 M; and C_8SS: 0.00112 M (0.00256 M). The cmc values for C_6SS and C_8SS agree well with the values obtained from EMF measurements.[69] The degrees of dissociation for each surfactant, as determined from conductivity are: C_6SS: 0.523; C_7SS: 0.450; C_8SS: 0.402. These values agree qualitatively with those obtained from the EMF measurements; for example, α = 0.63 at 0.0131 M C_6SS and α = 0.46 at 0.00171 M C_8SS. (In contrast, α = 0.34 for 0.07 M SDS.[112]) The decrease in α with

increasing surfactant chain length has been attributed to the increased charge density at the micellar surface.[63] With increasing concentration, the α values, as determined by the EMF measurements, are seen to decrease monotonically.

Results from ^{23}Na NMR measurements of C_6SS and C_7SS also support the finding that these surfactants form normal micelles in water. The NMR data were reproduced using a mass action model; a n_o of 30 was used to fit the C_6SS curve, whereas a n_o of 40 was used in fitting the C_7SS curve. In contrast, Kilpatrick and Miller[78] used a n_o of 50 for SDS and a n_o of 2 for Texas #1 (which they claimed did not form normal micelles). Thus, the sulfosuccinates exhibited behavior typical for double-tailed surfactants: these surfactants formed micelles having smaller aggregation numbers and higher degrees of counterion dissociation than do their single-tailed analogues.

SANS was utilized to study the following aspects of micellar behavior: (1) the determination of a realistic model for the micelles including the headgroup hydration and volume per monomer; (2) the determination of the rate of micellar growth as a function of surfactant and NaCl concentration; and (3) the determination of shape changes that occur as the micellar solubility limit is approached.

Internal and external contrast measurements were used to address the first aspect of micellar behavior. SANS measurement were made of C_7SS micelles in the presence of supporting electrolyte; under these conditions, the Guinier approximation can be applied to the small Q region. Analysis of the Guinier region yielded radii of gyration and

the intensity at zero Q. The R_g values obtained for the external contrast series decreased with increasing H_2O; this behavior is typical of a particle containing scattering length inhomogeneities. No such trend was found for the internal contrast series; incomplete deuteration of the tails may be the cause behind the lack of a trend.

Internal and external contrast variation measurements were also performed at 0.10 M C_7SS in the absence of salt; from fits of the full scattering curve, the volume of the dry monomer was determined to be 650 $Å^3$. A fraction of the alkyl tails (alf) was present in the shell; a value of 0.3 for alf appeared to provide the best fits. The number of solvent molecules associated with each surfactant monomer was determined from geometrical considerations; on the average, each monomer was associated with ten solvent molecules. This hydration number agrees fairly well with the numbers usually assigned to the headgroup and the counterion.

The size and shape of the micelles formed by C_6SS, C_7SS and C_8SS were determined by SANS. At concentrations near their respective cmc's, these surfactants all formed normal spherical micelles which were characterized by a "dry" hydrocarbon core surrounded by a hydrated shell. The micellar cores appeared to possess a substantial amount of disorder; at all concentrations a portion of the alkyl groups was present in the outer shell. This finding is consistent with the inferences that were drawn from the contrast variation measurements. The micellar size for these amphiphiles was lower than for single-tailed surfactants; for example, for 0.080 M C_7SS $\bar{n}$ = 42.3 whereas for 0.07 M SDS, $\bar{n}$ = 88. Upon

increasing the surfactant concentration, the extent of counterion dissociation decreased monotonically. The values of α as determined from SANS are in fairly good agreement with those obtained from EMF measurements: α = 0.26 for 0.0110 M C_8SS by SANS and α = 0.29 for 0.00750 M C_8SS by EMF. These micelles appeared to grow by incorporation of ion pairs because the charge remained the same over a range of concentrations. The aggregation numbers exhibited a dependence on surfactant concentration which is related to the micellar solubility of the surfactant. The quantity $\Delta\bar{n}/\Delta$(C-cmc) followed the micellar solubility: C_6SS (130, 1.2 M), C_7SS (284, 0.57 M) and C_8SS (930, 0.041 M). The addition of salt produced a large increase in the size of the micelles; the value of $\Delta\bar{n}/\Delta$[salt] for C_7SS was over twice that found for SDS, 970 compared to 350. Double-tailed surfactants, having larger headgroup areas, also have a larger amount of hydrocarbon-water contact at the micellar surface. Upon addition of salt, the inclination for growth is greater for the double-tailed surfactants due to the subsequent reduction in hydrocarbon-water contact.

As the surfactant concentration is increased and the micellar solubility boundary is approached, the aggregate size increased for C_6SS, C_7SS and C_8SS. For surfactants with a lamellar phase as the first liquid crystalline phase, the predicted shape change is that of a sphere to oblate ellipsoid. No shape change was seen in this region for C_8SS; a transition was seen for C_6SS; however, a distinction between oblate and prolate forms was not possible. Even at 0.40 M C_6SS, these micelles still showed only small deviations from sphericity; the axial ratio at this concentration was only 0.779. The C_7SS micelles were observed to

undergo a sphere to prolate ellipsoid transition at high concentrations; at 0.15 M the axial ratio was 3.0. As in the case of the n-hexadecyl-n-octyldimethylammonium bromides, the packing theory failed to predict the observed shape evolution. At high Q values, the calculated and experimental curves do not match; the presence of polydispersity in the micelle sizes may be the cause of this. The difference in behavior observed for C_6SS and C_7SS can be attributed to the fact that the measurements of the C_6SS solutions were not made close enough to its solubility limit; the highest concentration investigated was 0.40 M whereas the solubility limit at 45 C was 1.2 M for this surfactant. For C_7SS, measurements were made very close to its solubility limit and substantial deviation from sphericity was observed. In the case of the C_8SS surfactant, measurements were also made very close to its solubility limit; however, no deviation from sphericity was seen. It is quite possible, that for a surfactant of this chain length (octyl), that the sphere to ellipsoid transition is not thermodynamically favorable and a direct conversion to liquid crystal bilayers occurs instead.

Counterion effects for anionic surfactants are generally quite small; however, the addition of a macrocyclic ligand to solutions of anionic surfactants has been shown to alter the micellar structure.[6] The effect of the addition of the cryptand, C222, on the structure of micelles formed by SDS, C_7SS and $C_{10}SS$ was determined as a function of surfactant and salt concentration using SANS. In the case of SDS micelles with C222, the $\bar{n}$ were seen to remain small over a range of surfactant and salt concentrations when compared to SDS micelles

containing no C222. For example, for 0.25 M SDS $\bar{n}$ = 94.5 with no C222 and $\bar{n}$ = 51.5 with C222. The addition of salt to the SDS:C222 solutions had no effect; $\bar{n}$ = 51 at [NaCl] = 0.40 whereas $\bar{n}$ = 122 for [NaCl] = 0.30 M for SDS in the absence of C222. Opposite behavior was found for C_7SS micelles below 0.2 M, C_7SS:C222 micelles were larger with C222 present than without, (at 0.10 M $\bar{n}$ = 50.4 without C222, and $\bar{n}$ = 56 with C222). However, at 0.20 M, C_7SS micelles did become smaller when C222 was added. Below 0.20 M, the headgroup area of the C_7SS is sufficient to accommodate one C222:Na^+ complex and an increase in $\bar{n}$ is seen at these concentrations. Above 0.20 M, the area per headgroup is reduced; now there is insufficient room for the C222:Na^+ complex and a decrease in $\bar{n}$ is observed. This is also what is seen for the SDS micelles; the SDS headgroup area is not large enough to accommodate one C222 molecule per Na^+ and complexation results in an increase in the headgroup repulsion with a simultaneous decrease in $\bar{n}$. Additional interactions possible between the C_7SS micelle and C222 involve association of the complex with the micellar surface and local dipole-dipole interactions between the ester carbonyls and the C222:Na^+ complex. The addition of C222 to aqueous dispersions of $C_{10}SS$ at room temperature resulted in the formation of clear solutions. Using VEDICM, these solutions were seen to contain vesicles from concentrations of 10^{-4} M to 10^{-2} M. At 10^{-2} M, the vesicle-to-micelle transition is essentially complete.

CHAPTER VII

EXPERIMENTAL SECTION

A. Instrumental Methods and Techniques

1. Phase Studies

The phase studies were conducted in either a "primitive" constant temperature bath which consisted of a beaker of water, a hot plate/stirrer, a thermometer and a stirring bar or in a Lauda/Brinkmann Refrigerated Circulator whose temperature precision was ±0.01 to ±0.03°C.

The samples for the phase studies were prepared by weight and sealed in glass ampoules. The most dilute samples were based on a 4 g scale (total weight) while the remainder of the samples were prepared on a 2 g scale (total weight).

Phase boundaries were determined visually by comparison of the turbidities of the samples to the turbidity of water, which was used as the standard. Supercooling of the solutions occurred easily, especially for C_6SS; therefore, all temperatures reported were obtained by heating the samples.

2. EMF Measurements

EMF measurements were performed using either an Orion 9-11 sodium electrode with an Orion 90-02 double junction reference electrode or a Fisher 13-639-20 sodium electrode with a Corning Ag/AgCl reference electrode (Fisher 13-641-621). The Corning reference electrode's inner

chamber was filled with 4 M KCl and the outer chamber with 0.1 M NH_4Cl. When necessary, the electrodes were regenerated; regeneration of the Fisher sodium electrode required soaking the electrode in methanol and then in 0.1 M NaCl, while the Orion sodium electrode required soaking in 0.10 M ammonium bifluoride followed by soaking in 5 M potassium chloride. Measurements were made at 45.0 ±0.1°C employing an Orion 701 digital pH meter. Nernstian behavior was verified for the electrodes using sodium chloride solutions; measurements were then made on surfactant solutions prepared by the addition of concentrated surfactant solutions to stirred, distilled water. Equilibration times for the samples ranged from three to five minutes, which was the settling time for the mV reading.

3. Conductimetry

Two conductivity bridges were employed: (1) a Beckman RC18A conductivity bridge and (2) a Wayne-Kerr automatic precision bridge. The Beckman conductivity bridge was operated at a frequency of 1 and 3 kHz; the sample measurements did not exhibit a frequency dependence. The precision of the measurements was ±0.05% for the Beckman conductivity bridge. The Wayne-Kerr conductivity bridge was operated at a frequency of 1 kHz at which its precision was ±0.05% m Ω in the resistance range 0-10 MΩ. After a warm-up period of ten minutes, residual lead impedances were removed by trimming the instrument.

In order to obtain the greatest accuracy, the cell resistance, as "seen" by the bridge, should be within the range 100-100,000 ohms.

Adhering to this criterion required the use of three conductivity cells: (1) a 500 mL Kraus conductivity cell with a cell constant of 0.5418 cm^{-1} (2) a 500 mL Kraus cell having a cell constant of 1.0174 cm^{-1} and (3) a 500 mL "doughnut" cell with a cell constant of 6.9334 cm^{-1}. The cell constants were determined by the use of potassium chloride solutions whose conductivity was calculated by the conductance equation proposed by Lind, Zwolenick and Fuoss.[71]

Water was obtained either (1) by distillation of water from Kontes WS Still, followed by storage with drying tube filled with ascarite (to protect the water from the introduction of CO_2) or (2) from a Millipore Milli-Q Water Filtration System. The specific conductivity of the water was never larger than 1.5×10^{-6} S cm^{-1} at 45.00 ± 0.01°C; the temperature was controlled by a thermostatted oil bath.

Samples were prepared by weight, warmed until clear and then transferred to the conductivity cell. The concentrated surfactant solutions were diluted via (1) weighed aliquots of water (weighed in a glove bag under N_2 atmosphere in presence of Ascarite) or (2) dispensed through a Repipet (with a precision of ±0.5%). Resistance measurements were obtained after equilibration times of 20 and 30 minutes.

4. Nuclear Magnetic Resonance

All ^{23}Na NMR experiments were performed using a Nicolet NT200 FTNMR equipped with an Oxford magnet (field strength was 4.7 T), NIC 1180E data processor, NIC 293C programmable pulser and Control Data Corporation Cartridge disk drive. These experiments employed a 12 mm

multinuclear probe. A typical experiment used a pulse length of 25 μsec, a delay time of 2.0 sec and a sweep width of 1000-2000 Hz. Depending on the concentration, the number of acquisitions ranged from 32 (for 0.30 M) to 512 (5.0×10^{-4} M). The samples were prepared with Aldrich D_2O and all subsequent dilutions were made directly in the 12 mm sample tube. All chemical shifts were referred to 3% $NaB(C_6H_5)_4$ in CD_3CN as the reference; this solution was sealed in a 5 mm sample tube which was then positioned in a coaxial insert in the 12 mm sample tube. Transverse relaxation rates were determined from full widths at half height of the surfactant peak for each concentration using a Lorentzian line fitting program.

5. Sample Preparation for SANS

All SANS samples were prepared by weight in volumetric flasks and stored in the cold room overnight. The C222 samples were prepared in a glove bag under an inert atmosphere. The internal/external contrast samples were prepared by mixing appropriate volumes of either the surfactant in D_2O with the surfactant in H_2O or the deuterated surfactant in D_2O with the protiated surfactant in H_2O. Salt samples were prepared by the addition of small aliquots of 5 M NaCl by a microliter syringe to a stock solution; and then dilutions were made by mixing appropriate volumes of solutions with and without salt. Samples were contained in quartz spectrophotometric cells having 0.1, 0.2 or 0.5-cm pathlengths.

Transmission coefficients of the samples were determined by

$$T_s = (I_s - I_c)/(I_{empty} - I_c) \quad (85)$$

where I_s is the intensity of the sample, I_c is the intensity with Cadmium in the beam and I_{empty} is the intensity with no sample in the beam. For these determinations, the cells were placed at the source slit and the intensities were measured for 100 seconds. Glassy carbon is used to improve the accuracy of measurement of the transmission coefficients because it is a strong coherent scatterer.

6. Fluorescence Quenching Measurements

The fluorescence quenching measurements were performed at the Department of Biochemistry, University of Minnesota, employing a Spex Fluorolog 222 fluorometer. Ruthenium tris 2,2'-bipyridyl chloride was the fluorophore and 9-methylanthracene was employed as the quencher. The samples were excited at a wavelength of 453.5 nm and emissions were monitored between 610 and 645 nm.

7. Video Enhanced Differential Interference Contrast Microscopy

VEDICM measurements were performed by D. D. Miller of the University of Minnesota. Experimental details are presented elsewhere.[70]

B. Surfactant Synthesis and Materials

1. Synthesis of Sodium Di-n-Alkylsulfosuccinates

a. Preparation of Di-n-alkyl Fumarates. The fumarates were prepared according to the method of Raha,[141]

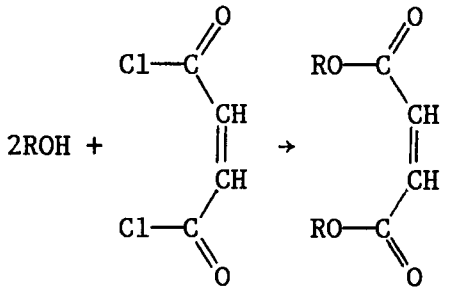

(85)

An example of the experimental procedure is presented here for n-heptanol. A 500 mL 24/40 round bottom three-necked flask was charged with 70.7 mL (0.5 mol) n-heptanol, 70 mL $CHCl_3$ (which had been stored over 4 Å sieves) and 125 mL N,N-dimethylaniline. The flask was equipped with an addition funnel and a reflux condenser which was protected by a drying tube containing $CaCl_2$. The reaction mixture was cooled to ca. 5°C with stirring, and 29.73 mL (0.28 mol) fumaryl chloride in 50 mL $CHCl_3$ was added dropwise over a two hour period. The reaction was strongly exothermic; the reaction flask was maintained in an ice bath during the addition and checked periodically for warming by stopping the addition, removing the ice bath and checking whether the flask was warm to the touch. The light brown reaction mixture was then refluxed for two hours, cooled and transferred to a separatory funnel to which 200 mL ice-cold 6 N H_2SO_4 was added. The product was extracted with three-150 mL portions of ether, which were combined and washed once with 6 N H_2SO_4, twice with distilled water, twice with saturated $NaHCO_3$ and once with saturated NaCl. The ether solution was then dried over anhydrous

sodium sulfate, filtered and treated twice with activated charcoal. After filtration through Celite, a bright orange solution was obtained. The ether was removed via rotary evaporation, and a Vigreaux distillation removed any unreacted alcohol. The product was then distilled twice using a short path condenser to obtain pure product in ca. 44% yield.

b. Sulfonation of Di-n-alkyl Fumarates. The preparation of the surfactant involved sulfonation of the di-n-alkylfumarate as shown in equation 86:

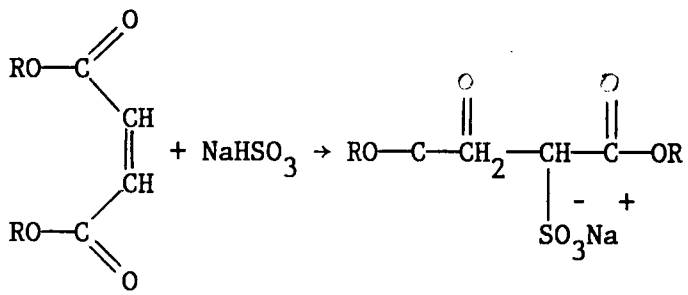

(86)

A 100 mL round bottom Bantamware flask was charged with 4.00 g (0.0128 mol) fumarate, 1.99 g (0.0192 mol, 0.5 mol excess) $NaHSO_3$, 10.0 mL 1,2-propanediol, 2.0 mL $CHCl_3$ and 1.0 mL H_2O. This mixture was stirred and heated to reflux for six hours; its progress was followed by TLC. The solvent mixture was then removed by vacuum distillation; the resultant yellow mixture was stirred overnight in dry methanol, filtered through a 0.5 μm membrane filter (suction) to remove any unreacted $NaHSO_3$, treated with activated charcoal and filtered through Celite. The surfactant obtained was then recrystallized from 50/50 v/v $MeOH/H_2O$

and dried under vacuum (C_6SS) or in a vacuum oven at 50°C (C_7SS, C_9SS, $C_{10}SS$). C_8SS was received as a 50% dispersion in 1,2-propanediol from American Cyanamid and purified as above. Table XXIX tabulates the carbon and hydrogen analyses.

2. Synthesis of Tail-Deuterated Sodium Di-n-Heptylsulfosuccinate

The surfactant $C_7SS\text{-}d_{30}$ was made for use in the SANS studies; a synthetic route for heptanol-d_{15} was needed. Two approaches were considered; the first approach is outlined in Scheme 1 (see Appendix). Due to the expense of preparing deuterated surfactants, all reaction yields were first maximized using the protiated reagents prior to the actual synthesis of the deuterated surfactants.

The first step in Scheme 1 utilizes the "acetylenic zipper" reaction,[142] in which a very strong base effects the migration of a triple bond along a straight chain. The product of this reaction is the salt of the terminal acetylene which is believed to be formed irreversibly. During the triple bond migration, the protons in the path of the triple bond are removed from the carbon skeleton and are replaced by protons from the base or solvent. Recently, Abrams[143] has demonstrated that these protons can be replaced by deuterium atoms if a deuterated base is employed. An advantage of this reaction is the mild conditions under which deuteration occurs. However, a major disadvantage of this reaction is the low yields involved upon changing from the protiated base to the deuterated base; a decrease of ca. 50% was reported.[143] Based on the highest yield obtained in our laboratories, 80 L D_2O

TABLE XXIX

CARBON AND HYDROGEN ANALYSES OF THE SULFOSUCCINATES

Surf	found % C	theoretical % C	found % H	theoretical % H
C_6SS	46.75	49.47	7.49	7.52
C_7SS	51.72	51.91	7.99	7.98
C_8SS	53.67	54.04	8.64	8.39
$C_{10}SS$	57.35	57.57	9.07	9.06

($35,200) would have been required to synthesize 1 g C_7SS. A second approach was then considered; this approach involved the palladium-catalyzed hydrogen exchange of hydrocarbons at atmospheric pressure. Both approaches to the synthesis of $C_7SS\text{-}d_{30}$ are outlined below.

a. Isomerization of 2-heptyn-1-ol by 1,3-diaminopropane. Lithium wire (2.74 g, 0.395 mol) was cut into 1 cm pieces, washed with hexanes and transferred to a 500 mL 24/40 round bottom flask equipped with a pressure equalizing dropping funnel, Ar inlet, condenser fitted with a KOH-filled drying tube, a magnetic stirring bar and a thermometer. All glassware had been dried overnight at 130°C. The flask was then charged with 170 mL 1,3-diaminopropane and the mixture was stirred for thirty minutes at room temperature at which time the lithium had partially reacted. The resultant blue mixture was then heated at 70°C until the blue color had discharged and a white suspension was obtained. The reaction mixture was then cooled to room temperature and potassium tert-butoxide (27.55 g, 0.25 mol) was added. After stirring a few minutes, the reaction mixture turned pale yellow. The solution was stirred for twenty minutes, cooled in an ice bath and then 2-heptyn-1-ol (5.9 mL, 0.047 g) was added dropwise over a period of ten minutes. The reddish-orange reaction mixture was stirred for 90 minutes at 18°C and overnight at room temperature. The reaction mixture was then poured into 500 mL of ice-water and the product extracted with four 200 mL portions of ether. The combined ether layers were washed with 500 mL each of distilled water, 10% HCl and saturated sodium chloride, and the ether

solution was then dried over anhydrous Na_2SO_4. The solution was filtered and the ether removed. The product was distilled using a Kugelrohr apparatus at 38°C at 100 microns. The highest yield obtained was 76%.

b. Deuteration of Heptanoic Acid by Catalytic Exchange. Deuterated heptanoic acids were prepared according to the methods of Hsaio et al.[144] and Atkinson et al.[145] An exchange cell of the type shown in Figure 50 was employed. A United Technologies Hydrogen generator produced the deuterium gas; the cell assembly consisted of a polymer electrode. Prior to the electrolysis, the cell assembly was flushed with D_2O (conductivity was within specifications) until aliquots taken from the cell assembly indicated that the water contained greater than 90% deuterium.

Heptanoic acid (18.73 g, 0.144 mol) was placed on 4 grams of 10% Pd on C spread out on the frit (the catalyst was covered by a layer of glass beads). After the heptanoic acid had settled through the catalyst, deuterium gas was bubbled through the frit at a flow rate of 40 cc/min. The cell was then lowered into an oil bath at 190°C which was heated by a Nichrome coil, wrapped with asbestos tape and stirred magnetically. An asbestos board was placed beneath the oil bath to protect the stir plate. A water cooled condenser connected to the reaction vessel was connected in series to a ethylene glycol cooled condenser (5°C) to prevent loss of heptanoic acid by volatilization. To obtain maximum use of the deuterium gas being generated, a second cell assembly could be placed after the first; however, attempts to do this

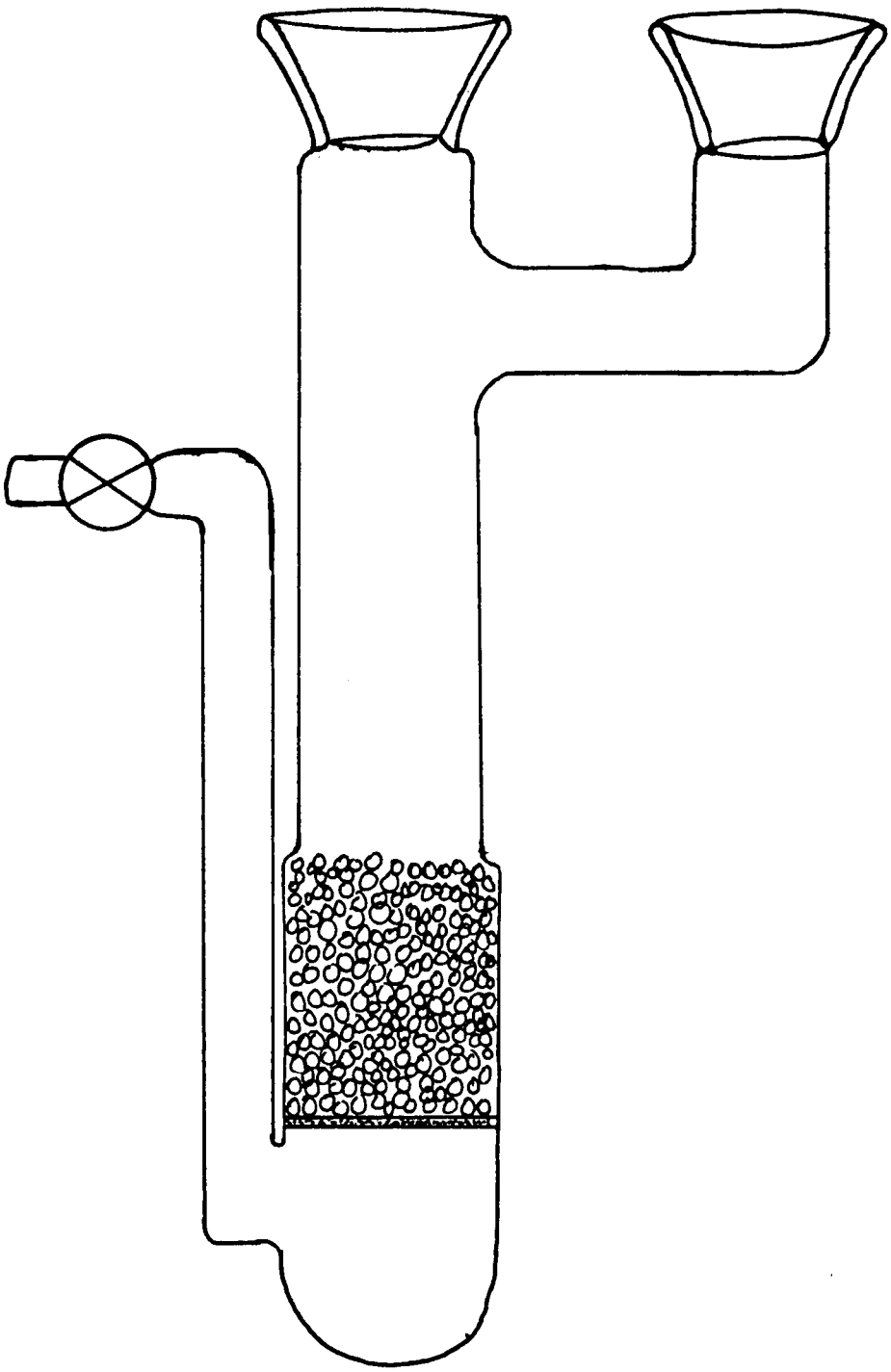

Figure 50. Exchange cell used for deuteration.

showed that the gas flow was greatly reduced at this point and the deuteration was determined to occur to a lower extent. Two Dry Ice-cooled traps were placed between the reactions to prevent carry-over from one experiment to the next.

The progress of the reaction was checked by NMR and IR. Samples were obtained by turning the gas flow off, raising the cell out of the oil bath and obtaining an aliquot through the sampling port. All samples were dissolved in ether, filtered through Celite and the ether removed. The reaction was stopped after 104 hours, at which time the product was 85% deuterated. The yield for this step was 71%.

c. Lithium Aluminum Deuteride Reduction of Hepta-noic Acid. To 300 mL dry ether in a 1 L round-bottom flask equipped with addition funnel, condenser with Ar outlet, and Gooch side arm, was added lithium aluminum deuteride (LAD) slowly under an Ar stream. Then, 7.827 g (0.0555 mol) heptanoic acid-d in 200 mL dry ether was added to the LAD solution cooled in an ice bath over a one hour period. The solution was then stirred for six hours under a positive pressure of Ar.

The excess LAD was killed by the slow addition of ca. 200 mL 10% H_2SO_4 solution. The layers were separated and the aqueous layer washed with two 250 mL portions of ether. The combined ether layers were dried over anhydrous K_2CO_3, filtered, the ether removed and the product vacuum distilled using a Kugelrohr apparatus. The product, heptanol-d_{15}, was confirmed by IR and NMR. The yield for this step was 90%.

The remainder of the reactions (preparation of fumaric acid, di-n-heptyl ester and of sodium di-n-heptyl-sulfosuccinate) were per-

formed in the same manner as for the protiated counterparts, only on a much smaller scale and with extreme care. The yield for the third step was 62% and for the fourth step, 69%. The overall yield for sodium di-n-heptylsulfosuccinate-$d_{25.5}$ was 27%. Hydrogen and carbon analyses for the deuterated compounds are tabulated in Table XXX.

3. Chemicals

a. N-hexanol. N-hexanol was obtained from Eastman Kodak and used as purchased.

b. N-heptanol. N-heptanol was used as purchased from Eastman Kodak.

c. N-nonanol. N-nonanol was purchased from Aldrich and used as received.

d. N-decanol. N-decanol was used as received from Eastman Kodak.

e. Fumaryl chloride. Fumaryl chloride was used as purchased from Aldrich.

f. N,N-dimethylaniline. N,N-dimethylaniline was used as received from Aldrich.

g. 1,2-propanediol. 1,2-propanediol was obtained from Aldrich and was used as received.

h. Heptanoic acid. Heptanoic acid was purchased from Eastman Kodak and distilled prior to use.

i. 10% Pd on Carbon. 10% Pd on C was used as received from Aldrich.

j. Lithium Aluminum Hydride (LAH) and Deuteride (LAD). LAH and LAD were used as received from Aldrich.

TABLE XXX

CARBON AND HYDROGEN ANALYSES OF DEUTERATED C_7SS

Compound	found % C	theoretical % C	found % H+D	theoretical % H + D
heptanoic acid-d	58.72	59.93	18.17	17.26
heptanol-d	63.32	65.01	22.31	22.62
di-C_7fum-d	63.07	63.94	17.12	17.13
C_7SS-d	48.28	48.89	13.41	13.32

k. 2-Heptyn-1-ol. 2-Heptyn-1-ol was purchased from Farchan Laboratories and distilled prior to use.

l. Lithium. Lithium was used as received from Aldrich.

m. Potassium tert-butoxide. Potassium tert-but-oxide was used as received from Aldrich.

n. 1,3-Diaminopropane. 1,3-Diaminopropane was purchased from Aldrich, distilled from BaO and stored over 4 Å sieves.

o. Barium oxide. Barium oxide was used as received from Aldrich.

p. 4,7,13,16,21,24-hexaoxa-1,10-diazacyclo-[8.8.8.]hexacosan (C222). C222 was used as received from Fluka or Aldrich.

q. Sodium dodecylsulfate (SDS). SDS was used as purchased from Aldrich.

r. Sodium bisulfite. Fisher certified ACS reagent sodium bisulfite was used as received.

s. Sodium tetraphenylborane. Aldrich ACS reagent Gold Label sodium tetraphenylborane was used as purchased.

t. Acetonitrile-d_3. Acetonitrile-d_3 was used as received from Norell.

u. Chloroform. Chloroform was obtained from Fisher and used as received.

v. Methanol. Methanol was obtained from Fisher or Mallinckrodt and stored over 4 A sieves prior to use.

w. Ether. Ether was purchased from Fisher, dried and distilled from sodium and benzophenone prior to use.

x. Deuterium oxide. Deuterium oxide was obtained from Norell, Aldrich or Cambridge and was 99+% isotopically pure.

y. Water. Water was distilled or passed through a Millipore filtration system.

REFERENCES

REFERENCES

1. Lindman, B.; Wennerstrom, H. "Micelles"; Topics in Current Chemistry, 87; Springer-Verlag: New York, 1980.

2. Fendler, E. J.; Fendler, J. H. Adv. Phys. Org. Chem. 1970, 8, 271.

3. Mukerjee, P.; Mysels, K. J. Critical Micelle Concentrations of Aqueous Surfactant Systems. NSRDS-NBS 36. Washington, D.C.: U. S. Government Printing Office 1971.

4. Jobe, D. J.; Reinsborough, V. C. Aust. J. Chem. 1984, 37, 303.

5. Mukerjee, P.; Mysels, K. J.; Kapauan, P. J. Phys. Chem. 1967, 71, 4166.

6. Evans, D. F.; Sen, R.; Warr, G. G. J. Phys. Chem. 1986, 90, 5500.

7. Emerson, M. F.; Holtzer, A. J. Phys. Chem. 1967, 71, 1898.

8. Hoffmann, H.; Nusslein, H.; Ulbricht, W. Micellization, Solubilization, and Microemulsions; Mittal, K., Ed.; Plenum Press: New York, 1977, Vol. 1, p. 263.

9. Carver, M. Ph.D. Dissertation, The University of Tennessee, Knoxville, Tennessee, 1986.

10. Corrin, M. J. Colloid Sci. 1948, 3, 333.

11. Hartley, G. Quart. Rev. Chem. Soc. 1948, 2, 152.

12. Benjamin, L. J. Phys. Chem. 1966, 70, 3790.

13. Harkins, W. D.; Matton, R. W.; Corrin, M. L. J. Colloid Sci. 1946, 7, 105.

14. Shinoda, K.; Hildebrand, J. H. J. Phys. Chem. 1958, 62, 295.

15. Shintzky, M.; Dianoux, A.; Gilten, C.; Weber, G. Biochemistry 1971, 10, 2106.

16. Waggoner, A. S.; Keith, A. D.; Griffith, O. H. J. Phys. Chem. 1968, 72, 4129.

17. Stigter, D. J. Colloid Interface Sci. 1967, 23, 379.

18. Menger, F. M.; Jerkunica, J. M.; Johnston, J. C. J. Am. Chem. Soc. 1978, 100, 4676.

19. Stigter, D. J. Phys. Chem. 1974, 78, 2480.

20. Dill, K. A.; Flory, P. J. Proc. Natl. Acad. Sci. 1981, 78, 676.

21. Fromherz, P. Chem. Phys. Lett. 1981, 77, 460.

22. Ulmius, J.; Lindman, B. J. Am. Chem. Soc. 1981, 85, 4131.

23. Menger, F. M. J. Phys. Chem. 1979, 83, 893.

24. Menger, F. M. Accts. Chem. Res. 1979, 12, 111.

25. Svens, B.; Rosenholm, B. J. Colloid Interface Sci. 1973, 44, 495.

26. Muller, N.; Birkhahn, R. H. J. Colloid Interface Sci. 1967, 71, 957.

27. Wennerstrom, H.; Lindman, B. J. Phys. Chem. 1979, 83, 2931.

28. Cabane, B.; Duplessix, R.; Zemb, T. J. Phys. 1985, 46, 2161.

29. Cabane, B. J. Phys. 1981, 42, 847.

30. Israelachvili, J.; Mitchell, D.; Ninham, B. J. Chem. Soc. Faraday Trans. 2 1976, 72, 1525.

31. Israelachvili, J.; Mitchell, D.; Ninham, B. Biochem. Biophys. Acta 1977, 470, 185.

32. Israelachvili, J.; Mitchell, D.; Ninham, B. J. Chem. Soc. Faraday Trans. 2 1981, 77, 601.

33. Wennerstrom, H.; Lindman, B. Phys. Rep. 1979, 52, 1.

34. Tanford, C. "The Hydrophobic Effect"; Wiley: New York, 1973.

35. Evans, D. F.; Wightman, P. J. J. Colloid InterfaceSci. 1982, 86, 515.

36. Evans, D. F.; Allen, M.; Ninham, B. W.; Fouda, A. J. Solution Chem. 1984, 13, 87.

37. Evans, D. F.; Ninham, B. W. J. Phys. Chem. 1986, 90, 226.

38. Lin, T.-L.; Chen, S.-H.; Gabriel, N. E.; Roberts, M.F. J. Phys. Chem. 1987, 91, 406.

39. Mazer, N. A.; Carey, M. C.; Benedak, G. B. in "Micellization, Solubilization and Microemulsions," Mittal,K. L., Ed.; Plenum: New York, 1977, Vol 1.

40. Lang, J.; Tondre, C.; Zana, R.; Bauer, R.; Hoffmann,H.; Ulbricht, W. J. Phys. Chem. 1975, 79, 276.

41. Muller, N.; Platko, F. J. Phys. Chem. 1971, 75, 547.

42. Fox, K. Trans. Faraday Soc. 1971, 67, 2802.

43. Takeda, K.; Yasunaga, T. J. Colloid Interface Sci. 1973, 45, 406.

44. Takeda, K.; Yasunaga, T. J. Colloid Interface Sci. 1972, 40, 127.

45. Lang, J.; Auborn, J. J.; Eyring, E. M. J. Colloid Interface Sci. 1972, 41, 484.

46. Aniansson, E. A. G.; Wall, S. N. J. Phys. Chem. 1974, 78, 1024.

47. Aniansson, E. A. G.; Wall, S. N. J. Phys. Chem. 1975, 79, 857.

48. Texas #1 is named due to its preparation by W. H. Wade and R. S. Schechter's enhanced oil recovery group at the University of Texas.

49. Hoffmann, H. Ber. Bunsenges. Phys. Chem. 1984, 88, 1078.

50. Kunitake, T. J. Macromol. Sci.-Chem. 1979, A13, 587.

51. Okahata, Y.; Tanamachi, S.; Nagai, M.; Kunitake, T. J. Colloid Interface Sci. 1981, 82, 401.

52. Deguchi, K.; Mino, J. J. Colloid Interface Sci. 1978, 65, 155.

53. Magid, L. J.; Shaver, R. J.; Gulari, E.; Bedwell, B.; Allkhafaji, S. Prepr. Div. Pet. Chem., Am. Chem. Soc. 1981, 26, 93.

54. Franses, E. I.; Puig, J. E.; Talmon, Y.; Miller, W. G.; Scriven, L. E.; Davis, H. T. J. Phys. Chem. 1980, 84, 1547.

55. Lianos, P.; Lang, J. J. Colloid Interface Sci. 1983, 96, 222.

56. Puig, J. E.; Franses, E. I.; Miller, W. G. J. Colloid Interface Sci. 1982, 89, 441.

57. Kaler, E. W.; Falls, A. H.; Davis, H. T.; Scriven, L. E.; Miller, W. G. J. Colloid Interface Sci. 1982, 90, 424.

58. Magid, L. J.; Triolo, R.; Johnson, J.; Koehler, W. J. Phys. Chem. 1982, 86, 164.

59. Martin, C. Ph.D. dissertation, The University of Tennessee, Knoxville, Tennessee, 1981.

60. Luisi, P. L.; Magid, L. J. CRC Critical Reviews in Biochemistry 1986, 20, 409.

61. Evans, H. C. J. Chem. Soc. 1956, 579.

62. Tausk, R. J. M.; Karmiggelt, J.; Oudshoorn, C.; Overbeek, J. Th. G. Biophys. Chem. 1974, 1, 175.

63. Zana, R. J. Colloid Interface Sci. 1980, 78, 330.

64. Miller, M. L.; Dixon, J. K. J. Colloid Sci. 1958, 13, 411.

65. Williams, E. F.; Woodberry, N. T.; Dixon, J. K. J. Colloid Sci. 1957, 12, 452.

66. Jobe, D. J.; Reinsborough, V. C. Can J. Chem. 1984, 62, 280.

67. Funasaki, N.; Hada, S. J. Colloid Interface Sci. 1978, 64, 454.

68. Balmbra, R. R.; Clunie, J. S.; Goodman, J. F. Proc. Royal. Soc. 1965, 285A, 534.

69. Magid, L. J.; Daus, K. A.; Butler, P. D.; Quincy, R. Q. J. Phys. Chem. 1983, 57, 5472.

70. Kale, K. M.; Cussler, E. L.; Evans, D. F. J. Phys. Chem. 1980, 84, 593.

71. Hoffmann, H.; Rehage, H.; Platz, G.; Schorr, W.; Thurn, H.; Ulbricht, W. Colloid Polym. Sci. 1982, 260, 1042.

72. Persson, B. O.; Drakenberg, T.; Lindman, B. J. ys. Chem. 1976, 80, 2124.

73. Lindblom, G.; Lindman, B.; Mandell, L. J. Colloid Interface Sci. 1973, 42, 400.

74. Ulmius, J.; Wennerstrom, H. J. Magn. Resonance 1977, 28, 309.

75. Ueno, M.; Kishimoto, H. J. Phys. Chem. 1983, 87, 850.

76. Gustavsson, H.; Lindman, B. J. Am. Chem. Soc. 1975, 97, 3923.

77. Gustavsson, H.; Lindman, B. J. Am. Chem. Soc. 1978, 100, 4647.

78. Kilpatrick, P. K.; Miller, W. G. J. Phys. Chem. 1984, 88, 1649.

79. Chen, S.-H.; Lin, T.-L. in "Methods of Experimental Physics--Neutron Scattering," Should, K.; Price, D. L., Eds.; Academic: New York, 1985, Vol. II.

80. Cabane, B. in "Surfactant Solutions: New Methods of Investigation," Zana, R. Ed.; Marcel Decker: New York, 1987.

81. Magid, L. J. in "Nonionic Surfactants" 2nd Edition, Shick, M., Ed.; Marcel Dekker: New York, 1986.

82. Magid, L. J. Colloids and Surfaces, 1986, 19, 129.

83. "Treatise on Materials Science and Technology, Vol. 15: Neutron Scattering," Kostorz, G., Ed.; Academic Press: New York, 1979, p. 5.

84. Hayter, J. B. in "Physics of Amphiphiles, Micelles, Vesicles and Microemulsions," Degiorgio, V.; Corti, M., Eds.; North Holland: Amsterdam, 1985, p. 59.

85. Hayter, J. B.; Penfold, J. Colloid Polym. Sci. 1983, 261, 1022.

86. Kotlarchyk, M.; Chen, S.-H. J. Chem. Phys. 1983, 79, 2461.

87. Glatter, O.; Kratky, O. "Small-Angle X-ray Scattering," Academic Press: New York, 1955.

88. Guinier, A.; Fournet, G. "Small-Angle Scattering of X-Rays," Wiley: New York, 1955.

89. Lord Rayleigh, Proc. Roy. Soc. London) 1914, A90, 219.

90. Patterson, A. L. Phys. Rev. 1939, 56, 972.

91. Ornstein, L. S.; Zernike, F. Proc. K. Ned. Akad. Wet. 1914, 17, 793.

92. Hansen, J. P.; Hayter, J. B. J. Mol. Phys. 1982, 46, 651.

93. Verwey, E. J. W.; Overbeek, J. Th. G. "Theory of the Stability of Lyophobic Colloids, " Elsevier, 1948.

94. Hayter, J. B.; Penfold, J. Mol. Phys. 1981, 42, 109.

95. Lebowitz, J. L.; Percus, J. K. Phys. Rev. 1966, 144, 251.

96. Hayter, J. B.; Zulauf, M. Colloid Polym. Sci. 1982, 260, 1023.

97. Reatto, L.; Tau, M. Chem. Phys. Lett. 1984, 108, 292.

98. Jacrot, B. Rep. Prog. Phys. 1976, 39, 911.

99. Cabane, B.; Zemb, T. Nature 1985, 314, 385.

100. Cabane, B.; Duplessix, R.; Zemb, T. in "Surfactants in Solution," Mittal, K.; Lindman, B., Eds.; Plenum Press: New York, Vol. 1, p. 373-404).

101. Hayter, J. B.; Zemb, T. Chem. Phys. Lett. 1982, 93, 91.

102. Berr, S. S.; Caponetti, E.; Johnson, J. S., Jr.; Jones, R. R. M.; Magid, L. J. J. Phys. Chem. 1986, 90, 5766.

103. Child, H. R.; Spooner, S. J. Appl. Cryst. 1980, 13, 259.

104. Jacrot, B.; Zaccai, G. Biopolymers 1981, 20, 2413.

105. Hayter, J. B.; Penfold, J. J. Chem. Soc., Faraday Trans. 1 1981, 77, 1851.

106. Bendedouch, D.; Chen, S.-H.; Koehler, W. C. J. Phys. Chem. 1983, 87, 2621.

107. Bendedouch, D.; Chen, S.-H. J. Phys. Chem. 1983, 87, 1653.

108. Bendedouch, D.; Chen, S.-H. J. Phys. Chem. 1984, 88, 648.

109. Bendedouch, D.; Chen, S.-H.; Koehler, W. C. J. Phys. Chem. 1983, 87, 153.

110. Chao, Y.-S.; Sheu, E. Y.; Chen, S.-H. J. Phys. Chem. 1985, 89, 4395.

111. Hayter, J. B.; Zemb, T. Chem. Phys. Lett. 1982, 93, 91.

112. Hayter, J. B.; Penfold, J. Colloid Polym Sci. 1983, 261, 1022.

113. Cabane, B.; Duplessix, R.; Zemb, T. in "Surfactants in Solution," Mittal, K. L., Ed.; Plenum Press: New York, Vol. 1, 1982.

114. Berr, S. C.; Coleman, M. J.; Jones, R. M. M.; Johnson, J. S. J. Phys. Chem. 1986, 90, 6492.

115. Chevalier, Y.; Belloni, L.; Hayter, J. B.; Zemb, T. J. Phys. 1985, 46, 749.

116. Quirion, F.; Magid, L. J. J. Phys. Chem. 1986, 90, 5193.

117. Quirion, F.; Magid. L. J. J. Phys. Chem. 1986, 90, 5435.

118. Magid, L. J.; Triolo, R.; Bedwell, B. in "Surfactants in Solution," Mittal, K. L., Ed.; Plenum Press: New York, Vol. 1, 1982.

119. Triolo, R.; Hayter, J. B.; Magid, L. J.; Johnson, J. S. J. Phys. Chem. 1983, 79, 1977.

120. Caponetti, E.; Triolo, R.; Ho, P. C.; Johnson, J. S.; Magid, L. J.; Butler, P.; Payne, K. A. J. Colloid Inter. Sci., 1987, 116, 200.

121. Magid, L. J.; Martin, C. A.; Caponetti, E. in "Proceedings of the 1984 Chemical Research and Development Center Conference on Chemical Defense Research.

122. Immirzi, A.; Perini, B. Acta Cryst. 1977, A33, 216.

123. Naegele, G.; Klein, R.; Medina-Noyola, M. J. Chem. Phys. 1985, 83, 2560.

124. Sheu, E. Y.; Wu, C.-F., Chen, S.-H., Blum, L. Phys Rev. A 1985, 32, 3807.

125. Evans, D. F.; Ninham, B. W. J. Phys. Chem. 1983, 87, 5025.

126. Tartar, H. J. Phys. Chem. 1955, 59, 1195.

127. Tanford, C. J. Phys. Chem. 1972, 76, 3020.

128. Magid, L. J.; Butler, P. D.; Daus, K. A. in "Proceedings of the 1983 Chemical Research and Development Center Conference on Chemical Defense Research"

129. Magid, L. J. Ph.D. Dissertation, The University of Tennessee, Knoxville, Tennessee, 1973.

130. Berr, S. S. Ph.D. Dissertation, Wake Forest University, Winston-Salem, North Carolina, 1986.

131. Carver, M.; Delichere, A.; Magid, L. J. Proceedings of the Symposium on Magnetic Resonance and Scattering from Surfactant Systems, Magid, L. J. Ed., Plenum Press: New York, in press.

132. Brady, J. E.; Evans, D. F.; Warr, G. G.; Greiser, F.; Ninham, B. W. J. Phys. Chem. 1986, 90, 1853.

133. Ninham, B. W.; Evans, D. F.; Wel, G. J. J. Phys. Chem. 1983, 87, 5020.

134. Talmon, Y.; Evans, D. F.; Ninham, B. W. Science 1983, 221, 1047.

135. Kachar, B.; Evans, D. F.; Ninham, B. W. J. Colloid Inter. Sci. 1984, 100, 287.

136. Vikingstad, E.; Badden, J. J. Colloid Inter. Sci. 1980, 74, 8.

137. Seno, M.; Tomiyuki, N.; Kise, H. Bull. Chem. Soc. Jpn. 1981, 54, 2841.

138. Miller, D. D.; Evans, D. F.; Warr, G. G.; Bellare, J.R. in press.

139. Turro, N. J.; Yekta, A. J. Am. Chem. Soc. 1978, 100, 5951.

140. Kachar, B.; Evans, D. F.; Ninham, B. W. J. Colloid Interface Sci. 1984, 100, 287

141. Raha, C. Organic Syntheses Collective Vol. IV, 263.

142. Brown, C. A.; Yamashita, A. J. Am. Chem. Soc. 1975, 97, 891.

143. Abrams, S. R. J. Org. Chem. 1984, 49, 3587.

144. Hsiao, C. Y. Y.; Ottaway, C. A.; Wetlaufer, D. B. Lipids 1974, 9, 913.

145. Atkinson, J. G.; Luke, M. O.; Stuart, R. S. Can. J. Chem. 1967, 45, 1511.

146. Lin, T.-L.; Chen, S.-H.; Gabriel, N. E.; Roberts, M. F. J. Am. Chem. Soc. 1986, 108, 3499.

147. Sheu, E. Y.; Chen, S.-H.; Huang, J. S. J. Phys. Chem. 1987, 91, 1535.

APPENDIX

SCHEME 1

(1). $HO\text{-}CH_2\text{-}C{\equiv}C\text{-}(CH_2)_3CH_3 \xrightarrow{\text{1,3-diaminopropane-d}} HO\text{-}CH_2(CD_2)_4\text{-}C{\equiv}C\text{-}D$

(2). $HOCH_2(CD_2)_4\text{-}C{\equiv}C\text{-}D \xrightarrow{D_2/Pt} HOCH_2(CD_2)_5CH_3$

(3). $HOCH_2(CD_2)_5CD_3 \xrightarrow{KMnO_4/H^+} HO\text{-}\overset{O}{\overset{\|}{C}}\text{-}(CD_2)_5CD_3$

(4). $HO\text{-}\overset{O}{\overset{\|}{C}}\text{-}(CD_2)_5CD_3 \xrightarrow{LAD} CD_3(CD_2)_6OH$

VITA

Kimberlee Daus Payne was born in Youngstown, Ohio on January 18, 1959. She attended elementary and junior high school in Youngstown, Ohio and high school in Huntingdon, Tennessee. She graduated from Huntingdon High School, as class valedictorian, in June 1977.

In September 1977 the author enrolled at the University of Tennessee at Martin. She finished her last year of undergraduate study at the University of Tennessee at Knoxville and graduated with high honors in June 1982 with a B.A. in Chemistry.

She entered the graduate school of the University of Tennessee in September 1982 where she held a teaching assistantship. In graduate school the author met her husband Don whom she married on August 10, 1985. In June 1987 she received the Ph.D. in Chemistry and accepted a research position with Hercules Incorporated.